CRANFIELD UNIVERSITY

OGHENERUONA ENDURANCE DIEMUODEKE

MODELLING OF LIQUID BREAKUP MECHANISMS IN ENGINEERING SYSTEMS

SCHOOL OF ENGINEERING
Energy And Power Engineering Division

PhD
Academic Year: 2013 - 2014

Supervisor: Dr. Ilai Sher
September 2014

CRANFIELD UNIVERSITY

SCHOOL OF ENGINEERING
Energy And Power Engineering Division

PhD

Academic Year: 2013 - 2014

OGHENERUONA ENDURANCE DIEMUODEKE

Modelling of Liquid Breakup Mechanisms in Engineering Systems

Supervisor: Dr. Ilai Sher
September 2014

ABSTRACT

Effective design of liquid fuel injection systems is a function of good understanding of liquid breakup mechanisms. A transient liquid breakup model is developed on the classical interfacial breakup theory by modifying the classical linear perturbation process to include time-dependent base and perturbed flow parameters. The non-isothermal condition on liquid jet instability and breakup is theoretically modelled; with the particular consideration of a spatially variation of surface tension along the liquid-gas interface. The model combines the classical interface hydrodynamic instability and breakup theory and heat-transfer through semi-infinite medium. Analytical liquid breakup model, which combines transient and non-isothermal effects on liquid jet breakup, is suggested. The suggested model could be simplified to the transient breakup model and the non-isothermal breakup model equivalents. A novel mechanistic model, which is based on a simple momentum balance between the injected jet and the aerodynamic drag force, is suggested for breakup length. A new model, which combines energy criterion and dual-timescale for turbulent shear in droplet dispersion, is suggested for droplet breakup criteria on the basis of critical Webber number. All developed models showed good predictions of available experimental data, and established empirical correlation, within the operational conditions of contemporary ICEs, specifically diesel engines. Continued research in these areas could benefit the development of the next generation of liquid fuel injectors and combustors – by accounting for transient effects and non-isothermal conditions in liquid jet breakup, and turbulent shear in droplet breakup.

Keywords: Analytical Modelling, Droplet Breakup Criteria, Instability Theory, Linear Perturbation, Non-Isothermal Effects, Transient Effects, Turbulent Shear

DEDICATION

This Thesis is dedicated to:

The Almighty God – Jehovah – *The Know-It-All.*

ACKNOWLEDGEMENTS

The input, help, patience and friendship, not to mention the advice and the knowledge of liquid breakup mechanisms and thermofluid systems modelling, of my supervisor, Dr. Ilai Sher, were sometimes all that kept me going. I would particularly also like to thank him for being an open person to ideas, and for encouraging and helping me to design my interest and ideas. The good advice and support of my co-supervisor, Prof. Hoi Yeung, has been invaluable on both an academic and a personal level, for which I am extremely grateful.

My mentor, Prof. Chika Ogbonna Chima Oko, of the University of Port Harcourt, is happily acknowledged – his advice and moral support stimulated me thus far.

I would particularly thank the Nigerian Government for financial sponsorship towards this research. The Cranfield University Bursary Award and the *Paul Eisenklam* Award for Young Researchers are sincerely appreciated.

I would like to thank my amiable wife, Eseoghene, and my lovely kids (Oghenemeru and Ogheneyoma) for their personal support and great patience at all times. My parents, sister, brothers and in-laws have given me their unequivocal support throughout, as always, for which my mere expression of thanks likewise does not suffice. The family of Mr. James Ogheneovo Atikporu is sincerely appreciated for its hospitality and assistance since the start of my PhD programme.

I would like to express my deepest appreciation to my pastor, Pastor Christina Emmanuel-Odiachi of the G&F Ministries Int., UK, for her spiritual tutelage and motherly care. The entire membership of the G&F Ministries Int., especially the Maintenance Team, is sincerely acknowledged.

To all staff and my office mates and colleagues in Cranfield University, I say a great thank you for your friendship.

TABLE OF CONTENTS

LIST OF FIGURES

LIST OF TABLES

NOMENCLATURE

A. English Symbol	Quantity	Unit(s)
a	Acceleration	[m/s2]
A	Area; Integration constant	[m^2];[-]
B	Integration constant	[-]
c	Specific heat capacity	[J/kgK]
C	Coefficient	[-]
E	Deformed Droplet Energy	[J]
e	Droplet Energy	[J]
$\bar{h}$	Mean convection coefficient	[W/m2K]
H	Functional parameter	[1/m]
I	First kind Bessel function	[-]
k	Wavenumber; Thermal conductivity	[1/m]; [W/mK]
K	Functional, Second kind Bessel function	[1/m]; [-]
L	Length	[m]
L_{bu}^{*}	Dimensionless breakup length	[-]
$\bar{N}$	Mean Nusselt number	[-]
m	Mass	[kg]
Oh	Ohnesorge number	[-]
p	Pressure	[Pa]
p'	Perturbed pressure	[Pa]
$\bar{p}$	Base pressure	[Pa]
$\hat{p}$	Initial pressure disturbance amplitude	[Pa]
Pr	Prandtl number	[-]
$\dot{Q}$	Liquid volume flow rate	[m^3/s]
r	Radial dimension; droplet radius	[m]; [m]
R_0	Unperturbed jet radius	[m]
Re	Reynolds number; Real value	[-];
t	Time	[s]
T	Temperature	[K]

t'	Turbulence timescale	[m]
t^*	Thermal penetration time	[s]
u	Velocity	[m/s]
U	Velocity	[m/s]
u'	Perturbed velocity	[m/s]
$\bar{u}$	Base velocity	[m/s]
$\hat{u}$	Initial velocity component amplitude	[m/s]
V	Volume	[m^3]
We	Webber number	-
z	Axial dimension	[m]
z	Axial direction	[m]

B. Greek Symbol	Quantity	Units
Δ	Differential	
Λ	Wavelength	[m]
Ψ	Smooth function	[-]
Ω	Nozzle entrance constant	[-]
ν	Kinematic viscosity; wave growth rate velocity	[s/m]; [m/s]
α	Thermal diffusivity; curve fit parameter	[m^2/s]; [-]
β	Functional parameter; curve fit parameter	[m^2]; [-]
γ	Functional parameter	[m]
δ	Surface perturbation	[m]
ε	Constant parameter	[-]
θ	Azimuthal direction	[rad]
κ	Experimental fit constant	[-]
μ	Dynamic viscosity	[kg/ms]
ξ	Functional parameter	[-]
ρ	Density	[kg/m^3]
σ	Surface tension	[N/m]
τ	Shear stress	[Pa]
φ	Proportionality constant	[-]
ω	Disturbance growth rate	[1/s]

C. Subscript	Meaning
0	Initial condition; zero-order
1	First-order
∞	Ambient parameter
b	breakup
bu	Breakup
c.v	Control volume
cr	Critical condition
D	Drag
d	Discharge
diss.	dissipative
f	Frontal
g	Gas phase
i	Initial parameter; parameter index; imaginary part; injection
j	Coordinates, jet
l	Liquid phase; laminar
max	maximum
opt	Optimum
p	Constant pressure; particle
p	penetration
r	radial direction; real part
rt	Relative turbulence
s	surface
T	Temperature gradient
z	Axial direction
zg	Axial parameter in gas phase
zl	Axial parameter in liquid phase
θ	Azimuthal direction

LIST OF ABBREVIATIONS

Abbreviation	Definition
2-D	Two-dimensions
ALE	Arbitrary Langragian Eulerian
CFD	Computational Fluid Dynamics
DDI	Diesel direct injection
DNS	Direct numerical simulation
HCCI	Homogenous charge compression ignition
HIP	High-injection-pressure
IC	Internal combustion
ICEs	Internal combustion engines
IPI	Interferometric Particle Imaging
KH	Kelvin-Helmholtz
LDA	Laser Doppler Anemometry
LES	Large eddy simulation
NSEs	Navier-Stokes Equations
PDA	Phase Doppler Anemometry
PDPA	Phase Doppler Particle Analyser
PIV	Particle Image Velocimetry
PLIF	Planer Laser Induced Fluorescence
RANS	Reynolds-Averaged Navier-Stokes Equations
RT	Rayleigh-Taylor
SMD	Sauter Mean Diameter
TAB	Taylor Analogy Breakup
UDF	User define function
VOF	Volume-of-Fluid

1 INTRODUCTION

1.1 Preamble

The design of modern Internal Combustion Engines (ICEs) is challenged with legislation, competitive economy, performance and manufacturing costs. Fuel injector performance has a direct effect on the combustion efficiency, pollutant emissions and combustion instability of internal combustion engines. The ever growing interests for low pollutant emissions and improved fuel economy of combustion systems have necessitated the quest for improved liquid fuel combustion efficiency. The combustion efficiency is dependent on liquid fuel breakup mechanisms – primary and secondary. The physical phenomenon of the breakup of bulk liquid volume to fine droplets is known as atomisation in most literature (Lefebvre, 1989). Government legislations against emissions, to make the environment friendlier, are becoming stringent with heavy penalties. To avoid the hammer of these legislations, therefore, there is a need for more effective design of fuel combustion systems.

The effective design of combustion systems is a function of good understanding of liquid fuel breakup processes. The design processes of injection systems, however, are mostly based on trial and error, which may introduce increased cost and time (Shinjo and Umemura, 2011b). The link between liquid fuel breakup processes and fuel-air mixing processes with the engine combustion efficiency and emissions have been acknowledged by many studies (Beaumgarten, 2006; Som and Aggarwal, 2009; Kourmatzis et al., 2013; Payri, et al., 2013). Many of the combustors use either the pressure swirl (simplex) atomisers, or pre-filming air-blast atomisers, or plain orifice pressure techniques (which are the most commonly used in common rail injection) for the breakup of bulk liquid fuel. The aim is to introduce the bulk liquid fuel in a much higher surface area to volume ratio for a stable combustion process.

The process surrounding the injection of liquid through a small aperture and the subsequent breakup of the bulk liquid may seem as a simple process, but the physics of spray formation has proved to be extremely complex. Nevertheless,

there is ever growing interests on liquid breakup mechanism, which is attributed to its importance to range of industries such as the combustion, crop spray, coating, metal deposit, chemical synthesis (Beaumgarten, 2006; Stiesch, 2010) and in fuel cells (Shepard Jr. and Palan, 2006). Although the physics of spray formation is complex, it plays a very important role in internal combustion engines; and its investigation can be categorised into three broad categories: experimental measurements, mathematical (analytical) and Computational Fluid Dynamics (numerical) modelling.

Experimental measurements have contributed significantly to the understanding and development of liquid breakup technology over the last twenty-five years (Siebers, 1999; Cossali, Marengo and Santini, 2005a; Madsen, 2006; Dumouchel, 2008; Chen et al., 2013). However, the experimental investigations of liquid fuel breakup may be limited by densely cloud of droplets around the liquid core, high velocity of droplets, highly transient nature of the liquid injection process and sometimes hostile environmental conditions in which the atomisation processes take place (for example, in ICEs). The experimental limitations sometimes propagate into experimental uncertainties, which may render the understanding of the breakup processes to be deficient.

The analytical category is concerned with the fundamental understanding of the physical process in a closed mathematical term. The analytical investigation either based on basic experimental results or based on theoretical derivation of basic transport governing equations, validated with available experimental data, may give appreciable insight into the breakup mechanisms of liquid. A predictive model for the liquid breakup mechanisms is offered by analytical methods. Furthermore, a validated analytical model would be a useful tool to optimise pertinent injection or combustion system parameters. However, the difficulties surrounding the two-phase flow phenomena, due to different length and time scales, have, in most cases, encouraged the analytical investigation category to be abandoned for, or interfaced with, the Computational Fluid Dynamics (CFD) codes (numerical) category (Kumar et al., 2013).

The numerical category involves the use of approximate mathematical formulations combined with empirical and/or semi-empirical formulations implemented into practical CFD codes. The CFD codes are satisfactory in some practical spray applications (Gorokhovski and Herrmann, 2008; Postrioti et al., 2014). However, it is worth noting that CFD codes assumptions may make simulations physically unrealistic in some spray applications (Shinjo and Umemura, 2011a). For example, the blobs model assumption for a dominant interfacial breakup phenomenon in two-phase flow may introduce considerable error due to the physical modelling error. Although some of the hindrances to the CFD investigation of liquid breakup, as acknowledged in Hardalupas and Chigier (1994), have been allayed in Mohan, Yang and Chou (2014), little has been done on the application of CFD to the parametric investigations of liquid breakup, as a majority of CFD codes is closed by empirical and/or semi-empirical correlations. Furthermore, the CFD investigation of liquid breakup mechanisms requires considerable amount of time investment and specialised and structured knowledge for a sufficiently detailed and accurate simulations. Majority of CFD investigations of liquid breakup mechanisms are built on the classical Kelvin-Helmholtz (KH) Instability model and the Rayleigh-Taylor Instability model, which are complemented by semi-empirical relations (Kalaaji et al., 2003). The semi-empirical relations in the form of mechanistic models, which complement the CFD codes, have not been fully exploited, because of the complexity surrounding the physics of liquid breakup.

Majority of combustion systems operate at relatively high-pressure sprays, which currently have few detailed primary breakup models. The few that are available, in most cases, are not simple in form and mainly difficult to implement (Shinjo and Umemura, 2011a). One of the challenging ways forward is the development of simplified and easy to implement models, without significantly compromising accuracy. Simplified models include more assumptions, require less input data, and may introduce disconnection between the nozzle flow and the primary mechanism, however, some important and specific details of the breakup mechanisms are achievable through the use of simplified basic

mathematical models, as demonstrated in Shepard Jr. and Palan (2006), Desantes et al. (2006), Sher (2010) and Qian et al. (2011).

Modelling of liquid breakup mechanisms may account for cavitation or turbulent or aerodynamic forces or impingement or the combination. It is generally acknowledged, however, that, in some conditions, the aerodynamic forces (interfacial breakup) are the major controlling factor of the liquid breakup mechanism (Sazhin et al., 2011; Turner et al. 2012; Radev et al., 2013). The classical hydrodynamic instability and breakup model (breaking of interfacial surfaces), the WAVE model (Reitz and Bracco, 1982), assumes that the physics of the liquid breakup is quasi-steady, as the base and perturbed parameters used in the modelling are assumed to be steady.

In practical fuel injection systems, some of the injection parameters, for example, injection velocity and pressure are highly transient in operation. Experimental results have shown that different engine load demands can also introduce transient operations, and have a direct consequence on spray formations (Kennaird et al., 2002), which the combustion process is strongly dependent upon. The quasi-steady assumption may be attributed to some of the deviations regarding the theoretical predictions and experimental observations of the primary atomisation mechanism (Dumouchel, 2008). It is expected that transient effects on spray structures would be more evident with the advent of pulsed-injection technique, which is employed in contemporary combustion engines, as it is shown to maintain better fuel economy and exhaust emissions (Satkoski et al., 2011).

The theory of jet instabilities and breakup has been developed under several assumptions, including assumptions that the jets are steady and isothermal (Reitz and Bracco, 1982). It has been stressed in Sazhin et al. (2011) that practical engineering spray systems are transient, which Bae and Kang (2006) have shown to have significant effects on the spray structure. Furthermore, absolute majority of available models treat liquid breakup mechanisms as an isothermal process, but in some practical spray systems, combustion systems for example, liquid fuel is injected into an elevated ambient temperature, which

may affect temperature dependent liquid properties. The surface tension, which predominantly controls the interfacial surface breaking, is highly temperature dependent. This suggests that non-isothermal conditions may have a significant influence on the breaking of interfacial surfaces.

Secondary breakup, which occurs after the primary breakup, involves the breakup of droplets induced by aerodynamic forces and droplet-wall interactions, which Cossali, Marengo and Santini (2005b) have extensively studied. The general stipulation, for aerodynamic induced secondary breakup, is that a droplet is deformed without breaking up, if Weber (We) < 12 – 13 (Stiesch, 2010; Faeth, 2002). The general stipulation, for droplet breakup holds only for the laminar flow around the droplet; hence, the breakup criterion may be changed considerably when a droplet is shot into a turbulent flow field, as the case for droplet instability and breakup in diesel sprays (Vuorinen et al., 2010). This expectation is attributed to a wide range of dynamic forces due to growing eddies (Vuorinen et al., 2010). Han, Luo and Liu (2011) have theoretically shown the prevalence of turbulent flow field on droplet breakup, as the work focuses on the drop size distributions in turbulent dispersions. However, minimum theoretical breakup criterion for droplet in gaseous flow field has not been fully investigated. Moreover, there has been no consensus in droplet breakup criterion from CFD simulations of spray flows, especially in turbulent flow field, see Liao and Lucas (2009), Vuorinen et al. (2010) and Han, Luo and Liu (2011) for a complete review.

1.2 Aim and Objectives

The aim of this research study is the analytical modelling of the liquid fuel breakup mechanisms – primary and secondary – for the development of the next-generation liquid fuel injectors. In what follows, the main objectives of the study are:

(a) Development of simplified analytical model to investigate the transient effects on liquid jet breakup mechanism.

(b) Development of simplified model for the investigation of liquid jet breakup in non-isothermal conditions.

(c) Theoretical investigation of simultaneous effects of liquid jet acceleration and elevated ambient temperature on the breakup of liquid jets.

(d) Development of a mechanistic model for liquid breakup length to complement CFD codes.

(e) The establishment of theoretical droplet breakup criteria in turbulent flow fields.

1.3 Methodology

The modelling of the liquid breakup mechanisms involves basic fluid mechanics, hydrodynamic instability theory, energy balance and heat transfer. The Kelvin-Helmholtz (KH) instability breakup theory is modified for transient and non-isothermal conditions. The modified KH instability breakup theory and a simple momentum balance – coupled with macro models – are considered for the modelling of the primary breakup mechanisms. Whereas energy balance criterion for droplet breakup is considered for the modelling of the secondary breakup mechanism. The detailed modelling methodology and sequence follow, thus,

1.3.1 Transient Jet Breakup

The transient jet investigation is done in two steps (details are presented in Chapter 3):

(i) Modification of KH Instability Model: The classical KH Instability and breakup model utilizes the following linearization parameters, see Reitz and Bracco (1982) for details,

$$u_j = \bar{u}_j + u_j'; \; j \in [r, \theta, z] \qquad \text{(1-1a,b)}$$

and $p = \bar{p} + p'$ (1-1c)

where the over bar parameters are the base parameters, which are treated as steady state parameters, and prime parameters represent perturbed parameters; the perturbed parameters are assumed to have the following forms, based on plane wave expansion:

$$u_r' = \Psi(r)\hat{u}_r e^{ikz+n\theta+\omega t} \quad \text{(1-2a)}$$

$$u_z' = \Psi(r)\hat{u}_z e^{ikz+n\theta+\omega t} \quad \text{(1-2b)}$$

$$u_\theta' = \Psi(r)\hat{u}_\theta e^{ikz+n\theta+\omega t} \quad \text{(1-2c)}$$

and $p' = \Psi(r)\hat{p}e^{ikz+n\theta+\omega t}$ (1-2c)

The classical KH development procedure is adhered to, but with modifications to the linearization parameters as follow:

$u_j = \bar{u}_j(t) + u_j'; \; j \in [r, \theta, z];$ (1-3a,b)

and $p = \bar{p}(t) + p'$, (1-3c)

with the perturbed parameters postulated to take the following forms:

$$u_r' = \Psi(r)\hat{u}_r e^{ikz+n\theta+\omega(t)} \quad \text{(1-4a)}$$

$$u_z' = \Psi(r)\hat{u}_z(t) e^{ikz+n\theta+\omega(t)} \quad \text{(1-4b)}$$

$$u_\theta' = \Psi(r)\hat{u}_\theta(t) e^{ikz+n\theta+\omega(t)} \quad \text{(1-4c)}$$

and $p' = \Psi(r)\hat{p}(t)e^{ikz+n\theta+\omega(t)}$ (1-4d)

These forms are less restrictive than the ones postulated by the classical hydrodynamic instability theory. These forms enable time dependency of perturbation to be non-linear, with the principle of separable variable still being maintained, and assume a different form for each parameter. Furthermore, the present postulations acknowledged the fact that a range of disturbances, wave packet (Turner et al., 2012), grow along the liquid-gas interface prior to breakup (Domann and Hardalupas, 2004) as against a single wave postulation of the classical postulation. However, it is argued that the critical wave (on the basis of maximum growth rate), which may results from self-growing or constructive wave interference, controls the breakup.

The formulation follows by substituting the perturbed parameters into the Navier-Stokes equation, by making use of basic assumptions and neglecting second order and products of perturbed terms. The analysis proceeds by noting that the conservation equation holds for both perturbed and unperturbed flow. Solving the resulting equation with appropriate boundary conditions, kinematic and dynamic, gives the transient KH instability dispersion equation, this is solved for the breakup controlling transient KH parameters: growth rate and wavenumber.

(ii) Macro model: The breakup controlling parameters from the transient KH instability step, the Reitz and Bracco (1982) spray angle model, and the coupling of penetration and breakup lengths, given in Eq.(1-5), on the account of mass and momentum balances were used to obtain the spray angle, breakup length and penetration length.

$$\int_0^{L_p} L_p \, dL_p = L_{bu} \int_0^t \bar{u}_z(t) dt \tag{1-5}$$

where L_p is penetration length and L_{bu} is the breakup length.

1.3.2 Non-isothermal Jet Breakup

The analytical investigation adopts the classical linearization postulations; however, the dynamic boundary condition imposed is modified thus

$$p_l - p_g = \sigma(z)K \text{ and } r = R_0 + \delta \tag{1-6a,b}$$

where $\sigma(z)$ denotes the axial variation of surface-tension due to transient heat transfer; with $K = div\,(\nabla G/|\nabla G|)$, where $G(r,z) = 0$ denotes the surface for which K has to be determined, it follows thus

$$K = \frac{1}{R_0} - \frac{\delta}{R_0^2} - \frac{\partial^2 \delta}{\partial z^2} \equiv \frac{1 - \delta/R_0}{R_0} - \frac{\partial^2 \delta}{\partial z^2} \tag{1-7}$$

where g and l stand for gas and liquid, respectively; whereas R_0 and δ denote the unperturbed jet radius and surface perturbation, respectively.

This particular postulation is necessary to capture the spatially variation of surface tension along the liquid-gas interface. In what follows, the $d\sigma/dz$ from the hydrodynamic analysis is coupled to heat transfer into a semi-infinite medium via the solution of the following governing heat transfer equations

$$\frac{1}{\alpha}\frac{\partial T}{\partial t} = \frac{\partial^2 T}{\partial r^2} \tag{1-8}$$

with the initial and boundary conditions given as

$$T(r,0) = T_i, \tag{1-9a}$$

$$T(\infty, t) = T_i \tag{1-9b}$$

and $$-k\frac{\partial T}{\partial r}\Big|_0 = \bar{h}\big(T_\infty - T(0,t)\big) \tag{1-9c}$$

In these expressions $\alpha \equiv k_l/\rho c_p$ is the thermal diffusivity, k is the thermal conductivity, T_i is the initial temperature, T_∞ is the ambient temperature and $\bar{h}$ is the mean convection coefficient. See Chapter 4 for details.

1.3.3 Transient Non-isothermal Jet Breakup

This involves a holistic modelling approach by combining the modelling postulations in the transient jet breakup, Eqs(1-3) and (1-4), and the assumption – axial variation of surface-tension – in the non-isothermal jet breakup, Eqs(1-6a,b) and Eq.(1-9a). The detailed analysis is presented in Chapter 5.

1.3.4 Mechanistic Model for Breakup Length in the Atomisation Breakup Regime

In this analysis, a control volume is defined to include the intact segment of the jet, just down to the breaking tip. Thereafter, a simple momentum balance between the injected jet and the aerodynamic drag force due to the surrounding gas, according to Eq.(1-10), which complements the classic hydrodynamic instability breakup mechanism, is done. The resulting equation is solved, with some basic assumptions, to arrive at breakup length.

$$\frac{d(mU)_{c.v}}{dt} = \pi\rho_j r_j^2 U_0^2 - \frac{1}{2}\rho_g C_D A_f U^2 \quad (1\text{-}10)$$

The details of this modelling aspect are presented in Chapter 6.

1.3.5 Turbulent Induced Droplet Breakup

The energy criterion, on a symmetrical breakup, for a disturbed parent droplet to disintegrate, see Eq.(1-11), is adopted, from Sher and Sher (2012), for the analysis of a droplet breakup.

$$E_s = ne_s + E_{diss} \quad (1\text{-}11)$$

It is argued that the droplet breakup is due to the simultaneous mechanisms of drag induced deformation (laminar drag breakup) and turbulence vortex induced breakup, the faster breakup mechanism being the relatively dominant.

The laminar drag breakup timescale, t_{bu}, and the turbulence breakup timescale, t', are coupled through the dual-timescale for turbulent energy transfer in droplet dispersion (Pai and Subramaniam, 2007), according to Eq.(1-12), to the dissipation timescale in the breaking droplet, t, which is the timescale in the energy balance for droplet breakup, that is, a balance of deformed surface energy and breakup dissipation.

$$\frac{1}{t} \sim \frac{1}{t'} + \frac{1}{t_{bu}} \quad (1\text{-}12)$$

The turbulence time scale, $t'[s]$, is generally given as (Stiesch, 2010)

$$t' = \frac{l}{u'} \equiv \frac{l}{I_{rt}U} \quad (1\text{-}13)$$

The analysis yields analytical minimum criteria for droplet breakup in turbulence flow field in the Weber-turbulence intensity and the Weber-Ohnesorge representations.

In what follows, from the methodologies (subsections 1.3.1–1.3.5), simple pseudo-code algorithms were devised, based on the models developed, and

converted into computer codes in MATLAB® programming environment; interfaced with Microsoft Excel® spreadsheet. Validations of the models with available published experimental data were achieved.

1.4 Thesis Layout

Chapter 2 deals with an in-depth review of the literature on the investigation of liquid breakup mechanisms and general information on liquid breakup. Chapter 3 is on the modelling of transient liquid jet breakup mechanism with emphases on breakup length, penetration length and spray angle. The chapter that follows, the 4th chapter, entails the analytical investigation of liquid jet breakup in non-isothermal condition. Chapter 5 involves the investigation of the simultaneous effects of acceleration and non-isothermal condition on liquid jet breakup. Subsequently, Chapter 6 is on the development of mechanistic model for the breakup length of liquid fuel breakup mechanism in the atomisation regime, which is the dominant regime in engine operation, as liquid fuel injection systems utilise high-injection-pressure. Chapter 7 analytically investigates the effects of turbulent flow field on the breakup criterion of droplet. The final chapter, Chapter 8, is on the conclusions drawn from the entire research study, which partly features summary of publications based on the research work, and recommendations for further study. Expanded mathematical formulations are presented in the Appendices A and B.

2 LITERATURE REVIEW

2.1 Brief History of Liquid Breakup Studies

Young and Laplace are considered as the pioneer researchers that set the stage opened for the systematic mathematical study of surface tension driven liquid breakup. However, Savart in 1833 was the first to propose that liquid jet breakup are controlled by some physical laws. Savart attributed the physical laws to intermolecular attraction without the recognition of the important effect of surface tension. Plateau in 1849, however, recognised the important role the surface tension plays in liquid breakup, as pioneered by Young and Laplace. Experimental observations of Savart and Plateau were advanced by Rayleigh in 1891. The second half of the nineteenth century, which coincided with the industrial revolution, pushed forward the role of surface tension in liquid breakup – theoretical and experimental wise. Notable contributors to the theory of liquid breakup are: Eötvö in 1886, Quincke in 1877, Lenard in 1887 and Bohr 1901. Theoretically, Rayleigh's linear instability analyses were the cornerstones for the analyses of liquid breakup mechanism. The expanded history of liquid breakup can be found in Eggers (2006), as this brief history is adapted from it.

2.2 Liquid Breakup Techniques

The underline principle behind liquid breakup techniques is on the process of energy conversion. Most practical liquid breakup techniques are basically, therefore, classified by the prevailing working principle, examples are: pressure, rotary, air-assisted, air-blast, flashing liquid jet and effervescent (Lefebvre, 1989, pp. 5-9). However, there are other forms of atomisers developed, which are useful in special applications (namely electrostatic, ultrasonic, whistle, windmill, vibrating capillary).

2.2.1 Pressure Technique

The pressure technique works by converting high pressure energy into kinetic energy through a small constriction called nozzle. The pressure technique comes in the form of plain orifice, pressure-swirl, duplex, dual orifice, fan spray, square spray and spill return, which are commonly utilised in internal

combustion engines. A major drawback of some of the pressure technique is that the volume flow rate of the liquid is directly proportional to the half power of the injection differential pressure, according to the Bernoullis' energy conservation. A typical liquid fuel injector that utilises pressure energy as a liquid breakup technique is shown in Figure 2-1.

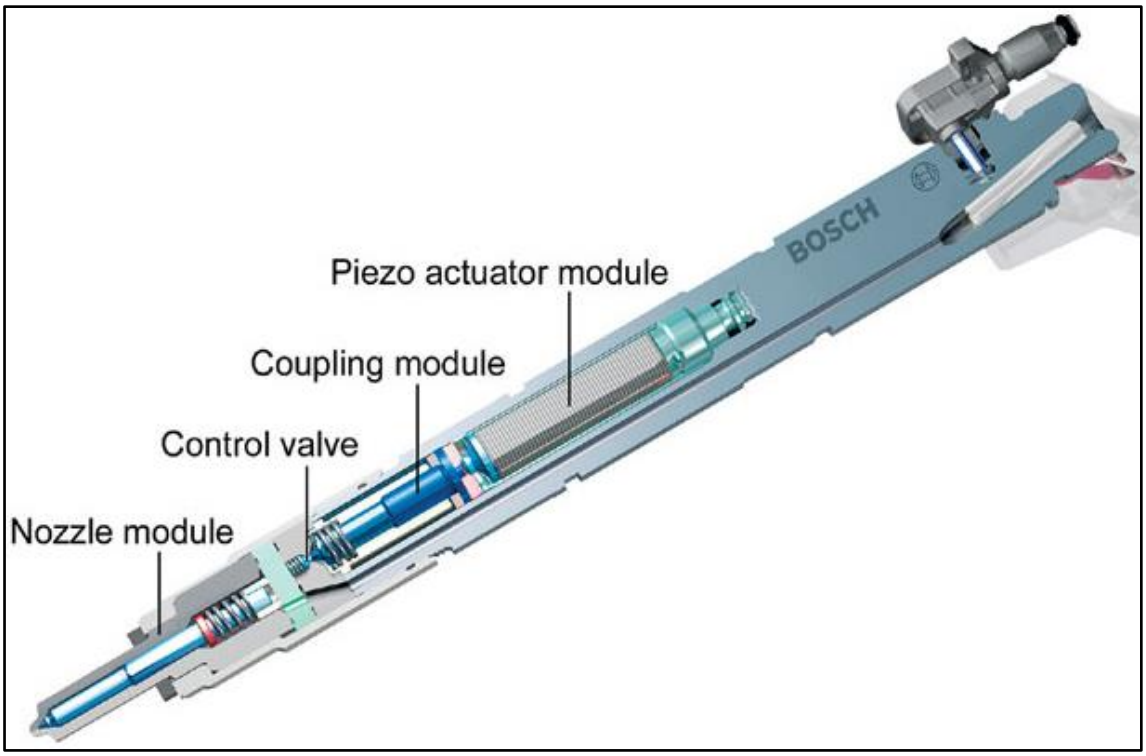

Figure 2-1 Typical Pressure Atomiser (Courtesy of Bosch Pty Ltd)

Plain orifice liquid breakup technique is achieved by forcing a high speed liquid through a circular orifice or nozzle to form a round jet of liquid, which is discharged into the ambient gas. The action of the ambient on the liquid jet results in the formation of droplets. The smaller the orifice diameter the smaller the droplet formed. They are the most commonly used in common rail injection systems.

Pressure-swirl liquid breakup technique is achieved by issuing liquid through the circular nozzle of plain orifice, and preceded by a swirl chamber through which the liquid is discharge via tangential holes. The pressure-swirl performance is practically good, but maximum atomisation occurs at wide spray angles and high injection pressures.

Duplex liquid breakup technique is attained by fitting the pressure-swirl chamber with two liquid distributor holes, each having separate liquid supply lines. The duplex technique is advantageous over all other pressure liquid breakup techniques, as it is not limited by the proportionality of the liquid flow rate to the half power of the supply pressure differential. The flow rate achievable by the duplex technique is of order four of the pressure-swirl.

Dual liquid breakup technique is the modification of the duplex breakup technique. The modification is in the presence of two separate swirl chambers, the primary flow handles one and the other is handled by the secondary flow. The two chambers are concentrically arranged and housed in a single nozzle squirrel. The primary nozzle is designed for a low flow rates and the secondary nozzle is designed to handle high flow rates. The design logic is that at low flow rates the whole liquid flows through the primary nozzle, but at high flow rates most of the liquid bypasses the primary nozzle to flow through the secondary nozzle.

2.2.2 Rotary Technique

The rotary technique employs the use of spinning disk or a rotating cup. The spinning disk has a rotating disk with a centre opening through which the liquid is being introduced. Ligaments or droplets from the broken bulk liquid are discharged radially (through the disk edge) with high velocity after axially introducing the bulk liquid. The disk comes in different forms such as a smooth and flat or may contain vanes and slots to guide the liquid toward the edge of the rotating disk. Droplet formation processes are dependent on the flow rates of the bulk liquid introduced. A high flow rates start with the formation of ligaments or sheets at the disk edge, which culminate into droplets as a result of surface tension; but for a relative low flow rates direct generation of droplets is achieved. The rotary cup, which is relatively smaller than the spinning disk, normally has an elongated bowl profile. In some cases, the cup is serrated for even distribution of droplet size. The rotary technique is advantageous in that it encourages the independent control of liquid flow rate, which makes it more

flexible in operation. However, it produces 360^{o} spray pattern and at times it is coupled with air-blast liquid breakup technique around the periphery.

2.2.3 Air-assisted/Air-blast Liquid Breakup Technique

This technique is achieved by accelerating the breakup of liquid from the injector nozzle by an external air stream directed through an annular. The aim is to promote the liquid breakup by increased relative velocity, which accelerates the liquid instability. The air-assisted technique and air-blast technique are differentiated by the quantity of air and its velocity. The external air stream enhances the breakup mechanisms, which results in smaller droplets, than without the external air. The air-assisted technique is used in other applications, which require fine breakup, where the pressure-swirl technique is used.

2.2.4 Flash-boiling and Effervescent Breakup Techniques

The flash-boiling breakup technique involves the introduction of a volatile liquid into a less volatile one to from a homogenous mixture. The mixture is then passed through an expander, which reduces the pressure of the mixture below the saturation pressure, and the dissolved volatile liquid is flash-boil at the expander to form bubbles and cavitate when approaching the exit of the injector. The cavitation phenomenon causes turbulence, which is attributed to breakup mechanisms. In the effervescent breakup technique a non-condensable gas is introduced into the liquid fuel at low velocity in a mixing chamber to produce bubbly two-phase flow. The bubbles explode at the lower pressure near the exit of the injector nozzle to cause turbulence that enhances the liquid breakup. The two techniques are similar at the downstream of the injector nozzle.

2.3 Liquid Breakup Mechanisms

The liquid breakup mechanisms – referred to as atomisation in most literature – is regarded as the breaking up of large volume of liquid into relatively small droplets for a relatively large surface to volume ratio. The atomisation processes play a significant role in the combustion of liquid fuels in internal combustion engines (ICEs) and other combustor systems (for example gas

turbine and incinerators) in order to achieve proper mixing of fuel and air for rapid evaporation and combustion (Stiesch, 2010; Mohan, Yang and Chou, 2014). The breakup of liquid sprays is divided into two main processes: the primary breakup and the secondary breakup, as illustrated in Figure 2-2.

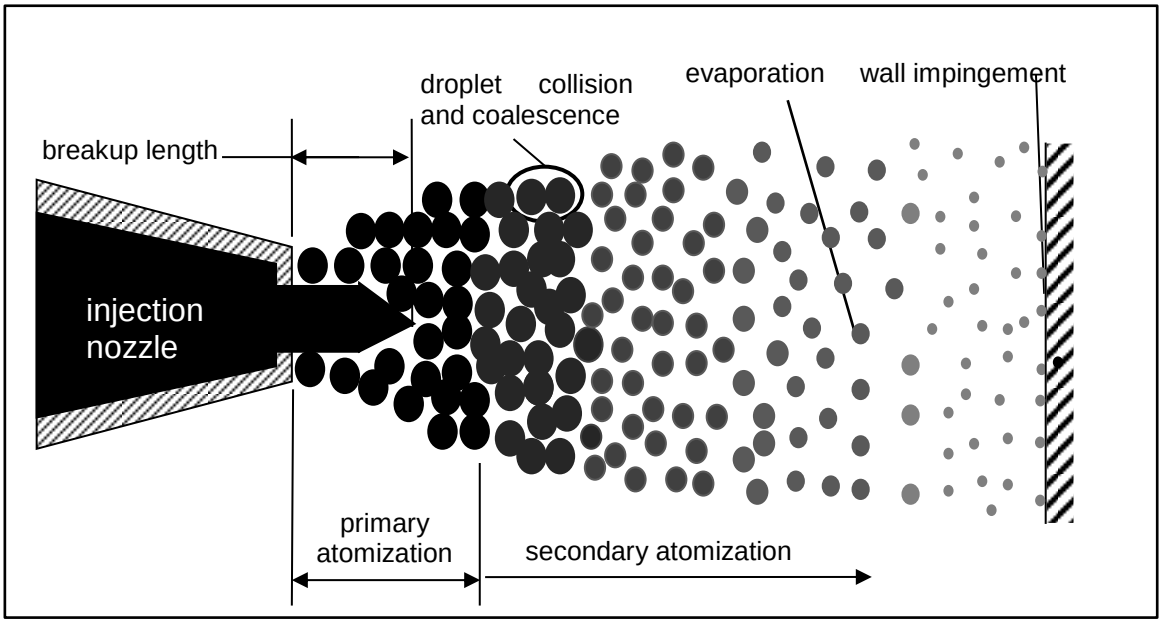

Figure 2-2 Illustration of Liquid Breakup Mechanisms

2.3.1 Primary Breakup

The primary breakup mechanism involves the breaking up of liquid jet – it takes place in the near nozzle region. The primary breakup combined the effects of aerodynamic and hydrodynamic interactions with ambient gaseous phase and the internal phenomena of the nozzle flow, namely cavitation and turbulence. The primary breakup has caught interest of several researchers, as the final droplet sizes are dependent on it, and is being investigated experimentally and mathematically to ascertain the exact mechanism of liquid jet disintegration into droplets. However, the investigation of the micro structure (namely breakup length) of the primary breakup is very difficult, as the region is covered by very dense spray. There are divided opinions on the existence of a liquid core (the breakup length) extending from the exit of the injection nozzle. Some of the researchers are of the view that liquid core exists, from which stripping of the core boundary layer occurs to form droplets, around a hundred of the exit

nozzle diameters; whereas others are of the view that breakup occurs right at the nozzle exit. However, a good number of current studies on near nozzle spray structure showed that there exists a liquid core around a few nozzle diameters from exit of the nozzle (Boggavarapu and Ravikrishna, 2013).

The breakup of the bulk liquid, which may be classified as jets, sheet and film, is as a result of several complex physical interactions in form of forces or energies: aerodynamic, surface tension, viscous and inertial. These energies determine the breakup characteristics of the spray, namely, breakup time and length, droplet size, spray angle and velocity distribution. There is high uncertainty about the actual mechanisms involved in the primary breakup process, but it is mainly attributed to the interaction of aerodynamic and hydrodynamic forces (see Sazhin et al. (2011) and Turner et al. (2012) for examples)

In the investigation of liquid breakup for combustion applications, of most interest are the breakup and penetration lengths, breakup time, drop size and spray angle (Lefebvre, 1989). The disturbance growth rate in liquid jets, which is created by the interaction of cohesive and disruptive forces, is measured by the breakup length. The breakup length, also, defines the point or region where the primary breakup terminates and the start of the secondary breakup mechanism (the fully dispersed two-phase flow region). This is why the primary breakup mechanism is mainly investigated and characterised by the breakup length (Dumouchel, 2001). The graphical representation of the breakup length and the injection velocity is called the stability curve, as illustrated in Figure 2-3, and is used to characterise the primary breakup mechanism.

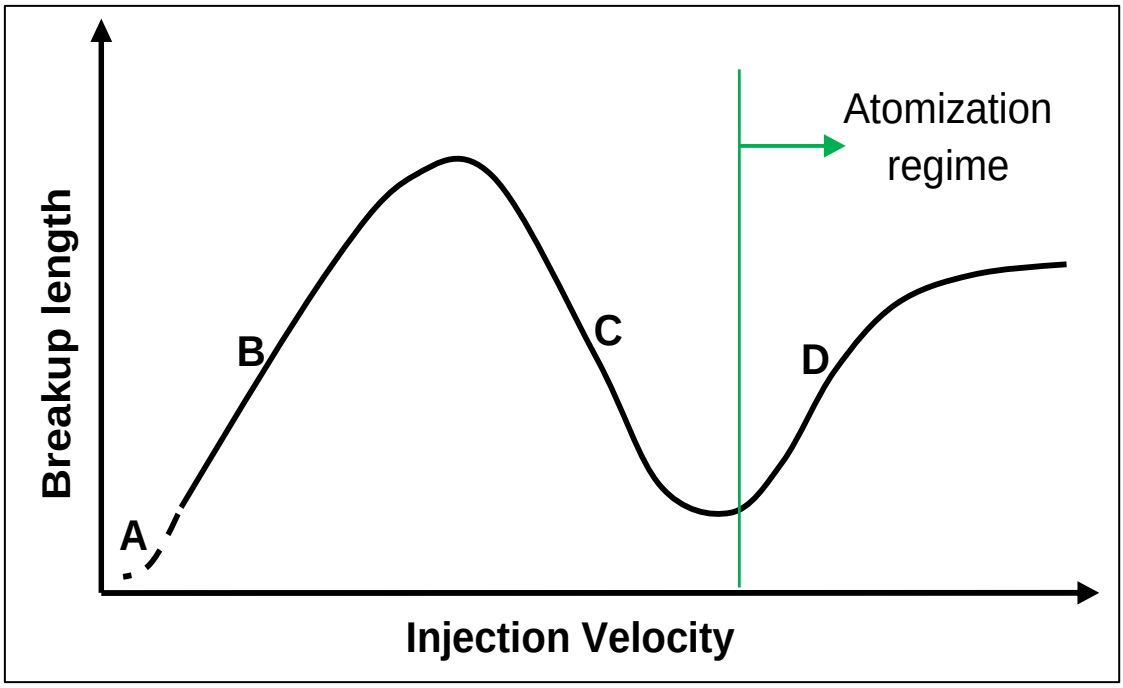

Figure 2-3 Stability Curve showing Primary Breakup Mechanisms

Figure 2-3 shows the predominant breakup mechanisms of the primary breakup of a round liquid jet (Lin and Reitz, 1998); characterised by the Webber number ($We_g = \rho_g U_j^2 d/\sigma$). The Letters, A, B, C, and D in Figure 2-3, stand for the Rayleigh, first-wind induced or wind assisted, second-wind induced and atomisation regimes, respectively, of the primary breakup mechanisms. The atomisation regime of the primary breakup, as shown in Figure 2-3, is the relevant regime for diesel direct injection systems and in most combustion systems (Stiesch, 2010).

Table 2-1 Breakup Regimes for Primary Breakup of a Cylindrical Jet in a Quiescent Air (Lin and Reitz, 1998)

Mechanism	Predominant Breakup Mechanism	Criteria*
Rayleigh Jet Breakup (Varicose Breakup)	Surface tension force	$We_g < 0.4$
First Wind-Induced Breakup (Sinuous Wave Breakup)	Surface tension force , dynamic pressure of ambient air	$We_g < 0.4 < 13$
Second Wind-Induced Breakup (Wave-like Breakup with Air Friction)	Dynamic pressure of ambient air	$We_g < 13 < 40.3$
Atomisation	Unknown, but could be attributed to: aerodynamics interaction, turbulence, cavitaion	$We_g > 40.3$

*$We_g = \rho_g U_j^2 d/\sigma$, where $U_j$is the jet velocity and ρ_g is the ambient gas density

2.3.2 Secondary Breakup

The secondary breakup mechanism takes place down the flow stream; it does not depend on the nozzle internal flow, but on the aerodynamic forces acting on droplets as a result of complex interaction processes with the surrounding gas (Madsen, 2006), and, in some applications, on droplet interactions with the wall (Moreira et al., 2006). There is a significant reduction in droplet size down the spray axis (see Figure 2-2), which suggests that droplets from the primary are breakup further broken up into smaller droplets. The complex interaction of the droplets with the surrounding gas, for a wholly droplet-gas interaction, gives difference in forces experienced by droplets, which results in various breakup regimes or mechanisms, as shown in Table 2-2.

Products of the primary breakup, that is droplets, are highly unstable and are, therefore, subjected to further breakup. The secondary breakup mechanism concerns the breakup of droplets, resulting from the primary breakup, as a result of aerodynamic forces brought by the relative velocity between unstable droplets and the surrounding gas, and droplet-wall interaction (droplet impingement), which is reported to play a vital role in the control of Homogenous Charged Compression Ignition (HCCI) combustion (Moreira et al., 2006). Droplet-wall interactions, which has been extensively studied by Cossali, Marengo and Santini (2005), has been shown to contribute to droplet breakup in the secondary breakup regime in ICEs, however, the phenomenon is given no further consideration in this work, as it is outside the scope of the present work. Forces inducing droplet deformation – outside droplet-wall interaction – are categorized, to a large extent, into two distinct mechanisms: turbulent and laminar drag forces. The mechanism of the secondary breakup is very important, as droplet size distribution is dependent on it. The successive breakup of the relatively unstable droplets into smaller droplets continues, until the breakup driving force is just below the surface tension. Figure 2-5, the exploded view of Figure 2-3, illustrates the relationship between the primary and secondary breakup mechanisms.

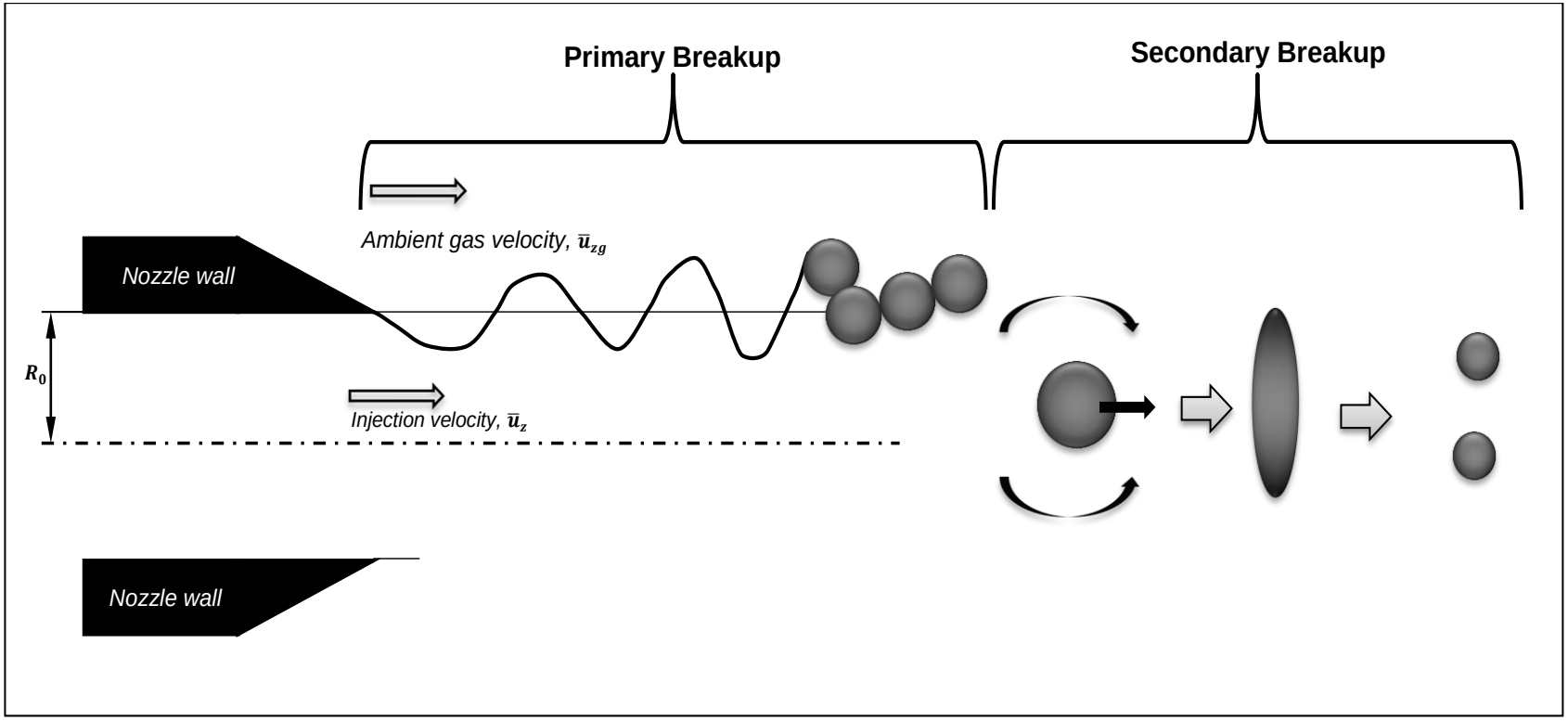

Figure 2-4 Illustration of the Relationship between Primary and Secondary Breakups

Table 2-2 Breakup Regimes for Secondary Atomisation (Wierzba, 1990)

Mechanisms	Breakup sequence				Criteria*
Vibration breakup					$We_g \approx 12$
Bag breakup	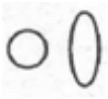				$We_g < 20$
Bag/streamer breakup	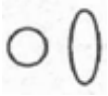				$We_g < 50$
Stripping breakup					$We_g < 100$
Catastrophic breakup					$We_g > 100$

*$We_g = \rho_g U_j^2 r/\sigma$, where r is droplet radius

The mechanism of the secondary breakup is very important, as droplet size distribution is dependent on it. The emphasis, in liquid combustion, is on the combustion of liquid droplets, which has been a topical issue since the last five decades, in the utilisation of liquid fuel in internal combustion engines (Awasthi, Gogos and Sundararajan, 2013); especially Diesel. It has been shown that the size of stable droplets has significant effects on liquid fuel combustion (Hayashi, Fukui and Akamatsu, 2013), however, the minimum criterion for droplet breakup in complex mechanism (namely simultaneous turbulent and laminar drag) has not been fully studied.

The general assumption is that droplet can be deformed without being breakup, if Weber (We) < 12 – 13 (Stiesch, 2010; Faeth, 2002). The general criterion for droplet breakup holds only for the laminar flow around the droplet; hence, the breakup criterion may be changed considerably when a droplet is shot into a turbulent flow field, as the case for droplet instability and breakup in diesel sprays (Vuorinen et al., 2010). This expectation is attributed to a wide range of dynamic forces due to the growing eddies (Vuorinen et al., 2010). Han, Luo and Liu (2011) have theoretically shown the prevalence of turbulent flow field on droplet breakup. The mechanism of the secondary breakup is very important, as droplet size distribution is dependent on it. The emphasis, in liquid combustion, is on the combustion of liquid droplets, which has been a topical issue in the last five decades, in the utilization of liquid fuel (especially diesel) in internal combustion engines (especially Diesel) (Awasthi, Gogos and Sundararajan, 2013).

2.4 Investigation of Liquid Breakup Mechanisms

The investigation of liquid breakup mechanisms is difficult in that the mechanism of liquid breakup is still not well understood; and that the mechanism may differ appreciably from one situation to another according to the obvious reasons of: varied liquid physical properties, injection operations, type of injector (geometrical factor), ambient conditions and droplet-droplet and droplet-wall interactions. Basically, the investigation approach takes the following categories: experimental measurements, mathematical (analytical)

and CFD (Numerical) modelling. Figure 2-5 summaries the investigation approaches and stresses the mathematical approach, which forms the basic objective of this research. Specifically, the continuous line rectangles, in Figure 2-5, are the main methodology adopted in this research work.

Experimental measurements have contributed significantly to the understanding and development of atomisation technology over the last twenty-five years (see Siebers (1999), Sallam et al. (1999), Madsen (2006), Dumouchel (2008) and Park et al. (2009) for examples). The analytical category is concerned with the fundamental understanding of the physical process in wholly mathematical terms (Reitz and Bracco, 1982; Marek, 2013). The CFD category involves the use of mathematical-numerical formulations, combined with empirical or semi-empirical formulations, implemented in computer codes (see Sazhin et al. (2013) for example).

Experimental investigations of liquid fuel breakup are may be limited in some applications due to densely cloud of droplets around the liquid core, high velocity of droplets and highly transient nature of the liquid injection processes and, of course, extreme environmental conditions in which the processes take place in some applications (for example, in ICEs). The experimental difficulties sometimes increase the experimental uncertainty, which may render the understanding of the breakup processes to be deficient. However, analytical and CFD investigations either based on basic experimental results or based on theoretical derivation of basic transport governing equations, validated with available experimental data, may give appreciable insight on the breakup mechanisms of liquid. Furthermore, validated analytical or CFD models would be useful tools to optimise pertinent injection or combustion system parameters. To a greater extent, all the three investigation approaches play a complementary role among each other – see Figure 2-6 for the illustration.

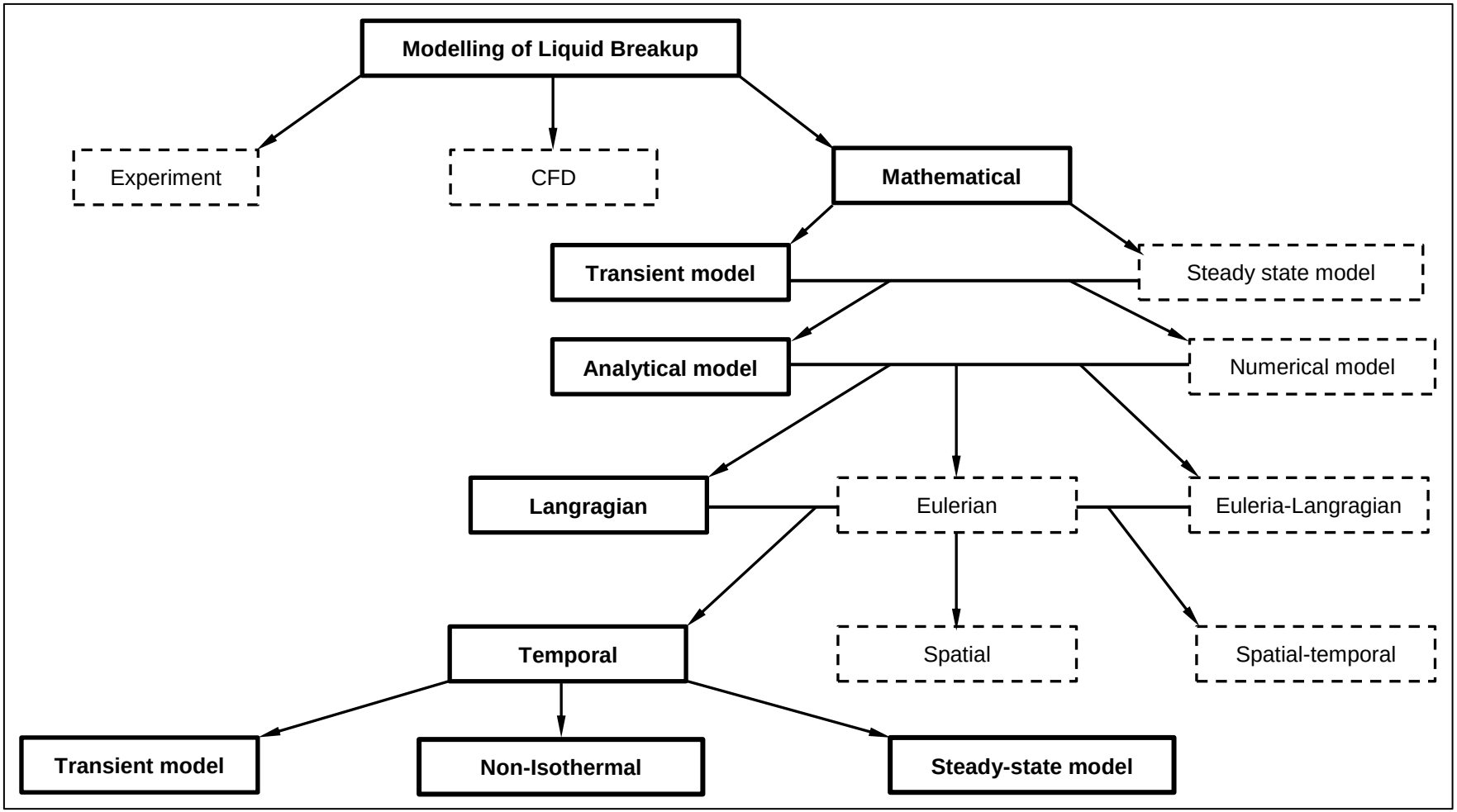

Figure 2-5 Approaches in the Investigation of Liquid Breakup Mechanisms

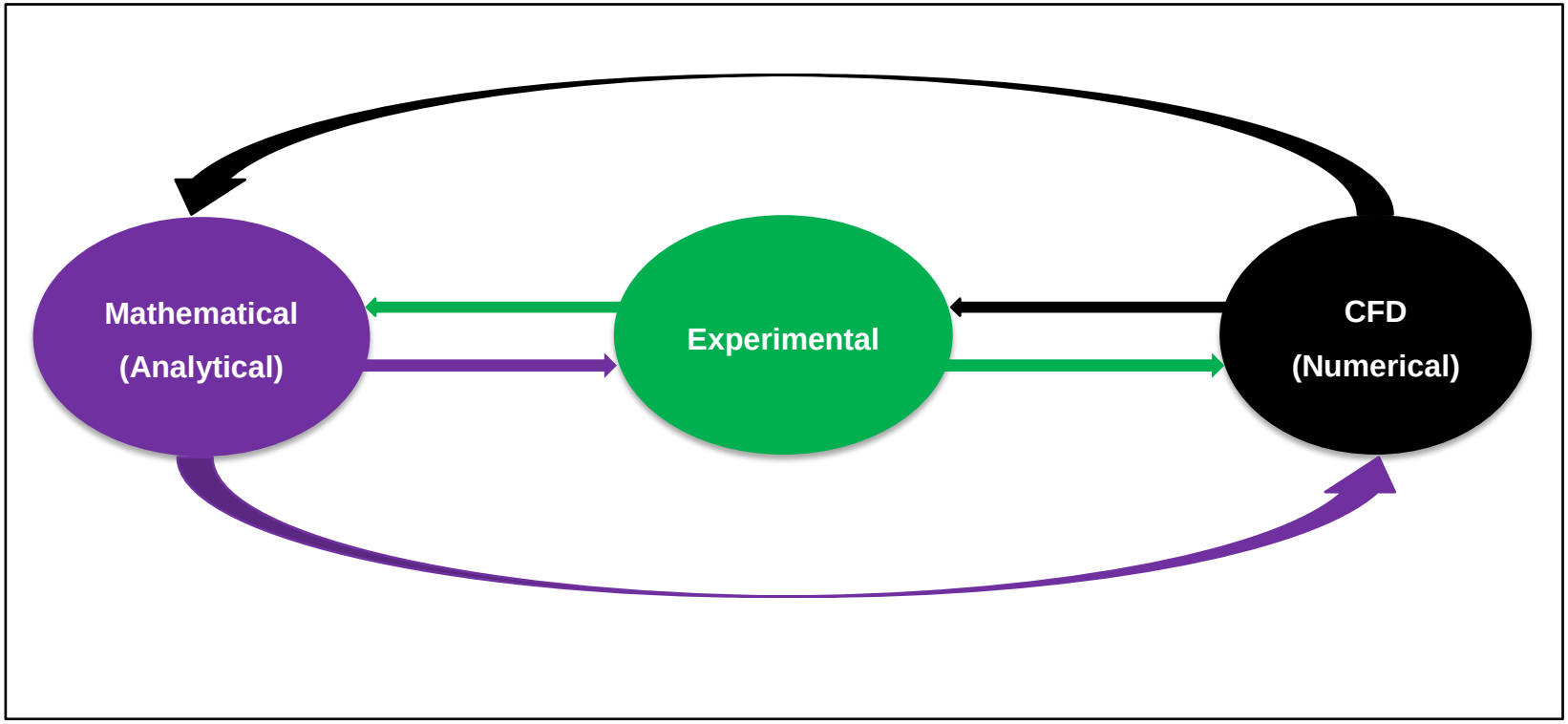

Figure 2-6 Complementary Role of the Liquid Breakup Investigation Approaches

2.4.1 Experimental Investigation

There are three basic classes of experimental methods used in atomisation and spray investigations, which are mechanical methods, electrical methods and optical methods. The optical methods are the most advanced and developed methods for investigating atomisation and spray evolution. Some of the optical experimental techniques used in spray investigation are Visualization (High-Speed Photography), Phase Doppler Anemometry (PDA), Particle Image Velocimetry (PIV), Planer Laser Induced Fluorescence (PLIF) and Phase Doppler Particle Analyser (PDPA) etc., see Dumouchel (2008) and Soid and Zainal (2011) for the complete review.

The visualization techniques are used to investigate macroscopic structure such as spray angle, penetration length and wall impingement; while the others are used to capture the microscopic structure (breakup length, droplet diameter, breakup time, velocity, concentration etc) of the atomisation and spray evolution. PDA is widely used for the measurement of drop size and velocity in sprays (Wigley, Godwin and Blondel, 2004). PDA combines the measurement of scattered light intensity with Laser Doppler Anemometry (LDA) to obtain simultaneous droplet size and velocity measurements. The breakup of liquid jet and the dense spray region is normally not considered in the use of LDA. PDA is a point measurement technique and as such cannot be used to obtain instantaneous spatial information on velocity, droplet size and concentration. The shortcomings of the PDA could be resolved with the relatively new imaging technique, called Interferometric Particle Imaging (IPI), which instantaneously captured spatial information. The PIV measures the distance travelled by particles in the flow field for a given time interval and is applied to the measurement of fuel spray flow and instantaneous whole field velocities. PLIF measurements are based on the principle of excitation of molecule from its ground electronic level to an upper electronic level as a result of laser beam, with area of application in fuel concentration and liquid and vapour fuel. The main limitation of some of these techniques is that they cannot be appropriately used at high droplet concentrations, which is typical of the primary breakup.

The experimental investigation of the primary breakup imposes some difficulties, which pave way for curve fitting spray characteristics, for example cone angle, breakup length or mean drop diameter, with selected breakup parameters like liquid properties, nozzle shape, injection pressure etc, as demonstrated in Qian, Lin and Xiong (2009). However, the trend is drastically changing since the emergence of new sophisticated experimental techniques such as ballistic image techniques, X-ray extinction techniques, optical probe techniques and the infrared laser extinction technique (Dumouchel, 2008; Madsen, 2006). Som and Aggarwal (2009), however, stressed that these experimental techniques, in most cases, are difficult to implement and are very expensive to setup.

The importance of transient liquid breakup mechanisms in the development of new injection technologies, for example the multi-pulse injection, employed in internal combustion systems has intensified efforts on the investigation of transient breakup characteristics. Kim and Lee (2008) investigated the transient breakup characteristics of a single-hole diesel spray using 2-D Phase Doppler Particle Analyser (PDPA) technique in order to clarify the time dependent of droplet formation process. They concluded that transient effect plays a major role in the Sauter Mean Diameter (SMD) analysis of the whole flow field and that the SMD gradually reached a maximum with time and then decreased.

2.4.2 Mathematical Investigation

The most basic analytical tools for investigating liquid breakup are the Taylor Analogy Breakup (TAB) model, and the linear instability theory(Reitz and Bracco, 1982; Eggers and Villermaux, 2008; Sazhin et al., 2013). In the TAB model, the breakup is conceptualised as a spring–mass system; whereas the linear instability model, which is known as WAVE model (Reitz, 1987), uses the linear instability theory of small perturbation waves on the liquid–gas interface.

The TAB model considers the droplet oscillation and distortion as analogous to simple forced harmonic oscillation of a spring-mass system. Although the TAB model has been advanced in Marek (2013) to include double-mass model, however, the concept is in analogous to a spring-mass system; where the

aerodynamic force is equivalent to the external excitation; the surface tension is equivalent to the spring restoring force; and the damping force is synonymous to the liquid viscosity force. Of course, balancing these forces leads to some characteristics equations. It has been shown that the TAB model underestimates some basic spray characteristics, in view of this some researchers modified the original constant in other to obtain more realistic predictions (Tanner, 1997; Bianchi et al., 2007), but the modified model poorly predicts the spray angle. More recent, in Marek (2013), the TAB model has been extended to consider the droplet breakup as analogous to a double-mass system. The approach yields a characteristic equation, which establishes a criterion for a droplet breakup in an ambient flow, without consideration to the effect of free stream turbulence on the droplet breakup.

In the linear hydrodynamic instability analysis, the liquid breakup is due to unstable wave growth as a result of aerodynamic interaction between the bulk liquid and ambient gas. Reitz and Bracco (1982) proposed a KH Instability model on the bases: the flow is assumed to be incompressible, a cylindrical coordinate system that moves with the jet (Langragian system), and base parameters are steady (quasi-steady flow). The linearized Navier-Stokes' equations for the surrounding gas and liquid velocity and pressure perturbations can be written and solved by introducing a velocity potential and stream functions. The solution of the analysis leads to dispersion equation, which relates the wave growth and the wavenumber, extensive literature review on the theory of liquid distortion can be found in Sirignano and Mehring (2001). Another form of the hydrodynamic instability model is the Rayleigh-Taylor (RT) model, which describes the instabilities that develop on a liquid-gas interface as a result of normal acceleration or deceleration towards the gas phase. It is, generally, assumed that the KH is responsible for the primary breakup; whereas the RT and KH compete for the secondary breakup (Som and Aggarwal, 2009). On this basis, some researchers combined the KH and RT as a hybrid hydrodynamic instability model for the secondary atomisation, as demonstrated in Beale and Reitz (1999) and Hossainpour and Binesh (2009).

There are divided opinion on the actual mechanism that controls the breakup process, but it is widely acknowledged that the interaction of aerodynamic and hydrodynamic forces are the major controlling factors of the breakup process (Sazhin et al., 2011; Turner et al., 2012; Radev et al., 2013). In the WAVE model, it is assumed that only the fastest growing perturbation growth rate, which corresponds to the optimum wavenumber, will ultimately control the breakup. The form and presentation of the hydrodynamic instability model depend on: the linear theory, and the postulation of the perturbation form.

Yoon and Heister (2003) presented three types of linear theories for the analysis of liquid breakup: temporal, spatial and spatio-temporal. The temporal theory, which is most commonly used, assumes that the disturbance responsible for the breakup grows temporally at the same rate in space; whereas the spatial theory assumes disturbance grows in space, given that the breakup appears to take place in the region downstream of the location where the liquid is introduced. The most complete theory is that of spatio-temporal instability. This theory has not yet been widely applied because of its mathematical and numerical complexity, as noted in Lin (2006).

The classical hydrodynamic instability analysis, the KH and RT instability models, start with the equations for liquid jet in a cylindrical material coordinate system as follows:

Continuity Equation:

$$\frac{u_r}{r}+\frac{\partial u_r}{\partial r}+\frac{1}{r}\frac{\partial u_\theta}{\partial r}+\frac{\partial u_z}{\partial z}=0 \qquad (2\text{-}1)$$

Momentum Equation:

r-direction momentum

$$\frac{\partial u_r}{\partial t}+u_r\left(\frac{\partial u_r}{\partial r}\right)+\frac{u_\theta}{r}\left(\frac{\partial u_r}{\partial \theta}\right)+u_z\left(\frac{\partial u_r}{\partial z}\right)=-\frac{1}{\rho}\left(\frac{\partial p}{\partial r}\right)+v\nabla^2 u_r \qquad (2\text{-}2)$$

θ-direction momentum

$$\frac{\partial u_\theta}{\partial t} + u_r\left(\frac{\partial u_\theta}{\partial r}\right) + \frac{u_\theta}{r}\left(\frac{\partial u_\theta}{\partial \theta}\right) + u_z\left(\frac{\partial u_\theta}{\partial z}\right) = -\frac{1}{\rho}\left(\frac{\partial p}{\partial \theta}\right) + v\nabla^2 u_\theta \quad (2\text{-}3)$$

z-direction momentum

$$\frac{\partial u_z}{\partial t} + u_r\left(\frac{\partial u_z}{\partial r}\right) + \frac{u_\theta}{r}\left(\frac{\partial u_z}{\partial \theta}\right) + u_z\left(\frac{\partial u_z}{\partial z}\right) = -\frac{1}{\rho}\left(\frac{\partial p}{\partial z}\right) + v\nabla^2 u_z \quad (2\text{-}4)$$

The velocity (u) and pressure (p) are linearized by decomposing as follows:

$$u_j = \bar{u}_j + u_j'; j \in [r, \theta, z]; p = \bar{p} + p' \quad (2\text{-}5a,b)$$

where over bar parameters are the base parameters, which are treated as steady state parameters in the classical postulation; prime parameters represent perturbed parameters; v[s/m] is the kinematic viscosity.

The perturbed parameters are postulated to have the following forms, based on plane wave expansion (Reitz and Bracco, 1982; Vladimir, Igor and Oleg, 2009):

$$u_r' = \hat{u}_r(r)e^{ikz+n\theta+\omega t} \quad (2\text{-}6a)$$

$$u_\theta' = \Psi(r)\hat{u}_\theta e^{ikz+n\theta+\omega t} \quad (2\text{-}6b)$$

$$u_z' = \Psi(r)\hat{u}_z e^{ikz+n\theta+\omega t} \quad (2\text{-}6c)$$

and

$$p' = \Psi(r)\hat{p}e^{ikz+n\theta+\omega t} \quad (2\text{-}6d)$$

where k [1/m] is the streamwise wavenumber, n [-] is the azimuthal wavenumber, ω [1/s] is the growth rate, $\hat{u}_j$ [m/s] are the respective initial velocity components disturbance amplitude, $\hat{p}$ [N/m^2] is the initial pressure disturbance amplitude and $\Psi(r)$is the smooth functions.

The complexity surrounding the analytical solution to Eqs (2-1)-(2-4) is overwhelming. However, the mathematical complexity could be resolved by some specific basic assumptions and the use of simplified basic mathematical models, as demonstrated in Shepard Jr. and Palan (2006), Desantes et al.

(2006), Sher (2010) and Qian et al. (2011). The simplified models require less input data, but it may introduce disconnection between the internal nozzle flows. However, detailed models require comprehensive input data regarding the injector flow, which may be obtained either from experiment or CFD simulation or both. Nevertheless, the simplified models are of advantage in that they have a wider area of application because of their global modelling, as noted by Beaumgarten (2006).

The classical instability model has a fundamental drawback – the quasi-steady state and the isothermal assumptions – since practical liquid fuel injection systems operate under transient and non-isothermal conditions. Kim and Lee (2008) have shown from their experimental results that transient effect of injection affects spray formation process. Turner et al. (2012) incorporated the transient effects of the injection process by the introduction of jet acceleration into the constant parameters of the classical WAVE model. Domann and Hardalupas (2004) suggested an interface tracking method; followed by the temporal and spatial evolution of all the disturbances on the surface of accelerated liquid jet, based on the assumption of wave packet. The theory of the wave packet analysis was advanced in Turner et al. (2012) CFD code for the calculation of liquid breakup length. However, these approaches are built on the classical perturbation postulations; moreover, the transient effects have never been fully considered, especially non-isothermal conditions.

2.4.3 Computational Fluid Dynamics (CFD) Investigation

The computational fluid dynamics combines numerical schemes of fluid flow equations and empirical (constructed experimental data best fit) or semi-empirical formulations into computer codes. The governing equations of fluid flow are the popular Navier-Stokes Equations (NSEs) and are generally valid for both laminar and turbulent flow regimes. On the foregoing merit, the early computational fluid dynamics directly solved the fluid flow equations, to resolve the smallest length scales. This approach is termed the direct numerical simulation (DNS); it considers the length scales as the smallest eddies. The investigation of primary breakup mechanism by DNS is still in its infancy,

apparently due to the attendant high computational cost and numerical complexities. In some situation the method is abandoned, for example, the typical conditions inside an air-cooled small engine combustion chamber requires about 10^{12} grid points to accurately resolve length scales, which, of course, is above the computational capacity of 10^{6} grid points of the contemporary computer systems (Stiesch, 2010).

Nevertheless, a number of studies have demonstrated the plausibility of analysing the liquid breakup processes using numerical approaches (Wang, 2010). Further development in the CFD modelling efforts adopted a single phase approach, not the DNS in the sense, in which the whole flow field is considered as liquid phase and the liquid-gas interface is presumed to attain zero value of the axial velocity (Stiesch, 2010). This gives way to the large eddy simulation (LES) approach, in which only the large-scale eddies of the flow fields are resolved. In the LES approach, all the LES sub-grid terms, which arise from the presence of small-scale interfacial controlling forces, e.g. the surface tension force, are neglected. The DNS resolves all spatial and temporal perturbation of the fluid flow fields whereas the LES under-resolves the DNS of the phases interface by considering a local average of the whole flow field (Gorokhovski and Herrmann, 2008; Wang, 2010). However, the LES approach can yield significant insight into the primary breakup process, if the large-scale resolved phase-interface dynamics is not substantially affected by the small-scale unresolved phase-interface dynamics. Large-scale and small-scale eddies are established by filtering the flow field by a specific cut-off length scale that is appropriate for the problem at hand. LES approach has its own fundamental problem in the selection of the cut-off length scale. Therefore, a third approach, which absorbs itself from some of the DNS and LES problems, is the Reynolds-Averaged Navier-Stokes Equations (RANS) in which quantities of turbulent flows are splinted into an average base quantity and a perturbation value (Ferziger and Peric, 2002).

The RANS method deals with average of the entire turbulent flow field rather than the instantaneous flow field; details can be found in Stiesch (2010). Recent

advancements in CFD have shown other means of tracking the interface in order to establish the two-phase flow fields. One of them, as seen in Xue et al. (2002), is the Arbitrary Langragian Eulerian (ALE) method and another one is the Volume-of-Fluid (VOF), which is the fraction of liquid volume in a given computational cell (Ibrahim, Jog and Jeng, 2005; Hansen et al., 2002). These methods form the foundation for most CFD softwares (Fluent, CFX, Star-CD, KIVA III etc). Wang (2010) noted that the investigation of liquid jet flows must take into account free surface motion and interface, but there is inherent complexity to accurately establish and track the interface between the liquid and the gas phase in the CFD modelling of two-phase flow.

Most researchers found the CFD codes satisfactory; judging from volume of publications on the CFD applications in liquid breakup (Gorokhovski and Herrmann, 2008; Boggavarapu and Ravikrishna, 2013). Although the CFD codes might be useful in some specific applications, however, their use may be complicated by interfacial two-phase flow phenomenon that controls the interfacial breakup mechanisms, which may be attributed to the ever growing numerical techniques on the CFD simulation of liquid jet breakup for efficient methodology to capture the interface phenomena (see Jiang et al. (2010) for completeness). The hydrodynamic models in CFD codes are complemented with empirical formulations (Kalaaji et al. 2003), which may render parametric investigations in CFD to be difficult, as acknowledged in Hardalupas and Chigier (1994). The numerical simulation (CFD codes) requires huge amount of time investment and specialised and structured knowledge to produce sufficiently detailed and accurate simulations; whereas some of the important and specific details of the breakup process could be achieved through the use of simplified basic mathematical models. Absolute majority of the breakup models implemented in CFD codes are based on the quasi-steady-state and isothermal fluid flow conditions, which, of course, in real practical applications, for example liquid fuel combustion systems, the spray injection process is transient and non-isothermal.

2.5 Combustible Mixture Preparation

The ever growing interests for low pollutant emissions and improve fuel economy of combustion systems have necessitated the quest for improved design of internal combustion (IC) engines. Several methodologies have been adopted to solve the problem of exhaust emissions: exhaust gas after-treatment, sophisticated design and control of fuel-injection systems and the combination. While all these have been proved useful, however, it has been stressed in Karimi (2007) that the most important approach of reducing emission should be at source.

Reducing exhaust emissions at source is based on good mixture preparation, which has it epicentre on efficient liquid-fuel breakup processes. The overall aim of the liquid-fuel breakup processes is to introduce the liquid-fuel in a much higher surface area to volume ratio for high fuel evaporation rates. The sequence of processes in combustion mixture preparation of liquid-fuel fired internal combustion engines are: fuel injection, breakup, evaporation and mixing of vapour with air, ignition and finally combustion. The first process, i.e. the fuel injection, has a task of forcing the bulk liquid-fuel, with high pressure, through a small aperture to obtain small droplets with average diameter smaller than that of the nozzle diameter. The fine droplets are subsequently converted to vapour by evaporation process.

The vapour is mixed with appropriate amount of charged air to form a homogenous mixture, which is ignited once the condition for ignition is met. The injector is responsible for the injection of the liquid-fuel, which has the capabilities of metering the appropriate amount of fuel, depending on engine load and speed; and to inject the fuel, at the desired rate, at the appropriate time. The influence of liquid breakup processes on IC engines is varied. In diesel engines it is the combustion rate, which is controlled by the evaporation of droplets, whereas in spark-ignited engines the mixture preparation is influenced by the quality of breakup processes (Liu, Mather and Reitz, 1993).

2.5.1 Diesel Engine

The compression ignition (diesel) engines have excellent engine power density than the spark ignition engines. The diesel engine has, in recent years, attracted research attention apparently because of its excellent fuel efficiency, which can be above 40% and 50% for small and large applications, respectively (Constantine and Evangelos, 2009). Diesel engines have been noted for moderate sensitivity to air-fuel ratio, absence of throttling, high tolerability in peak cylinder pressures and temperatures and high output torque. These characteristics favour the applications of other engine efficiency improvement techniques – for example supercharging. Although diesel engines have enjoyed appreciable patronage, however, there are research concerns about the conflict between exhaust particulate emissions and fuel consumption. The concerns for the exhaust particulate emissions have necessitated the application of other injection strategies or exhaust gas after-treatment.

One of the developments in diesel direct injection (DDI) engines is the utilization of electronically controlled high-injection-pressure (HIP) fuel system, which is aimed at achieving high-power-density low-emission DDI engine (Mahr, 2002). In the HIP fuel system liquid fuel is injected at a very high pressure, as high as near 200MPa (see Figure 2-7); which is later converted to a corresponding high velocity, at near sonic speed, by the injector nozzle. The combination of common-rail solenoid-actuated fuel injection with the HIP has made the independent control of injection pressure, timing, volume of fuel and multi pulses of injection in a thermodynamic cycle (Satkoski et al., 2011). This advancement has led to appreciable reductions in emissions. Beside the reduction in emissions, for example particulate matter and nitrogen-oxides, there has been appreciable decrease in noise and fuel consumption as noted by Satkoski et al. (2011).

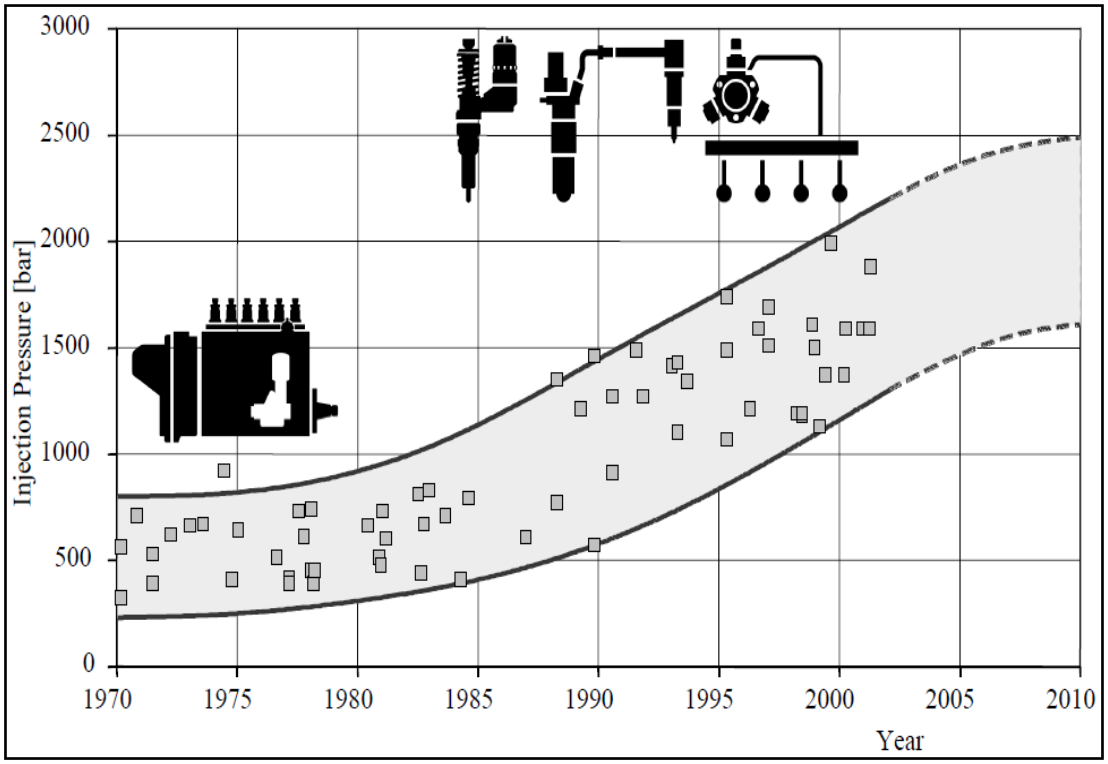

Figure 2-7 Trend of Injection Pressure for DDI engine (adapted from Mahr (2002))

The utilisation of multi-pulse injection means that the volume of liquid injected into the combustion chamber is split into a number of pulses, see Figure 2-8. The injection process starts with a pilot injection, which takes place earlier before the cylinder reaches the top dead centre and spreading it through to achieve a homogenous combustion mixture for an efficient and clean combustion. It should be noted, from Figure 2-8, that the multi-pulse injection is predominantly transient (changing velocities) as against the conventional injection.

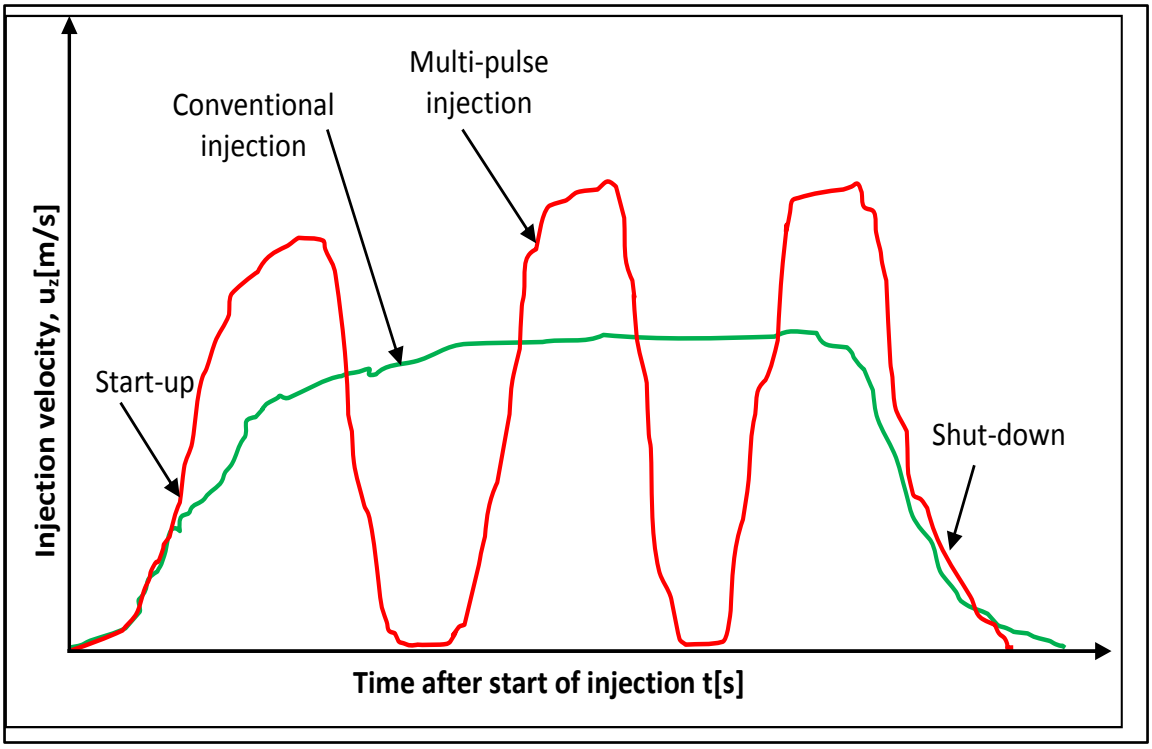

Figure 2-8 Velocity Evolution after Start of Injection for Convectional and Pulsed Injection

2.6 Summary and Knowledge Gap

The theory of jet instabilities has been developed under several assumptions, including the assumption that the jets are quasi-steady and isothermal (Reitz and Bracco, 1982; Radev et al., 2013). It has been stressed in Sazhin et al. (2011) that practical engineering spray systems are transient, which has been shown to have significant effects on the spray structure (Bae and Kang, 2006). It is expected that liquid fuel breakup mechanisms would be substantially affected by the transient effects, especially with the recent fuel injection technology, the pulsed-injection, which is highly transient in operation.

Sazhin et al. (2011) stressed the transient effects on liquid jet breakup by considering the jet acceleration in the classical instability model constants. Domann and Hardalupas (2004) suggested an interface tracking method; followed by the temporal and spatial evolution of all the disturbances on the surface of accelerated liquid jet, based on the assumption of wave packet. The theory of the wave packet analysis was advanced in Turner et al. (2012) CFD

code for the calculation of liquid breakup length. It is noted, however, that these approaches were built on the classical perturbation postulations, and that not all transient effects have been fully considered.

Absolute majority of available models treat liquid breakup mechanisms as an isothermal process, but in some practical spray systems, for example in combustion systems, liquid fuel is injected into an elevated ambient temperature, which may affect temperature dependent liquid properties (namely surface tension). The surface tension, which predominantly controls the interfacial surface breaking, is temperature dependent. It has been shown that the variety of liquid properties, such as surface tension, have a strong effect on atomisation spray performance (Chhetri and Watts, 2013). This suggests that non-isothermal effects may have a significant role to play in the breaking of interfacial surfaces.

The majority of CFD investigations of liquid breakup mechanism are built on classical instability models, which are complemented by semi-empirical relations (Kalaaji et al., 2003). Mechanistic models that complement CFD codes have not been fully exploited, seemingly because of the complexity surrounding the physics of liquid breakup. However, some important specific details of the breakup process can be achievable through the use of simplified basic mathematical models.

The sequence of processes in liquid-fuel fired internal combustion engines are fuel injection, breakup, evaporation and mixing of vapour with air, ignition and finally combustion. The intermediate process, the liquid-fuel breakup, has not been fully understood, because of experimental difficulties – associated with transient operation, high ambient temperatures and injection velocities, and near lack of access for optical measurement techniques in engines – and the mathematical complexity. Secondary breakup, which occurs after the primary breakup, involves the breakup of droplets induced by aerodynamic forces. The general assumption is that a droplet can be deformed without breaking up, if Weber (We) < 12 – 13 (Stiesch, 2010; Faeth, 2002). The general criterion for droplet breakup holds only for the laminar flow around the droplet; hence, the

breakup criterion may be changed considerably when a droplet is shot into a turbulent flow field, as the case for droplet instability and breakup in diesel sprays (Vuorinen et al., 2010). This expectation may be attributed to a wide range of dynamic forces due to the growing eddies (Vuorinen et al., 2010). There is inherent difficulty to experimentally and analytically capture all the phenomena of droplet breakup in a turbulent flow field.

Minimum breakup criterion for droplets has not been fully investigated for all flow fields. Moreover, there has been no consensus on droplet breakup criterion from CFD simulations of spray flows, especially in turbulent flow field, see Liao and Lucas (2009), Vuorinen et al. (2010) and Han et al. (2011) for a complete review. It is of importance, especially in diesel engines, where liquid fuel combustion is in the liquid droplet regime, to devise a simplified mathematical model for the critical Weber number, which would account for the turbulent effects.

Thus, some important physical behaviour, which might arise from the transient, non-isothermal spray and turbulent flow field, is not yet fully investigated. Both experimental and numerical data is therefore scarce on these phenomena, however, since its effects are expected to be significant, simplified basic analytical models, are developed in expectation to obtain some insight into the breakup processes of transient jet, non-isothermal jet and turbulent flow field sprays.

3 TRANSIENT LIQUID JET INSTABILITY AND BREAKUP MODEL

3.1 Background

Many of the combustion systems use either the pressure swirl (simplex) atomizers, or pre-filming air-blast atomizers, or plain orifice pressure atomizers for the breakup of bulk liquid fuel. The aim is to introduce the liquid fuel in a much higher surface area to volume ratio for a stable combustion process. The process surrounding the injection of liquid through a small aperture and the subsequent breakup of the bulk liquid may seem as a simple process, but the physics of spray formation has been proven to be complex (Eggers and Villermaux, 2008).

The most basic analytical tools for the investigation of liquid breakup are the Taylor Analogy Breakup (TAB) model, and the linear instability theory (Reitz and Bracco, 1982; Eggers and Villermaux, 2008; Sazhin et al., 2013). In the TAB model, the breakup is conceptualised as a spring–mass system; whereas the linear instability model, which is known as WAVE model (Reitz, 1987), uses the linear instability theory of small perturbation waves on the liquid–gas interface. The interaction between aerodynamic forces and the jet hydrodynamic forces induce surface waves, as shear flow, because of the relative velocity between the liquid phase and gas phase, see Figure 3-1. Absolute majority has acknowledged that the interaction of aerodynamic and hydrodynamic forces are the major controlling factors of the liquid jet breakup process (Turner et al., 2012; Radev et al., 2013), which the WAVE model is based on (Reitz, 1987).

The WAVE model is on the Kelvin-Helmholtz (KH) interfacial instability model for liquid breakup, which was suggested by Reitz and Bracco (1982) on the basis of surface waves formation as a result of hydrodynamic and aerodynamic forces interactions. The model is constructed on the basis of a first order linear analysis of a KH instability growing on the surface of a cylindrical liquid jet that is penetrating into a quiescent incompressible gas with a relative velocity. Both

the liquid and the gas are assumed to be incompressible, and the gas is assumed to be inviscid. The dynamics of the liquid jet and gas interaction are described by the linearization of conservation equations for two-phase flow; based on steady base flow parameters. The liquid phase is assumed as the disperse phase and the gas phase as the continuous phase. The detailed analysis, which can be found in Reitz and Bracco (1982) and Reitz (1987), yields a dispersion equation relating the growth rate of a perturbation to its wavelength. The dispersion equation obtained is not amenable to analytical solution; however, numerical curve fit was sought, which shows that there exists a single maximum in the wave growth rate curve and assumed that the maximum growth rate controls the liquid breakup. On this basis, numerous research works have been devoted to the development of interfacial instability models for liquid breakup.

The theory of jet instabilities has been developed under several assumptions, including the assumption of steady jet. However, in most practical engineering applications these jets are highly transient. The acceleration of the liquid during start-up is in order of 10^6 [m/s^2] at the orifice exit for high Reynolds numbers (Jarrahbashi and Sirignano, 2013). The common-rail diesel fuel injection systems utilising pulsed injection, as demonstrated in Figure 2-8, have drastically improved the ability to lower emissions, noise, and fuel consumption. However, with the application of the injection technique (the pulsed injection) in modern engines, the transient effects on jet instability and breakup need to be investigated. Sazhin et al. (2011) stressed the transient effects on liquid jet breakup by considering the jet acceleration in the classical instability model constants. Domann and Hardalupas (2004) suggested an interface tracking method; followed by the temporal and spatial evolution of all the disturbances on the surface of accelerated liquid jet, based on the assumption of wave packet. The theory of the wave packet analysis was advanced in Turner et al. (2012) CFD code for the calculation of liquid breakup length. However, the transient effects have never been fully considered.

3.2 Modelling

This section presents the modelling of the transient effects on the liquid jet instability and breakups by analytical means, which is based on the modification of the linear perturbation of the conservation equations that considers time-dependent base flow parameters.

3.2.1 Hydrodynamic Governing Equations and Assumptions

The assumption that the interaction between aerodynamic forces and the jet hydrodynamic forces induce surface waves, as shear flow, because of relative velocity between the liquid and gas, is adopted. Considering the assumptions made by Reitz and Bracco (1982), hence, one proceeds with the conservation equations. Figure 3-1 illustrates the free-surface shear, on the liquid jet on the basis of perturbed parameters, in 2D axisymmetric cylindrical material coordinate system.

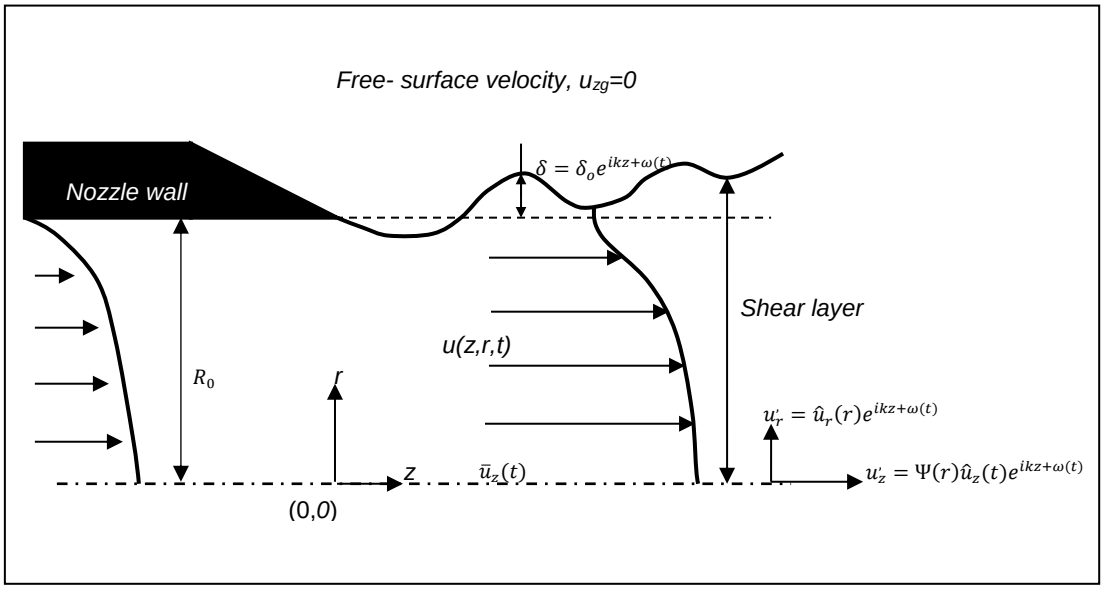

Figure 3-1 Free-surface Liquid Jet in 2D Cylindrical Material Coordinate System

The conservation equations for the 2D axisymmetric cylindrical material coordinate system(varicose deformation) – non-axisymmetric disturbances (sinusoidal deformation), $u_\theta = \partial/\partial\theta = 0$ can be taken as non-dominant since zero gas-to-liquid momentum ratio is here considered (Rangel and Sirignano, 1991) – are, therefore, obtained from Eqs(2-1)-(2-4) as follows:

The continuity equation

$$\frac{u_r}{r} + \frac{\partial u_r}{\partial r} + \frac{\partial u_z}{\partial z} = 0 \tag{3-1}$$

The momentum equation

r-direction momentum

$$\frac{\partial u_r}{\partial t} + u_r\left(\frac{\partial u_r}{\partial r}\right) + u_z\left(\frac{\partial u_r}{\partial z}\right) = -\frac{1}{\rho}\left(\frac{\partial p}{\partial r}\right) \tag{3-2}$$

z-direction momentum

$$\frac{\partial u_z}{\partial t} + u_r\left(\frac{\partial u_z}{\partial r}\right) + u_z\left(\frac{\partial u_z}{\partial z}\right) = -\frac{1}{\rho}\left(\frac{\partial p}{\partial z}\right) \tag{3-3}$$

where the r and z coordinates are the radial and axial coordinates, respectively, originating at the nozzle's tip centre (see Figure 3-1for the schematic description).

The governing equations are subject to the following three basic boundary conditions:

(i) To satisfy the kinematic boundary condition

$$u_{r=R_0} = \frac{\partial \delta}{\partial t} + u_z \frac{\partial \delta}{\partial z} \tag{3-4a}$$

(ii) To satisfy dynamic boundary condition at the liquid-gas interface

$$p_l - p_g = \sigma K; \text{ at } \quad r = R_0 + \delta \tag{3-4b}$$

with $K = div\,(\nabla G/|\nabla G|)$ where $G(r,z) = 0$ denotes the surface for which K has to be determined, it follows thus:

$$K = \frac{1}{R_0} - \frac{\delta}{R_0^2} - \frac{\partial^2 \delta}{\partial z^2} \equiv \frac{1 - \delta/R_0}{R_0} - \frac{\partial^2 \delta}{\partial z^2} \tag{3-4c}$$

where R_0 and δ denotes the unperturbed jet radius and surface perturbation, respectively.

(iii) To satisfy axisymmetric assumption (the varicose deformation)

$$\left.\frac{\partial u_r}{\partial r}\right|_{r=0} = 0 \qquad \text{(3-4d)}$$

The model is limited to the case of varicose deformation, which could be extended to include the sinusoidal deformation by superposition principle. However, the model sufficed for the case under consideration – zero gas-to-liquid momentum ratio.

Hydrodynamic assumptions

The theory of small perturbation decomposition is adopted (Reitz and Bracco, 1982). The perturbed parameters are represented as a sum of base, which are taken as time-dependent parameters, and perturbation values, thus, the linearization process follows by decomposing velocity, u, and pressure, p, as presented in Eqs (1-1a,b):

$$u_r = \bar{u}_r + u_r', \qquad \text{(3-5a)}$$

$$u_z = \bar{u}_z(t) + u_z' \qquad \text{(3-5b)}$$

and

$$p = \bar{p}(t) + p' \qquad \text{(3-5c)}$$

With Eqs (3-5a,b,c) been sufficient for the transient base parameters, it suffices to postulates that the initial amplitudes of transient parameters varies with time, thus, the perturbed parameters have the following forms, knowing that $n = 0$ in Eqs (2-6).

$$\delta = \delta_o e^{ikz+\omega(t)} \qquad \text{(3-6a)}$$

$$u_z' = \Psi(r)\hat{u}_z(t)e^{ikz+\omega(t)} \qquad \text{(3-6b)}$$

and

$$p' = \Psi(r)\hat{p}(t)e^{ikz+\omega(t)} \qquad \text{(3-6c)}$$

These linearized postulations are less restrictive than the ones postulated by the classical hydrodynamic stability theory. They also enable time dependency of perturbation to be non-linear, with the principle of separable variable still being maintained, and assume a different form for each parameter. Furthermore, the present postulation acknowledged the fact that a range of disturbances, wave packet (Turner et al., 2012), grow along the liquid-gas interface prior breakup (Domann and Hardalupas, 2004) as against a single wave postulation of the classical postulation. However, it is of the view that the wave with maximum growth rate, which may occur by self-growth or by constructive interference, controls the breakup according to the Reitz and Bracco (1982) assumption.

Jet's bulk velocity is simplified to be of a uniform axial velocity (no radial variation): $\frac{\partial \bar{u}_z}{\partial r} = 0$. As high speed jets with relatively moderate bulk velocity changes in time are considered, bulk radial velocity is assumed to be absent: $\bar{u}_r \approx 0$. Products of perturbed parameters are relatively too small, hence, neglected: $u_i' \frac{\partial u_i'}{\partial i} = u_i' \frac{\partial u_j'}{\partial i} \approx 0; i, j = r, z$.

3.3 Hydrodynamic analysis

The analysis follows by substituting the linearized parameters, Eqs (3-5a,b,c), into the conservation equations, Eqs (1-1a,b) through (1-3a,b,d); making use of the assumptions; subtracting the (continuity and momentum) equations for the non-perturbed parameters – momentum equations hold for both perturbed and unperturbed flows – and neglecting second order terms. Then the following equations are obtained for the perturbed continuity equation, r-direction and z-direction momentum equations, respectively, as:

$$\frac{u_r'}{r} + \frac{\partial u_r'}{\partial r} + \frac{\partial u_z'}{\partial z} = 0 \tag{3-7}$$

$$\frac{\partial u_r'}{\partial t} = -\frac{1}{\rho}\frac{\partial p'}{\partial r}, \tag{3-8}$$

and

$$\frac{\partial u_z'}{\partial t} + \bar{u}_z \frac{\partial u_z'}{\partial z} = -\frac{1}{\rho}\frac{\partial p'}{\partial z} \tag{3-9}$$

3.4 Analytical Formulation

Operating $\frac{1}{r}\frac{\partial}{\partial r}[r(\,)]$ and $\frac{\partial(\,)}{\partial z}$ on Eqs (3-8) and (3-7), respectively, gives

$$\frac{1}{r}\frac{\partial u_r'}{\partial t} + \frac{\partial^2 u_r'}{\partial r \partial t} + \frac{\partial^2 u_z'}{\partial z \partial t} + \bar{u}_z \frac{\partial^2 u_z'}{\partial z^2} = -\frac{1}{\rho r}\frac{\partial p'}{\partial r} - \frac{1}{\rho}\frac{\partial^2 p'}{\partial r^2} - \frac{1}{\rho}\frac{\partial^2 p'}{\partial z^2} \tag{3-10}$$

Differentiating Eq.(3-7) with respect to time (t) gives:

$$\frac{1}{r}\frac{\partial u_r'}{\partial t} + \frac{\partial^2 u_r'}{\partial r \partial t} + \frac{\partial^2 u_z'}{\partial z \partial t} = 0 \tag{3-11}$$

Substituting Eq.(3-11) into Eq.(3-10) and using Eqs (3-6b,c) in the resulting equation gives:

$$r^2\frac{\partial^2 \Psi}{\partial r^2} + r\frac{\partial \Psi}{\partial r} - k^2 r^2\left(1 + \frac{\rho \bar{u}_z \hat{u}_z}{\hat{p}}\right)\Psi = 0 \tag{3-12}$$

It is here suggested that $\hat{p} \gg \rho \bar{u}_z \hat{u}_z$, since pressure has a relatively high order of magnitude in comparison with the velocity in High-Injection-Pressure (HIP) systems, for the transient liquid injection breakup processes, thus, Eq.(3-12) becomes:

$$r^2\frac{\partial^2 \Psi}{\partial r^2} + r\frac{\partial \Psi}{\partial r} - k^2 r^2 \Psi = 0 \tag{3-13}$$

The two independent solutions of Eq.(3-13), second-order linear differential equation, are $I_0(kr)$ and $K_0(kr)$; where I_0 and K_0 are the modified zero-order Bessel function of the first and second kinds, respectively. However, boundary conditions dictate that, for the liquid phase side, $r \to 0$, $I_0(kr)$ is bounded; in converse, $K_0(kr)$ is bounded in the gas phase, $r \to \infty$, thus:

$$\Psi_l = \mathrm{A} I_0(kr) \tag{3-14}$$

and

$$\Psi_g = BK_0(kr); \tag{3-15}$$

where l and g stand for liquid phase and gas phase, respectively.

Integrate Eq.(3-7) to obtain:

$$u_r' = -\frac{1}{r}\int r\frac{\partial u_z'}{\partial z}dr \tag{3-16}$$

Using Eq.(3-14) in Eq.(3-6b); eliminating integration constants (A and B) by utilising Eq.(3-4c); substituting the resulting equation into the integral, Eq.(3-16); thereafter, considering the kinematic boundary condition – that is, Eq.(3-4a) – in the perturbed form, for the liquid and gas phases; and finally, substituting the resulting equation into Eq.(3-6b) give

$$u_{zl}' = \frac{\delta_0 I_0(kr)}{I_1(kR_o)}\left[i\frac{d\omega(t)}{dt} - k\bar{u}_{zl}(t)\right]e^{ikz+\omega(t)} \tag{3-17a}$$

and

$$u_{zg}' = -\frac{\delta_0 K_0(kr)}{K_1(kR_o)}\left[i\frac{d\omega(t)}{dt} - k\bar{u}_{zg}(t)\right]e^{ikz+\omega(t)} \tag{3-17b}$$

On the dynamic boundary condition, Eq.(3-4c); after substituting the linearized parameters, and noting that $\left(\bar{p}_l - \bar{p}_g\right)\big|_{r=R_0} = \frac{\sigma}{R_0}$, gives the perturbed dynamic boundary condition as:

$$p_l' - p_g' = \sigma\delta_o\left(k^2 - \frac{1}{R_0^2}\right)e^{ikz+\omega(t)} \tag{3-18}$$

Using Eqs (3-17a,b) in Eq.(3-9) subtracting the resulting equation for the liquid phase from that of the gas phase; and, thereafter, taking $\bar{u}_{zg} = 0$, for a quiescent ambient, and prescribing all parameters at $r = R_o$ give the dispersion equation as:

$$\left(\frac{I_0(kR_o)}{I_1(kR_o)}\rho_l + \frac{K_0(kR_o)}{K_1(kR_o)}\rho_g\right)\left[\frac{d^2\omega(t)}{dt^2} + \left(\frac{d\omega(t)}{dt}\right)^2\right]$$
$$+ \frac{I_0(kR_o)}{I_1(kR_o)}\rho_l\left[2ik\bar{u}_z(t)\frac{d\omega(t)}{dt} + ik\frac{d\bar{u}_z(t)}{dt} - k^2\bar{u}_z^2(t)\right] \quad (3\text{-}19)$$
$$+ \sigma k\left(k^2 - \frac{1}{R_0^2}\right) = 0$$

In spraying, short wave in comparison with the jet radius, R_o, are expected, thus, for $kR_o \to \infty$ approximation can be made as:

$$\frac{K_0(kR_o)}{K_1(kR_o)} \approx 1; \frac{I_0(kR_o)}{I_1(kR_o)} \approx 1 \quad (3\text{-}20a,b)$$

Using this pertinent approximation, Eqs(3-20a,b), hence the dispersion equation, Eq.(3-19), is simplified to give:

$$\left(\rho_l + \rho_g\right)\left[\frac{d^2\omega(t)}{dt^2} + \left(\frac{d\omega(t)}{dt}\right)^2\right]$$
$$+ \rho_l\left[2ik\bar{u}_z(t)\frac{d\omega(t)}{dt} + ik\frac{d\bar{u}_z(t)}{dt} - k^2\bar{u}_z^2(t)\right] \quad (3\text{-}21)$$
$$+ \sigma k\left(k^2 - \frac{1}{R_0^2}\right) = 0$$

It is assumed that the disturbance growth rate is approximately constant, $\frac{d\omega(t)}{dt} \approx const.$; and that the base velocity rate change is the jet acceleration, hence, $\frac{d^2\omega(t)}{dt^2} = 0$ and $\frac{d\bar{u}_z(t)}{dt} = a[m/s^2]$. With these assumptions, Eq.(3-21) is rearranged to give:

$$\frac{d\omega(t)}{dt} = \frac{-ik\rho_l\rho_g\bar{u}_z(t)}{\left(\rho_l + \rho_g\right)}$$
$$\pm\frac{\left(k\rho_l\rho_g\,\bar{u}_z^2(t) - \left(\rho_l + \rho_g\right)k\sigma\left(k^2 - \frac{1}{R_o^2}\right) - i\left(\rho_l + \rho_g\right)\rho_l ka\right)^{1/2}}{\left(\rho_l + \rho_g\right)} \quad (3\text{-}22)$$

Interest is on the real part of the dispersion equation, $Re\left(\frac{d\omega(t)}{dt}\right) \equiv \omega'[1/s]$; in the frame of temporal analysis, Eq.(3-23) is obtained, after a considerable algebraic exercise and rearrangement, as:

$$\omega' = \frac{(2^{-1}k)^{1/2}}{(\rho_l + \rho_g)}\left(\left(\left[\rho_l\rho_g\,\overline{u}_z^2(t) - (\rho_l + \rho_g)\sigma\left(k^2 - \frac{1}{R_o^2}\right)\right]^2 + \left[(\rho_l + \rho_g)\rho_l a\right]^2\right)^{1/2} + \rho_l\rho_g\,\overline{u}_z^2(t) - (\rho_l + \rho_g)\sigma\left(k^2 - \frac{1}{R_o^2}\right)\right)^{1/2} \quad (3\text{-}23)$$

The plots of Eq.(3-23) for constant axial velocities (50, 350 m/s) show that there exist maxima growth rate, as shown in Figure 3-2. The figure, also, indicates that increasing the injection velocity increases the disturbance growth rate as a result of increased relative velocity. This exemplifies the classical liquid jet breakup theory (Lefebvre, 1989). Furthermore, it is observed from the figure that increasing the acceleration widen the spectrum, which could be used to describe droplet distribution, with higher breakup rate, which confirms the description of experimental results in Domann and Hardalupas (2004). The dominant or the liquid breakup controlling wavenumber, k_{opt}, which corresponds to the maximum growth rate, $\omega'_{max}\,[1/s]$, is expected to occur at $\frac{dRe(\omega')}{dk} = 0$ (Reitz and Bracco, 1982).

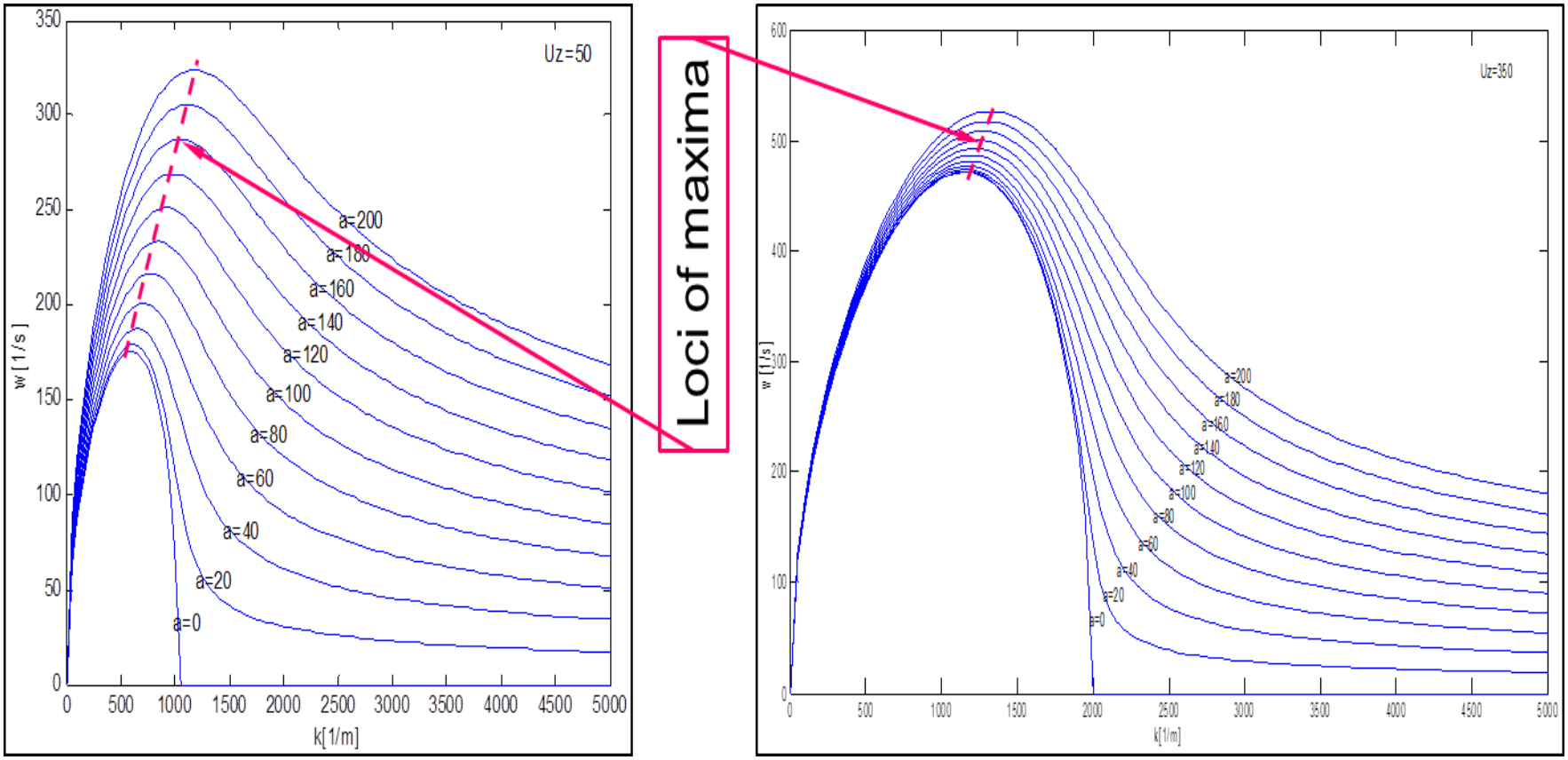

(a) Constant velocity of 50m/s ***(b) Constant velocity of 350m/s***

Figure 3-2 Variation of growth rate, ω'[1/s] with wavenumber, k[1/m] and jet acceleration, a[m/s^2] at constant velocities

The breakup controlling wavenumber and the corresponding growth rate are, therefore, given, respectively, as

$$k_{opt} = \left(\frac{\left(4\left[\rho_l \rho_g \, \overline{u}_z^2(t) + \frac{\sigma}{R_o^2}(\rho_l + \rho_g) \right]^2 + 3\left[(\rho_l + \rho_g)\rho_l a \right]^2 \right)^{1/2}}{3\sigma(\rho_l + \rho_g)} - \frac{\left[\rho_l \rho_g \, \overline{u}_z^2(t) + \frac{\sigma}{R_o^2}(\rho_l + \rho_g) \right]}{3\sigma(\rho_l + \rho_g)} \right)^{1/2} \tag{3-24}$$

and

$$\omega_{max}^{'} = \left(\frac{\left(\left[k_{opt}\rho_l \rho_g \, \overline{u}_z^2(t) - \left(\rho_l + \rho_g \right) \sigma k_{opt} \left(k_{opt}^2 - \frac{1}{R_o^2} \right) \right]^2 + \left[\left(\rho_l + \rho_g \right) \rho_l k_{opt} a \right]^2 \right)^{1/2}}{2\left(\rho_l + \rho_g \right)^2} + \frac{k_{opt}\rho_l \rho_g \, \overline{u}_z^2(t)}{2\left(\rho_l + \rho_g \right)^2} - \frac{\left(\rho_l + \rho_g \right) \sigma k_{opt} \left(k_{opt}^2 - \frac{1}{R_o^2} \right)}{2\left(\rho_l + \rho_g \right)^2} \right)^{1/2} \tag{3-25}$$

The interfacial instability model here developed accounts for transient effects, velocity and acceleration, of liquid jet breakup. It is expected that the wave with the highest growth rate, $\omega'_{max} = f(t)$, will finally be sheared off the jet and form droplets; this argument still holds even with the theory of wave packet advanced in Turner et al. (2012), since it is here argued that the critical wave (on the basis of maximum growth rate), which result from self-growing or constructive wave interference, controls the breakup. It is worth noting that the liquid breakup is insensitive to acceleration sign, as can be seen in Eqs(3-24) and (3-25); this implies that acceleration and deceleration may have the same breakup phenomena, which are expected to occur at the start-up and short-down of most injector operations, respectively.

Mainly, the spray angle and penetration length have been identified as pertinent macro parameters whereas the breakup length and breakup time as the pertinent micro parameters for the understanding of the atomisation and spray

processes in ICEs. Hence, one proceeds to seek macro models for these parameters as follow.

The relation for the half spray angle, $\theta/2$, in Trinh and Chen (2006) as proposed by Reitz and Bracco (1982) sufficed:

$$\tan\theta/2 = \Omega\frac{\Lambda\omega'_{max}}{\bar{u}_z} \tag{3-26}$$

where $\Omega[-]$ is a constant that accounts for the nozzle entrance shape, which must be fitted experimentally (Reitz and Bracco, 1982), and $\Lambda = 2\pi/k_{opt}[m]$ is the optimum wavelength.

The spray angle can also be obtained by geometrical consideration – approximating the half of the spray as an isosceles triangle with the height being the half penetration length (Naber and Siebers, 1996; Payri et al., 2012), as follows:

$$\tan\theta/2 = \frac{A}{(L_p/2)^2} \tag{3-27}$$

where $A\ [m^2]$ is the upstream half image projected spray area and $L_p[m]$ is the spray penetration length.

The penetration length is, thus, obtained, with consideration of Eq.(3-26), as:

$$L_p = \gamma\sqrt{\frac{\bar{u}_z}{\Lambda\omega'_{max}}} \tag{3-28}$$

where $\gamma[m] \equiv 2(A/\Omega)^{1/2}$

Forstall and Shapiro (1950) proposed a relation, as presented in Karimi (2007), between the spray penetration length and breakup length on mass and momentum balance; given as:

$$L(\bar{u}_p - \bar{u}_g) = L_{bu}(\bar{u}_z - \bar{u}_g) \tag{3-29}$$

where $\bar{u}_p[m/s]$ is the tip penetration velocity, $\bar{u}_g[m/s]$ is the ambient gas velocity and $L_{bu}[m]$ is the breakup length.

For a quiescent ambient gas, $\bar{u}_g = 0$.Then, taking $\bar{u}_p \approx \frac{dL}{dt}$; considering Eq.(3-29) and separating variables to give:

$$L_{bu} = \int_0^{L_p} L\, dL / \int_0^t \bar{u}_z(t)dt \tag{3-30}$$

It is assumed that $\int_0^t \bar{u}_z(t)dt \approx \kappa \bar{u}_z t$, where κ is an integration fit parameter; therefore, solving for L_{bu} by considering Eq.(3-28) gives:

$$L_{bu} = \frac{\beta}{\Lambda \omega'_{max} t} \tag{3-31}$$

where $\beta[m^2] \equiv \gamma^2/2\kappa$. The parameters Ω, κ and A are experimentally fitted.

3.5 Model Validation

Experimental data presented in Karimi et al. (2006) and Karimi (2007), for a 3 hole 0.2 mm diameter valve covered orifice (VCO) diesel injector at different injection pressures (60, 100, 140, 160 MPa), were used for the validation of the developed transient instability model. Karimi (2007) presented experimental data for discharge coefficient, $C_d(t)$, and instantaneous change in pressure, Δp_{inj}, for the four injection pressures. The injection velocity is here computed by utilizing the relation: $\bar{u}_z(t) = C_d(t)\sqrt{2\Delta p_{inj}/\rho_l}$. The curve fit suggested by Turner et al. (2012) for diesel injectors, $\bar{u}_z(t) = \alpha \tanh(\beta t)$, is here adopted to fit the Karimi (2007) experimental data; where α and β are the curve fit parameters, which depend on injection and back pressures. With these relations, the jet acceleration is computed accordingly: $a(t) \equiv d\bar{u}_z/dt = \alpha\beta[1 - \tanh^2(\beta t)]$. Figure 3-3 shows the Karimi (2007) constructed experimental data (dot) and the curve fits (line) for the various injection pressures.

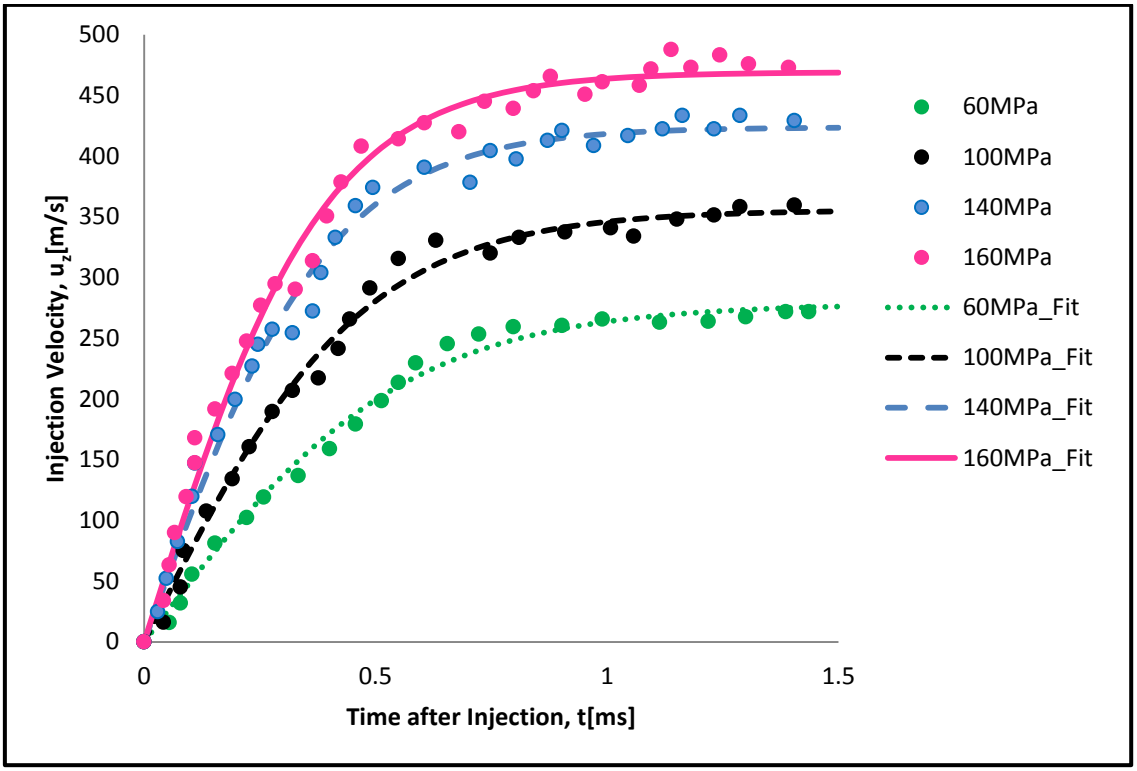

Figure 3-3 Constructed Injection Velocity from Experimental Data

Figure 3-4 shows the model prediction (line) and experimental (dot) spray angle data for transient fuel injection. The figure shows that there is a good agreement between the model predicted results and the experimental data. The spray angle is observed to be very high at the initial start of injection and later settled for a value around 17^{o} during the steady fuel injection. It is observed that the 60 [MPa] injection pressure has a wider spray angle compared to higher injection pressures. This observation may be attributed to the initial low penetration velocity into dense ambient, which requires more time to adjust to the surrounding gases, hence less constrained to expand. The significant difference in the spray angle in the accelerating region, 0-0.5 [ms] after the start of injection, and the steady region shows that the transient effects have a significant role on the liquid fuel breakup.

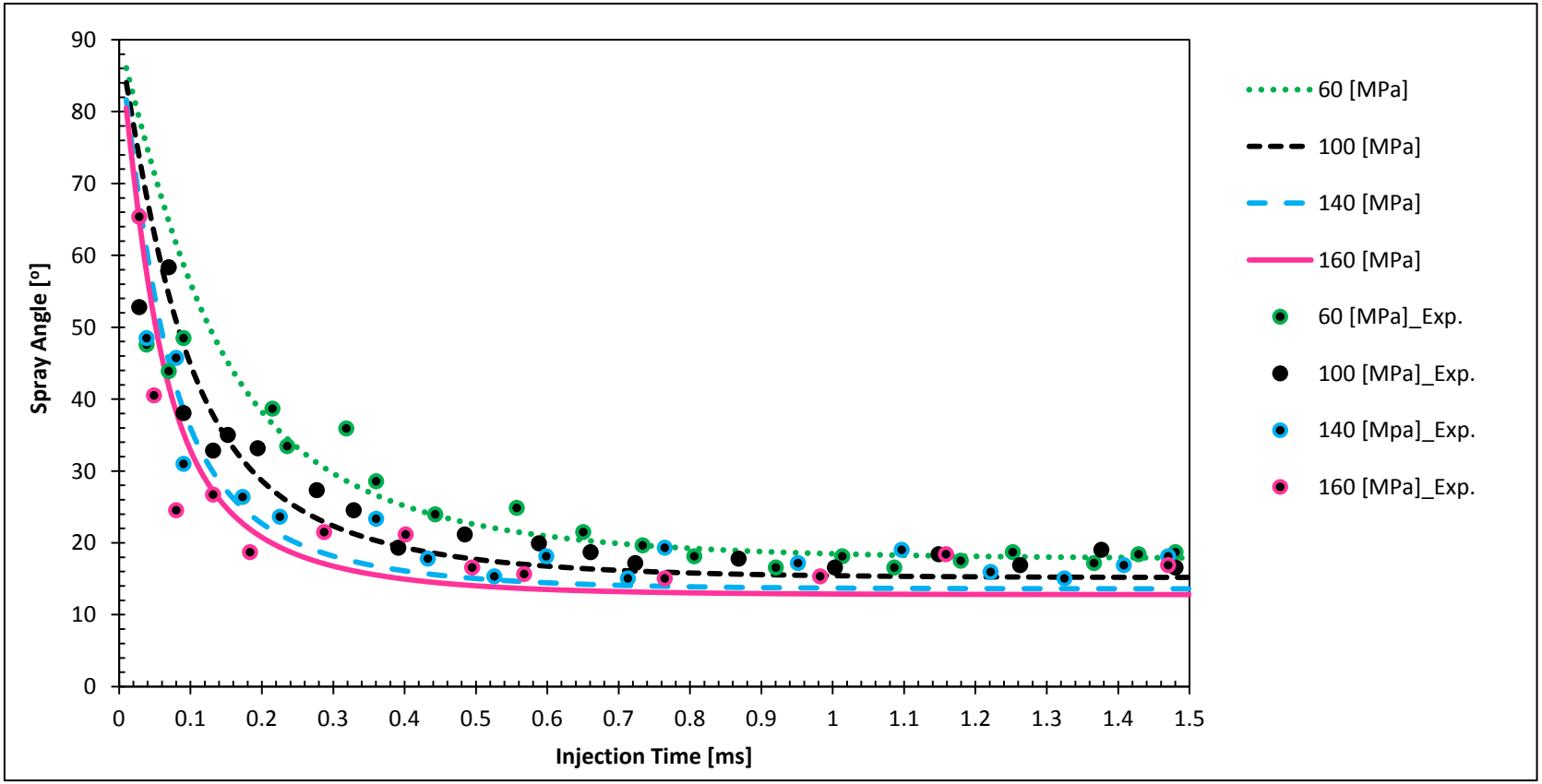

Figure 3-4 Variation Spray Angle with the Time after Start of Injection in an Ambient of Density 47 [kg/m^3] at various Injection Pressures

Figure 3-5 shows the transient breakup length at various injection pressures in an ambient density of 47 [kg/m^3]. It is observed from the figure that there is an appreciable agreement between predicted breakup length and experimentally obtained breakup length (Karimi, 2007); but it seems to be relatively poor in the steady state region. The poor prediction of the breakup model may be attributed partly to the indirect approach used in the determination of the experimental breakup length in Karimi (2007) and the approximation of the velocity integral used. Nevertheless, the predicted results are acceptable for investigation purposes considering negligible computational time investment, less than 1 minute, as compared to CFD simulation, which may take 100s of hours of time investment. It is also observed that the reduction in the breakup length with time after injection is more rapid as the injection pressure increases, which corresponds to increase in acceleration rate.

The reduction in breakup length may also be attributed to increased jet acceleration, since there is rapid increase in injection velocity. This observation is in agreement with Turner et al. (2012) and other researchers in the field (Domann and Hardalupas, 2004). The observation suggests that using the classical liquid jet breakup model (WAVE model), which does not account for transient effects (e.g acceleration), poor prediction of pertinent spray parameters, required for combustor design, may be significant. Most importantly, the poor prediction in jet breakup parameters would be more significant during the start of injection where acceleration is dominant, in the order of 10^6 [m/s^2] (Jarrahbashi and Sirignano, 2013). It suffices to say that poor prediction of some experimental jet breakup data, even up to 50%, as noted in Sazhin et al. (2008), by computational fluid dynamics (CFD) software may be strongly tied to the failure of the consideration of transient effects in the classical WAVE model.

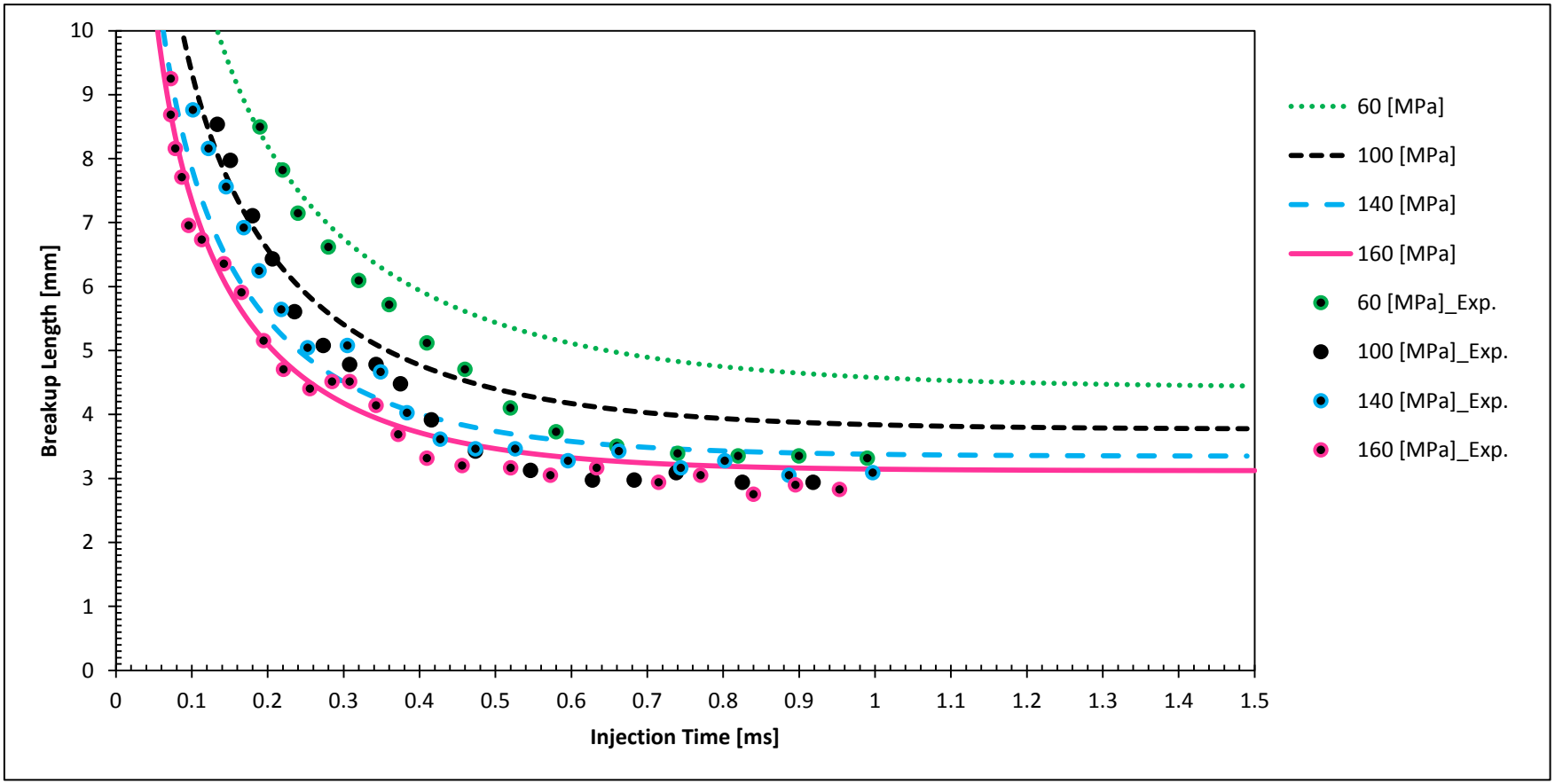

Figure 3-5 Transient Breakup Length at various Injection Pressures in an Ambient of Density 47[kg/m^3]

Figure 3-6 shows the variation of penetration length with injection time at various injection pressures in an ambient density of 47 [kg/m^3]. Figure 3-6 shows that there exists an agreement between transient KH instability model and the experimentally obtained penetration length in Karimi (2007). Critical observation of the figure shows that there exists a maximum in the predicted penetration length by the analytical instability model. This observation is in conformity with majority of experimental data presented in the literature (Ming et al., 2012). In terms of the injection pressure, it is observed that the liquid penetration reached the maximum value much faster with elevated injection pressure due to the higher jet velocity, which rapidly induces instability and breakup.

Figure 3-4 through Figure 3-6 show that there exist plausible agreements between the transient KH instability model and the experimentally obtained data for spray angle, breakup length and penetration length. However, better agreements are seen at higher injection pressures. It is hypothesised that the better agreement at higher injection pressures may be due to the increased dominancy of acceleration related instabilities at higher pressures, over other secondary phenomena that may exist, which are not accounted for in this model (as opposed to acceleration and velocity related instabilities).

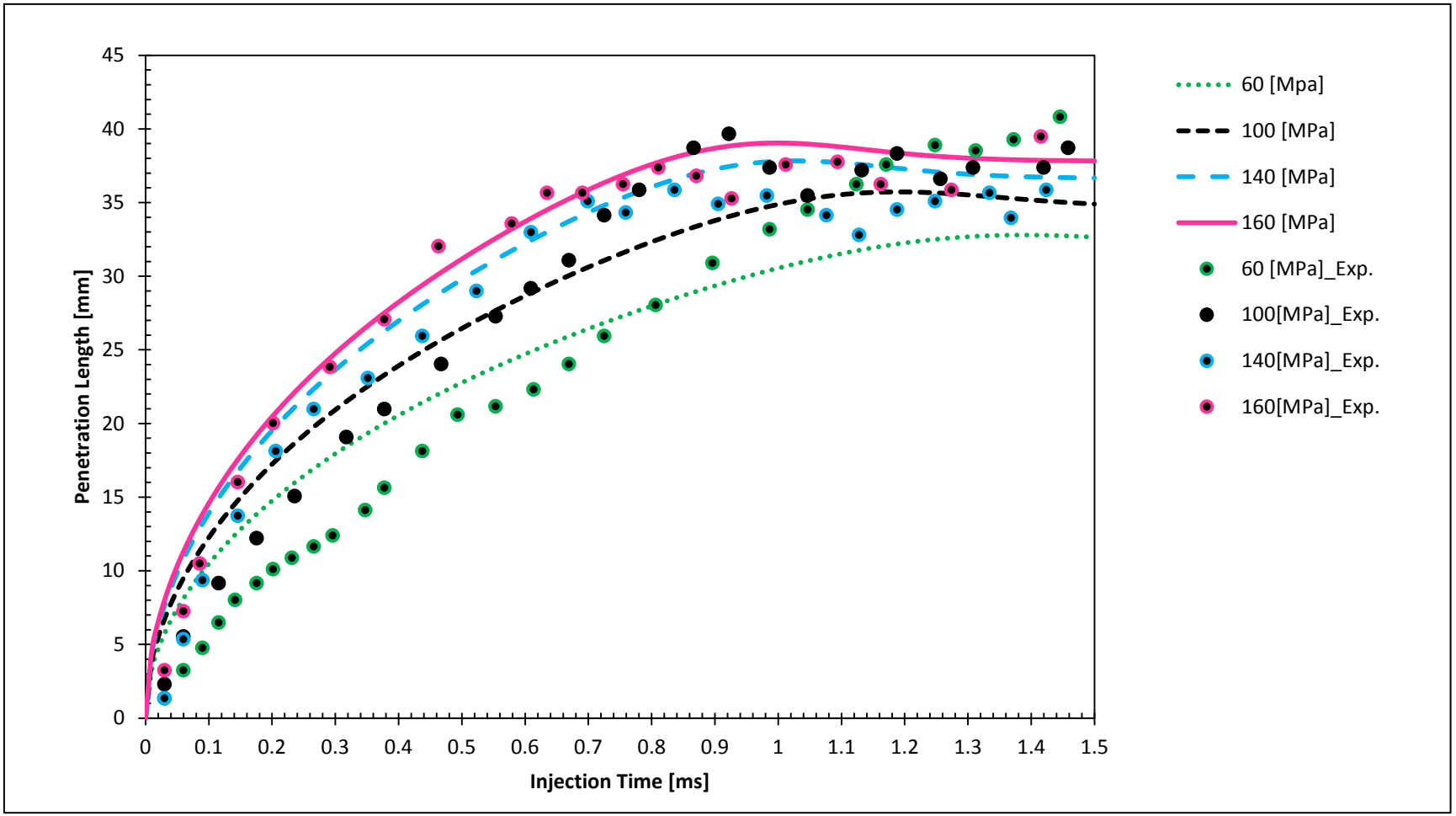

Figure 3-6 Penetration Length at various Injection Pressures in an Ambient of Density

3.6 Steady Jet Approximation

For a steady jet: $\bar{u}_z = const.$, and hence: $\frac{d\bar{u}_z(t)}{dt} = 0$, which is a special case of a transient jet. Therefore, for this case, Eq.(3-24) is simplified to:

$$\frac{d\omega(t)}{dt} = \frac{-ik\rho_l\rho_g\bar{u}_z(t) \pm \left(k\rho_l\rho_g\,\bar{u}_z^2(t) - (\rho_l+\rho_g)k\sigma\left(k^2 - \frac{1}{R_o^2}\right)\right)^{1/2}}{(\rho_l+\rho_g)} \tag{3-32}$$

The breakup controlling wave is expected to be the maximum growth rate, to occur at: $\frac{\partial Re(\omega)}{\partial k} = 0$. Hence, solving Eq.(3-32) for the breakup controlling wavenumber gives:

$$k_{opt} = \frac{\bar{u}_z^2 + \left\{\bar{u}_z^4 - \left(\sigma\frac{(\rho_l+\rho_g)}{\rho_l\rho_g}\right)^2\frac{3}{R_o^2}\right\}^{1/2}}{\frac{3(\rho_l+\rho_g)\sigma}{\rho_l\rho_g}} \tag{3-33}$$

For expected shortwave assumption, that is $kR_o \gg 1$, in Eq.(3-32), therefore, the breakup controlling wavenumber is obtained as:

$$k_{opt} = \frac{2}{3}\frac{\bar{u}_z^2}{\sigma}\frac{\rho_l\rho_g}{(\rho_l+\rho_g)} \tag{3-34}$$

Eq.(3-34) is synonymous to Eq.(124) of Eggers and Villermaux (2008), even with the different analysis approach.

In the case of a dripping flow, $\bar{u}_z \approx 0$, one gets, from Eq.(3-33), the breakup controlling wavenumber as:

$$k_{opt} = \frac{1}{\sqrt{3}R_o} \tag{3-35}$$

Eq.(3-35) gives the Rayleigh mode, which is numerically obtained as $k_{bu} = 0.70/R_o$ in Tjahjadi et al. (1992). The slight difference between Eq.(3-35) and the numerical solution may be attributed to the numerical approximations adopted in Tjahjadi et al. (1992).

3.7 Conclusion of Chapter Three

The theory of jet instabilities has been developed under several assumptions, which include the assumption that the jets are steady. However, practical fuel injectors' operations are normally transient; these transient operations will be dominant in most of the contemporary injection techniques utilised in the internal combustion engines, e.g the pulse injection that is known for better fuel economy and emission reduction. The steady jets assumption has been attributed to some of the deviations observed between theoretical predictions and experimental data. Therefore, this section has presented a new instability and breakup model for transient liquid jet, which considers the jet instantaneous velocity and acceleration. The model was developed from the conservation equations for two-phase flow, on the classical interfacial breakup theory, by the modification of the linear perturbation processes that consider time-dependent base flow parameters. The analytical model accounts for the transient effects on liquid jet breakup; with results obtained by the model being having a good agreement with experimentally obtained data for penetration length, breakup length and spray angle. The model is shown to maintain the plausibility of investigating liquid jet breakup mechanisms under accelerating conditions, which are dominant in modern practical fuel injection techniques.

4 NON-ISOTHERMAL LIQUID JET INSTABILITY AND BREAKUP MODEL

4.1 Background

The theory of liquid jet instabilities has been developed under several assumptions, which include the assumption that the jets breakup processes are isothermal. Liquid fuels are normally injected into an elevated combustion-chamber temperature to maintain a desirable homogeneous combustible mixture – liquid vapour and air. The Liquid fuels injected are inherently unstable and breakup to form droplets. The jet breakup may be induced by cavitation, turbulence, hydrodynamic and aerodynamic forces interactions and variation in fluid properties. Numerous research have been devoted to extensive study of some of the effects that cause jet instability and breakup (Sirignano and Mehring, 2001). It has been shown that the variety of liquid properties, such as surface tension, have a strong effect on atomisation spray performance (Chhetri and Watts, 2013).

However, the particular effects of non-isothermal conditions, through spatial variations of surface tension, on jet instability and breakup, have not been fully studied yet; despite their practical relevance in liquid fuel spray and combustion. Specifically, heat is transferred from the combustion-chamber gases to the liquid jet and carried downstream by the jet velocity, which gives rise to a transient spatially variation of surface tension (i.e. surface tension gradient) along the liquid-gas interface. This suggests that non-isothermal effects may have a significant role to play in the breaking of interfacial surfaces, since the surface tension predominantly controls interfacial breakup, in most breakup regimes. This may be expected to be significant in all atomisation mechanisms: primary and secondary.

Effect of surface tension variation on ink jet instability and breakup has been investigated by (Furlani, 2005) for a periodic heat source with relatively low excess temperatures, and low jet speeds. Hence, applicability to combustor environments may be limited.

In the preceding chapter, Chapter 3, the particular effects of unsteady jet have been addressed; therefore, in this present Chapter, a new linear theory model, on the KH instability is presented for non-isothermal conditions. The model is for the instability and breakup of largely non-isothermal liquid jets, with consideration of a spatially variation of surface tension along the liquid-gas interface. The spatial variation of surface tension is obtained through temperature-dependent surface tension and transient heat-transfer from the combusting gases to the liquid jet. The classical interfacial hydrodynamic breakup theory and the solution of heat-transfer in a semi-infinite medium are coupled through the surface tension gradient. The analytical model accounts for the non-isothermal effects on jet breakup. In-depth understanding of the non-isothermal effects on liquid jet breakup could pave way for the development of the next generation atomiser for better fuel efficiency and reduction in pollutant emissions from internal combustion engines.

Though the research problem has been partly considered for internal combustion engines in Payri et al. (2013) and Som & Aggarwal (2010) works, however, the approach presented here is original and unique in that: is devoted to primary breakup; analytical formulation of the dispersion equation; coupling heat transfer in the analysis; and no recourse to CFD applications as computations are done in MATLAB® programming environment, interface with Microsoft Excel® spreadsheet, with a negligible computation cost.

4.2 Mathematical Modelling

This section presents the modelling of the non-isothermal condition on the liquid jet instability and breakups by analytical means, which is based on the modification of the dynamic boundary condition, to include the spatial variation of surface tension.

4.2.1 Hydrodynamic Equations

The mathematical model describes wave growth at the interface, due to relative velocity between liquid and gas and surface tension variation due to temperature variation, as depicted in Figure 4-1.

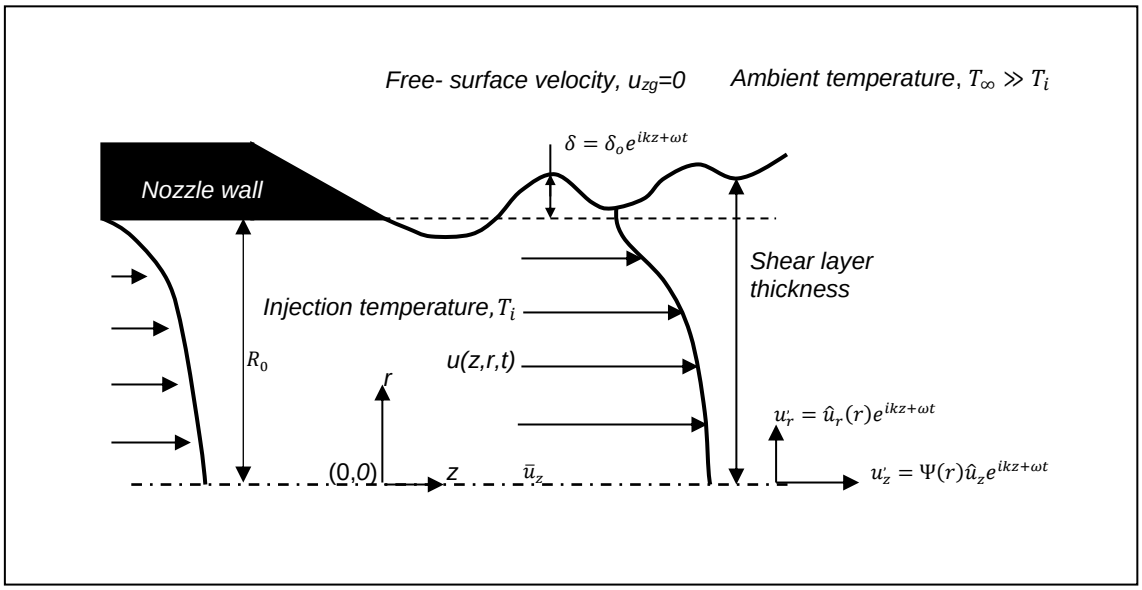

Figure 4-1 Free-surface Liquid Jet in 2D Cylindrical Material Coordinate System

The governing equations presented for the 2D cylindrical material coordinate system, maintaining the basic assumptions of (Reitz and Bracco, 1982), in §3.2.1 are appropriate. It is intended not to rewrite these equations here – interested readers should see Eqs (3-1)-(3-3) and (3-4a,d). However, the dynamic boundary condition at the liquid-gas interface, Eq.(3-4b), is presented as follows:

To satisfy dynamic boundary condition at the liquid-gas interface, considering spatial (axial) variation of surface tension as a result of surface temperature variation, thus

$$p_l - p_g = \sigma(z)K; \text{ at } \quad r = R_0 + \delta \tag{4-1a}$$

with $K = div\,(\nabla G/|\nabla G|)$ where $G(r,z) = 0$ denotes the surface for which K has to be determined, it follows thus:

$$K = \frac{1}{R_0} - \frac{\delta}{R_0^2} - \frac{\partial^2 \delta}{\partial z^2} \equiv \frac{1 - \delta/R_0}{R_0} - \frac{\partial^2 \delta}{\partial z^2} \tag{4-1b}$$

where R_0 and δ denotes the unperturbed jet radius and surface perturbation, respectively.

4.2.2 Hydrodynamic Assumptions

The theory of small perturbation decomposition is adopted (Reitz and Bracco, 1982). The perturbed parameters are represented as a sum of base and perturbation values, thus, the linearization process follows by decomposing velocity, u, and pressure, p, as stated in Eqs (1-1a,b).

With Eqs (1-1a,b) being sufficient, thus, the perturbed parameters are defined to take the following forms, after taking $n = 0$ and $u_\theta = \partial/\partial\theta = 0$ in Eqs (1-2a,b,c,d),

$$\delta = \delta_o e^{ikz+\omega t} \tag{4-2a}$$

$$u_z' = \Psi(r)\hat{u}_z e^{ikz+\omega t} \tag{4-2b}$$

and

$$p' = \Psi(r)\hat{p} e^{ikz+\omega t} \tag{4-2c}$$

It is assumed that radial variation of the jet's bulk velocity (base velocity) is negligible, thus, the jet's bulk velocity is simplified to be of a uniform axial velocity, $\partial\bar{u}_z/\partial r = 0$. Also, for a relatively high liquid injection speed, the bulk radial velocity is assumed to be relatively small, $\bar{u}_r \approx 0$.

4.2.3 Heat Transfer Equations

The liquid jet, which is suddenly exposed to an elevated ambient temperature, see Figure 4-1, could be described by heat conduction into a semi-infinite medium model, with the assumption that thermal radiation is negligible. Hence, the heat transfer governing equation is

$$\frac{1}{\alpha}\frac{\partial T}{\partial t} = \frac{\partial^2 T}{\partial r^2} \tag{4-3}$$

With the initial and boundary conditions given as:

$$T(r,0) = T_i \tag{4-4a}$$

$$T(\infty,t) = T_i, \tag{4-4b}$$

and

$$-k_g \frac{\partial T}{\partial r}\Big|_0 = \bar{h}\big(T_\infty - T(0,t)\big) \tag{4-4c}$$

In these expressions k is the thermal conductivity (g and l stand for gas and liquid, respectively), $\alpha \equiv k_l/\rho c_p$ is the thermal diffusivity, c_p is specific heat capacity, T_i is the initial temperature, T_∞ is the ambient temperature and $\bar{h}$ is the mean convection coefficient, where the approximations for the $\bar{h}$ is heavily dependent on the gas phase parameters and dynamics, which is estimated through the Nusselt number, $\bar{N} \equiv 2\bar{h}R_0/k_g$. However, the Nusselt number can be assumed as a steady parameter, which is universally accepted in most heat transfer analyses. Therefore, $\bar{N} = 0.26Re^{0.6}Pr^{0.36}$, with $Re \equiv \frac{2\rho_g u_z R_0}{\mu_g}$ and $Pr \equiv \frac{c_{pg}\mu_g}{k_g}$, is adopted according to Naterer (2003), where Re is Reynolds number, Pr is Prandtl number and μ is dynamic viscosity. Eq.(4-4c) suggests that all the heat supplied from the ambient to the jet is used to raise the surface temperature of the jet.

4.3 Analysis

The analysis follows by considering the hydrodynamic and heat transfer governing equations and, thereafter, coupling the hydrodynamic analysis and the heat transfer analysis through the surface tension gradient.

4.3.1 Hydrodynamic Analysis

Substituting the linearized parameters, Eqs (1-1a,b), into Eqs (3-1) through (3-3); considering all the hydrodynamic assumptions; and noting $u_i' \frac{\partial u_i'}{\partial i} = u_i' \frac{\partial u_j'}{\partial i} = \frac{\partial \bar{u}_j}{\partial t} = 0$; where $i,j \in [r,z]$, therefore, the following equations are

obtained for the perturbed continuity equation, r-direction momentum equation and z-direction momentum equation, respective, as:

$$\frac{u_r'}{r} + \frac{\partial u_r'}{\partial r} + \frac{\partial u_z'}{\partial z} = 0 \tag{4-5}$$

$$\frac{\partial u_r'}{\partial t} = -\frac{1}{\rho}\frac{\partial p'}{\partial r}, \tag{4-6}$$

and

$$\frac{\partial u_z'}{\partial t} + \bar{u}_z \frac{\partial u_z'}{\partial z} = -\frac{1}{\rho}\frac{\partial p'}{\partial z} \tag{4-7}$$

Operate $\frac{1}{r}\frac{\partial}{\partial r}[r(\,)]$ and $\frac{\partial(\,)}{\partial z}$on Eqs (4-6) and (4-7), respectively, to obtain

$$\frac{1}{r}\frac{\partial u_r'}{\partial t} + \frac{\partial^2 u_r'}{\partial r \partial t} + \frac{\partial^2 u_z'}{\partial z \partial t} + \bar{u}_z \frac{\partial^2 u_z'}{\partial z^2} = -\frac{1}{\rho r}\frac{\partial p'}{\partial r} - \frac{1}{\rho}\frac{\partial^2 p'}{\partial r^2} - \frac{1}{\rho}\frac{\partial^2 p'}{\partial z^2} \tag{4-8}$$

Differentiating Eq.(4-5) with respect to time(t); and following similar analysis as in Section 3.3 to give

$$r^2\frac{\partial^2 \Psi}{\partial r^2} + r\frac{\partial \Psi}{\partial r} - k^2 r^2\left(1 + \frac{\rho \bar{u}_z \hat{u}_z}{\hat{p}}\right)\Psi = 0 \tag{4-9}$$

As before in §3.3, the assumption that $\hat{p} \gg \rho \bar{u}_z \hat{u}_z$ holds, since the emphasis is on liquid fuel injection systems, hence, Eq.(4-9) becomes:

$$r^2\frac{\partial^2 \Psi}{\partial r^2} + r\frac{\partial \Psi}{\partial r} - k^2 r^2 \Psi = 0 \tag{4-10}$$

The two independent solutions to Eq.(4-10), second-order linear differential equation, are $I_0(kr)$ and $K_0(kr)$, where I_0 and K_0 are the modified zero-order Bessel function of the first and second kinds, respectively. However, boundary conditions dictate that, for the liquid phase side, $r \to 0, I_0(kr)$ is bounded; whereas $K_0(kr)$ is unbounded, hence, Ψ for the liquid phase is

$$\Psi_l = \mathrm{A} I_0(kr) \tag{4-11a}$$

and for the gas phase, $r \to \infty, K_0(kr)$ is bounded; whereas $I_0(kr)$ is unbounded, thus, Ψ for the gas phase is

$$\Psi_g = BK_0(kr) \tag{4-11b}$$

It should be noted that Eq.(4-5) is equivalent to $\frac{1}{r}\frac{\partial}{\partial r}(ru_r') = -\frac{\partial u_z'}{\partial z}$, which is integrated to obtain

$$u_r' = -\frac{1}{r}\int r\frac{\partial u_z'}{\partial z}dr \tag{4-12}$$

Using Eqs (4-11a,b) in Eq.(4-2b); eliminating integration constants with axisymmetric condition, hence, Eq.(4-12) gives, for the liquid phase and the gas phase, respectively, the following:

$$u_{rl}' = -iAI_1(kr)\hat{u}_{zl}e^{ikz+\omega t} \tag{4-13a}$$

and

$$u_{rg}' = iBK_1(kr)\hat{u}_{zg}e^{ikz+\omega t} \tag{4-13b}$$

Considering the kinematic boundary condition, Eq.(3-4a), in the perturbed form, from which the perturbed axial velocity is gotten, after equating Eqs (4-13a) and (4-13b) to Eq.(3-4a), for the liquid and gas phases; and, thereafter, substituting the resulting equations into Eq.(4-2a), respectively:

$$u_{zl}' = \frac{\delta_0 I_0(kr)}{I_1(kR_o)}\left(i\omega - k\bar{u}_{zg}\right)e^{ikz+\omega t} \tag{4-14a}$$

and

$$u_{zg}' = -\frac{\delta_0 K_0(kr)}{K_1(kR_o)}\left(i\omega - k\bar{u}_{zg}\right)e^{ikz+\omega t} \tag{4-14b}$$

Using Eqs (4-14a,b) in Eq.(4-7) and subtracting the resulting equation for the liquid phase from the gas phase gives:

$$\begin{pmatrix} -\rho_l \dfrac{\delta_0 I_0(kr)}{I_1(kR_o)}\{\omega(i\omega - k\bar{u}_{zl}) + ik\bar{u}_z(i\omega - k\bar{u}_{zl})\} \\ -\rho_g \dfrac{\delta_0 K_0(kr)}{K_1(kR_o)}\{\omega(i\omega - k\bar{u}_{zg}) + ik\bar{u}_{zg}(i\omega - k\bar{u}_{zg})\} \end{pmatrix} e^{ikz+\omega t} = \frac{\partial(p_l' - p_g')}{\partial z} \tag{4-15}$$

On the dynamic boundary condition, Eq.(4-1), after substituting perturbed parameters and noting that $(\bar{p}_l - \bar{p}_g)\big|_{r=R_0} = \frac{\sigma(z)}{R_0}$ gives

$$\frac{\partial(p_l' - p_g')}{\partial z} = \delta_o \left(\frac{d\sigma(z)}{dz} + ik\sigma(z)\right)\left(k^2 - \frac{1}{R_0^2}\right) e^{ikz+\omega t} \tag{4-16}$$

Combining Eq.(4-15) and Eq.(4-16); and, thereafter, taking $\bar{u}_{zg} = 0$, for a quiescent ambient, and prescribing all parameters at $r = R_o$ give the dispersion equation as:

$$\left(\rho_g \frac{K_0(kR_o)}{K_1(kR_o)} - \rho_l \frac{I_0(kR_o)}{I_1(kR_o)}\right) i\omega^2 + \rho_l \frac{I_0(kR_o)}{I_1(kR_o)} k(2i\bar{u}_z\omega + ik\bar{u}_z^2) - \left(\frac{\partial\sigma(z)}{\partial z} + ik\sigma(z)\right)\left(k^2 - \frac{1}{R_0^2}\right) = 0 \tag{4-17}$$

As before in §3.4, the expected short wave ($kR_o \to \infty$) assumption, Eqs (3-20a,b), is used; thus, Eq.(4-17) becomes

$$(\rho_l + \rho_g)\omega^2 + 2i\rho_l k\bar{u}_z\omega - \rho_l k\bar{u}_z^2 + k\sigma(z)\left(k^2 - \frac{1}{R_0^2}\right) - i\frac{d\sigma(z)}{dz}\left(k^2 - \frac{1}{R_0^2}\right) = 0 \tag{4-18}$$

Solving for the growth rate in Eq.(4-18) gives

$$\omega = \frac{-ik\rho_l \bar{u}_z}{(\rho_l + \rho_g)} \pm \left\{ \frac{\rho_l \rho_g k\, \bar{u}_z^2 - (\rho_l + \rho_g) k\sigma(z) \left(k^2 - \frac{1}{R_o^2}\right)}{(\rho_l + \rho_g)^2} + \frac{i(\rho_l + \rho_g) \frac{d\sigma(z)}{dz} \left(k^2 - \frac{1}{R_0^2}\right)}{(\rho_l + \rho_g)^2} \right\}^{1/2} . \quad (4\text{-}19)$$

Considering the real part, $Re(\omega)$, in the frame of temporal analysis, thus, Eq.(4-19) is obtained:

$$Re(\omega) = \frac{1}{2^{1/2}(\rho_l + \rho_g)} \{\beta_1 + (\beta_1^2 + \beta_2^2)^{1/2}\}^{1/2} \quad (4\text{-}20a)$$

where

$$\beta_1 \equiv \rho_l \rho_g k \bar{u}_z^2 - (\rho_l + \rho_g) k\sigma(z) \left(k^2 - \frac{1}{R_o^2}\right) \quad (4\text{-}20b)$$

$$\beta_2 \equiv (\rho_l + \rho_g) \left(k^2 - \frac{1}{R_0^2}\right) \frac{d\sigma}{dz} \quad (4\text{-}20c)$$

The plot of Eq.(4-20), for axial velocity of 200[m/s], shows that there exists a maximum (please see Figure 4-2). The dominant or the liquid breakup controlling wavenumber, k_{opt}, which corresponds to the maximum growthrate, ω_{max}, is expected to occur at $\frac{\partial Re(\omega)}{\partial k} = 0$, as acknowledged before.

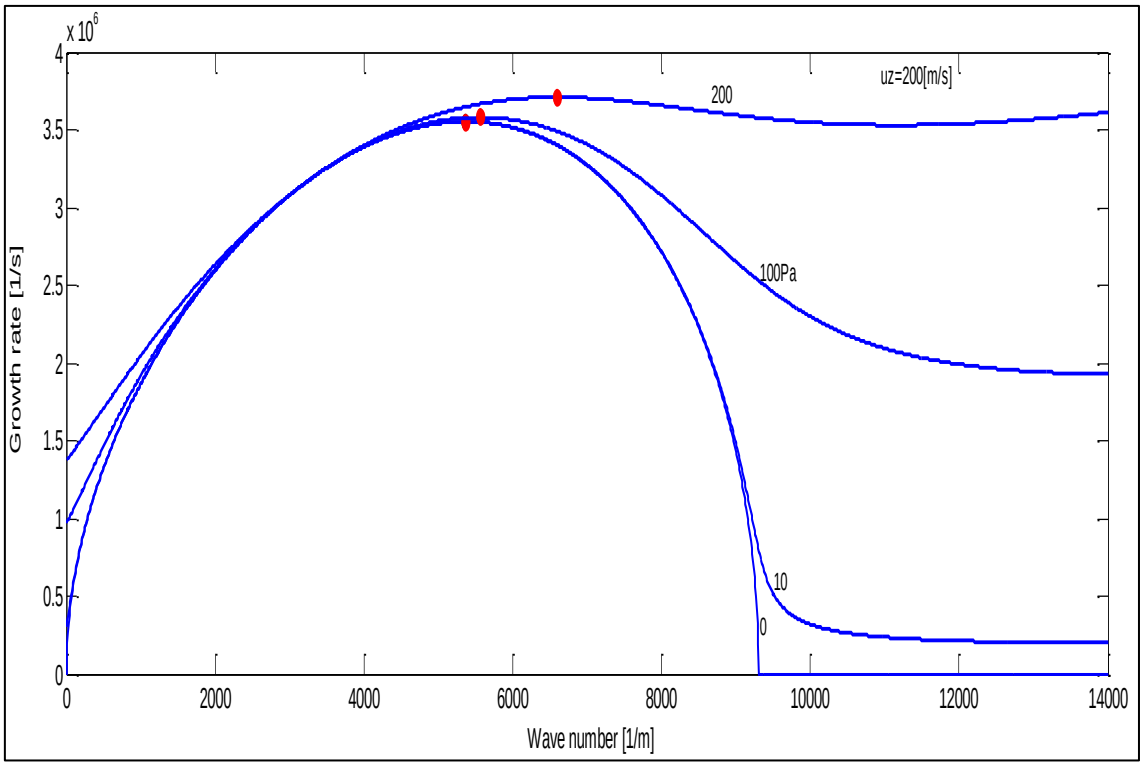

Figure 4-2 Variation of Growth Rate with Wavenumber and Surface Tension Gradient: 0, 10, 100 and 200 [Pa] at Injection Velocity, 200 [m/s]

It can be observed from Figure 4-2 that the breakup controlling parameters are dependent on the surface tension gradient, which exemplifies the claim that spatial variation of surface tension has a significant role to play in liquid atomisation and sprays (Mashayek and Ashgriz, 2006). Figure 4-3 shows the variation of the disturbance growth rate, with injection velocity, for the specific case of an isothermal condition (zero excess temperature), which indicates that increasing the injection velocity increases the disturbance growth rate as a result of increased relative velocity. This coincides with classical theory (Lefebvre, 1989). Figure 4-2 and Figure 4-3 suggest that increases in surface tension gradient and relative velocity may, respectively, have same effect on jet breakup.

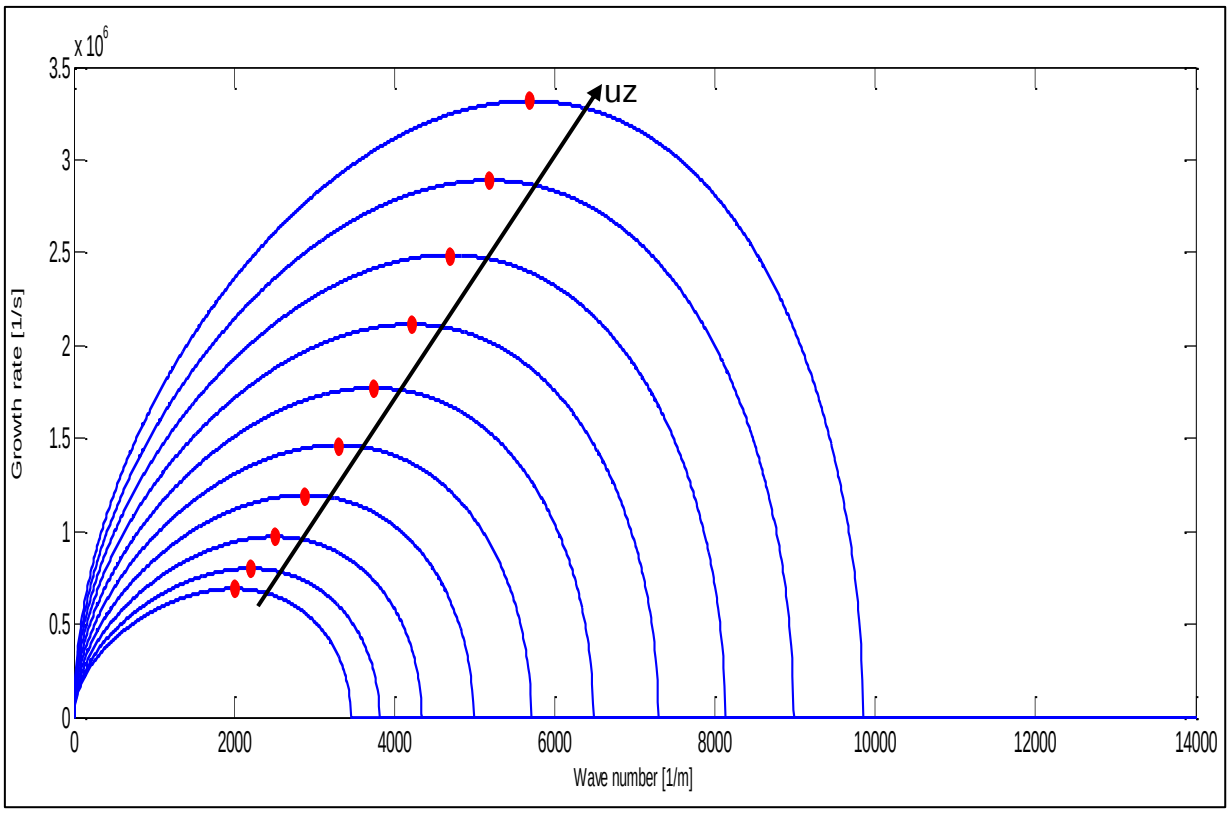

Figure 4-3 Variation of Growth Rate with Wavenumber and Injection Velocity (30 – 300 [m/s])

4.3.2 Coupling Heat Transfer Analysis

The coupling of the hydrodynamic analysis and the heat transfer is done through the surface tension gradient, $d\sigma/dz$.The analytical solution of the above heat transfer equations, Eqs (4-4), is well established, and can be found in classical heat transfer texts, for examples Naterer (2003) and Oko (2011), also see Appendix A for the detailed solution method. The solution is given, thus, as:

$$T(r,t) = T_i + T_{exc}\left\{erfc\left(\frac{r}{2\sqrt{\alpha t}}\right) - erfc\left(\frac{r}{2\sqrt{\alpha t}} + H\sqrt{\alpha t}\right)e^{(Hr+H^2\alpha t)}\right\} \qquad (4\text{-}21)$$

where $erfc(x) \equiv 1 - \frac{2}{\pi}\int_0^x e^{-t^2}dt$, $T_{exc} \equiv (T_\infty - T_i)$ is the excess temperature, and $H \equiv \bar{h}/k_g$.

On the Lagrange frame of reference, the axial velocity could be related as $u_z = \partial z/\partial t$, therefore, the following relation is applied to the axial temperature gradient.

$$\frac{\partial T}{\partial z} = \frac{1}{u_z}\frac{\partial T}{\partial t}\Big|_{\substack{r=R \\ t=t^*}} \tag{4-22}$$

In this expression, $t^* \sim R_0^2/\alpha \equiv \varepsilon R_0^2/\alpha$, denotes the thermal penetration time, where ε is a proportionality constant, which is expected to be $\varepsilon \ll 1$ for high liquid injection velocity; linear variation of the surface tension with temperature is adopted empirically as $\sigma = \sigma_i - \sigma_T(T - T_i)$; where σ_i denotes a reference temperature surface tension and σ_T denotes the gradient ($d\sigma/dT$), which is taken as σ_T= -0.0000519 N/mK for the diesel fuel according to experimental data presented in Chhetri and Watts (2013).

Differentiating Eq.(4-21) with respect to time (t) gives:

$$\begin{aligned}\frac{\partial T}{\partial t} = {} & \frac{R_0}{2\sqrt{\alpha\pi}}t^{-3/2}e^{-\frac{R_0^2}{4\alpha t}} - H^2\alpha e^{(HR+H^2\alpha t)}erfc\left(\frac{R_0}{2\sqrt{\alpha t}} + H\sqrt{\alpha t}\right) \\ & + \frac{1}{\sqrt{\pi}}\left\{\left(H\sqrt{\frac{\alpha}{t}} - \frac{R_0}{2\sqrt{\alpha}}t^{-3/2}\right)e^{-\left[\left(\frac{R_0}{2\sqrt{\alpha t}}+H\sqrt{\alpha t}\right)^2 + HR_0 + H^2\alpha t\right]}\right\}\end{aligned} \tag{4-23}$$

Substitute Eq.(4-23) into Eq.(4-22), and rearrange to obtain

$$\begin{aligned}\frac{\partial T}{\partial z} = {} & \frac{T_{exc}e^{-1/4}}{u_z R_0^2}\left\{\frac{1}{2}\left(\frac{\alpha}{\pi}\right)^{1/2} - H^2R_0^2 erfc\left(\frac{1}{2} + HR_0\right)e^{\xi_1}\right. \\ & \left. + \left(\frac{HR_0\alpha}{\sqrt{\pi}} - \frac{1}{2}\left(\frac{\alpha}{\pi}\right)^{1/2}\right)e^{-\xi_2}\right\}\end{aligned} \tag{4-24a}$$

where

$$\xi_1 = \frac{1}{4\varepsilon} + HR_0 + \varepsilon H^2 R_0^2 \tag{4-24b}$$

and

$$\xi_2 = \frac{1}{2\varepsilon} + 2HR_0^2 + 2\varepsilon H^2 R_0^2 \tag{4-24c}$$

Using $\frac{d\sigma}{dz} \equiv \frac{\partial T}{\partial z}\frac{d\sigma}{dT}$, yields:

$$\frac{\partial \sigma}{\partial z} = \frac{1}{u_z}\frac{d\sigma}{dT}\frac{T_{exc}\alpha e^{-1/4\varepsilon}}{R_0^2}\left\{\frac{1}{2}\frac{\varepsilon^{-3/2}}{\sqrt{\pi}} - H^2 R_0^2 erfc\left(\frac{1}{2\varepsilon} + \sqrt{\varepsilon}HR_0\right)e^{\xi_1} + \left(\frac{HR\alpha}{\sqrt{\varepsilon\pi}} - \frac{1}{2}\frac{\varepsilon^{-3/2}}{\pi}\right)e^{-\xi_2}\right\} \tag{4-25}$$

The estimate of the surface tension gradient, see Figure 4-2, for a diesel fuel injected into a hot ambient is modelled, based on the semi-infinite heat transfer model (Eqs (4-2), (4-3); (4-21) through (4-25)). The figure suggests that at high jet speeds, the very short time available for heat transfer between the ambient and the jet results in diminishing surface tension gradient.

For a typical common-rail diesel injection engine operation, it is noted that average injection velocity (~120m/s) and nozzle diameter (~0.1mm). For the diesel fuel injected, data presented in Sazhin et al. (2006) are adopted accordingly: liquid jets of an initial temperature of ~300K, are injected into hot ambient gas at a temperature of ~800K; (excess temperature of ~500K). The following thermo-physical properties, presented in Table 4-1, hold for the diesel fuel and the surrounding gas.

Table 4-1 Thermo-physical Properties of Fluids (Sazhin, 2006)

Fluid (i)	***Density,*** ρ_i ***[kg/m3]***	***Specific Heat at constant pressure,*** c_{pi} ***[J/kgK]***	***Thermal conductivity,*** k_i ***[W/mK]***
Gas, g	23.8	1120	0.061
Diesel fuel, l	600	2830	0.145

Figure 4-4 shows that the effect of elevated ambient temperature on surface tension reduces progressively as the injection velocity increases, this is expected because high injection velocity depicts that the thermal interaction between the hot ambient and the liquid fuel is very fast and, therefore, heat conduction into the liquid fuel, to increase the liquid temperature, is reduced. This suggests that surface tension gradient effects may be minimal, in view of Figure 4-2, for injection velocity above ~150m/s, even in a very hot ambient condition (~1000K). However, for the transient injection operation, where velocity varies with time, the non-isothermal condition on the liquid jet breakup may still be significant.

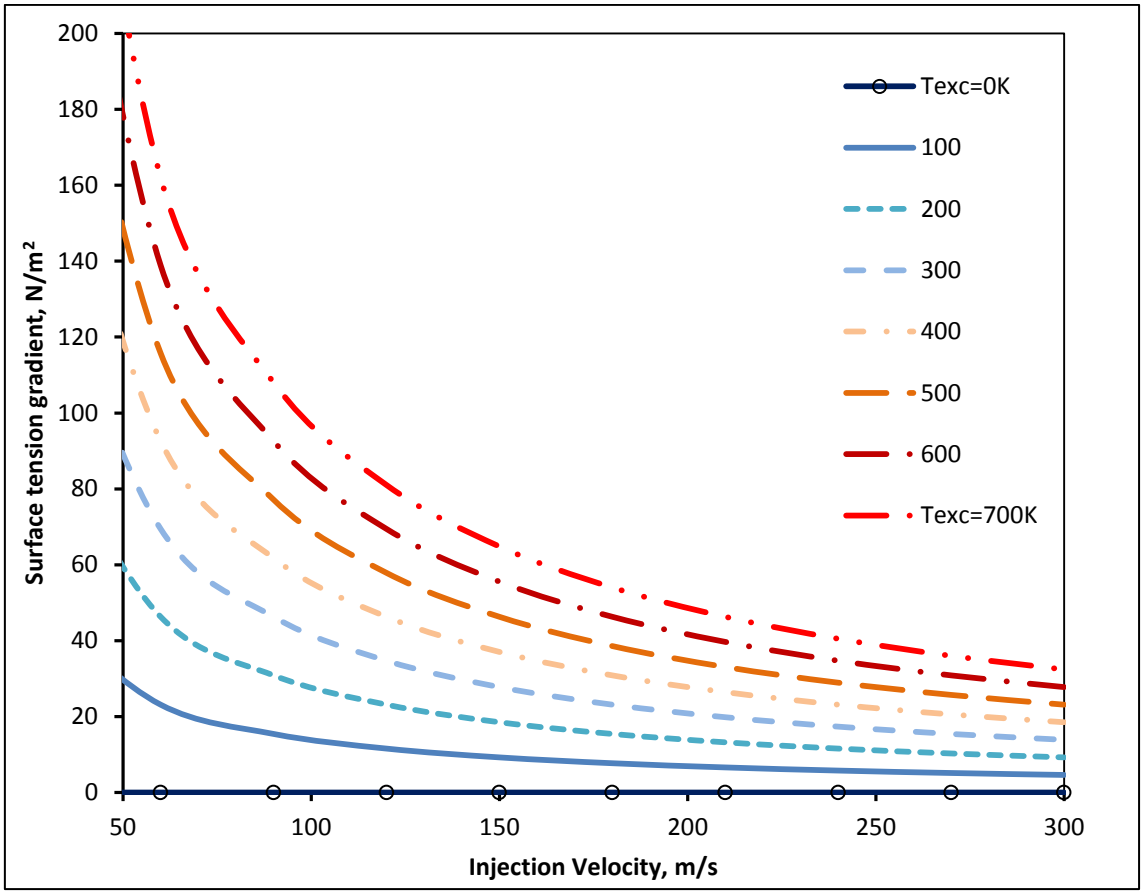

Figure 4-4 Variation of Surface Tension Gradient with Injection Velocity and Excess Temperature (0 –700[K])

With Eq.(4-25) being substituted into Eq.(4-20), hence, the coupled hydrodynamic and heat transfer liquid breakup model for a non-isothermal is readily obtained.

Typical wave growth velocity, at breakup, can be taken as

$$v_{bu} = \frac{\omega'_{max}}{k_{opt}} \tag{4-26}$$

and typical breakup time being

$$t_{bu} \approx \frac{R_0}{v_{bu}} \tag{4-27}$$

Therefore, applying Eqs (4-26) and (4-27) in this present non-isothermal jet breakup model case gives Figure 4-5. It is observed from the figure that liquid

jets instability is enhanced with increasing excess-temperature up to a high injection velocity where the non-isothermal effects become minimal beyond which the breakup mechanism coincides with the isothermal condition. This observation is attributed to the interfacial surface tension behaviour, which is directly related to the temperature at the interface.

At high jet speeds, the very short time available for heat transfer between the ambient and the jet results in diminishing interface excess temperature. This result implies that for transient liquid fuel injection, as velocity increases progressively with time (see Figure 2-8), the non-isothermal effects may influence the breakup mechanism significantly, while during high injection velocities the non-isothermal effects may attenuate. Similarly, for a very low injection velocity, injection is also expected to approximate the isothermal case (at ambient temperature).

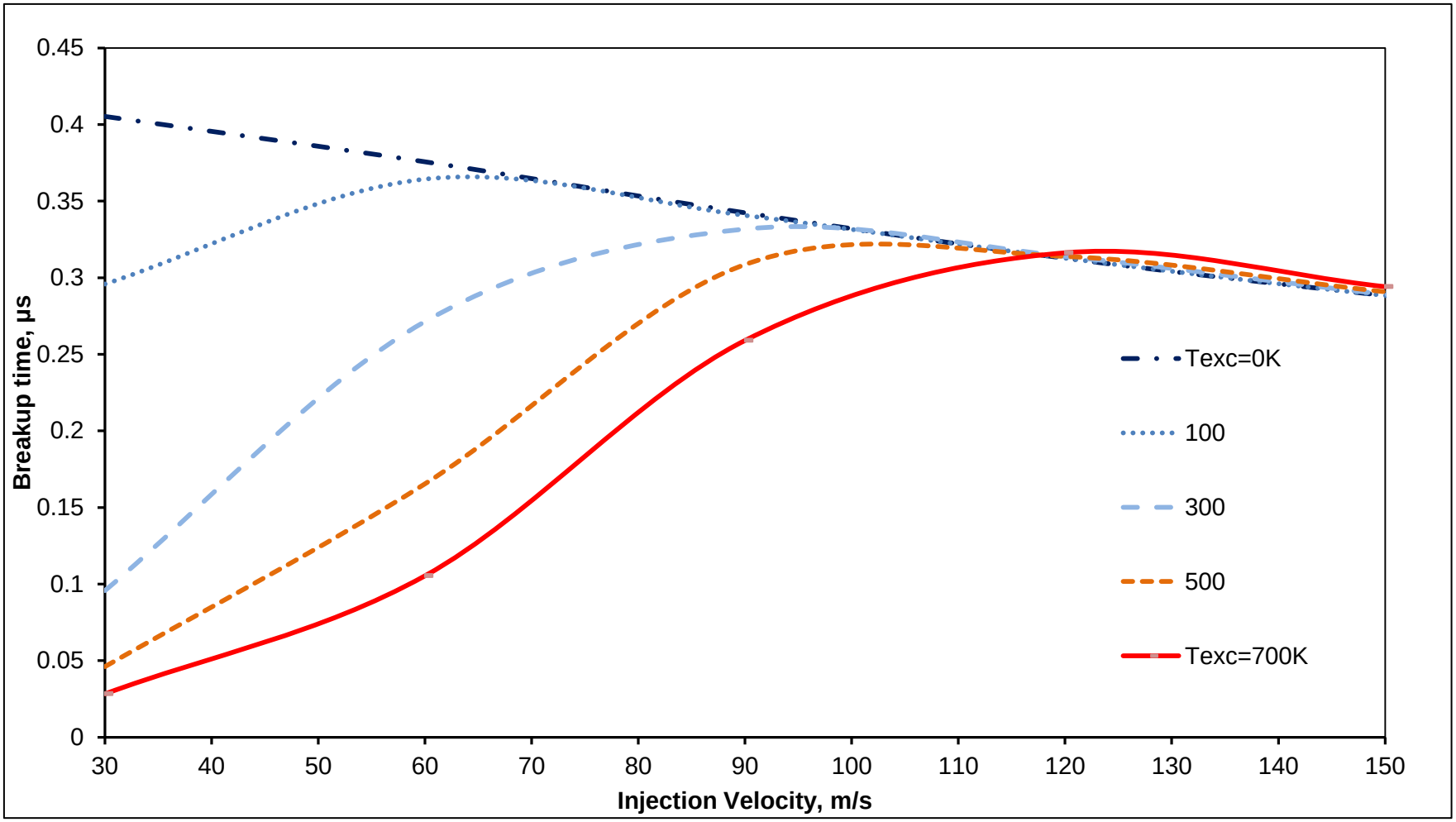

Figure 4-5 Variation of Breakup Time with Injection Velocity and Excess Temperature (0 –700[K])

4.4 Model Validation

There are no direct comparisons of the model predictions with experimental data. However, macro models that coupled primary and secondary atomisation are sought. The spray angle, penetration length and liquid length have been identified as the relevant macroscopic parameters for the understanding of the fuel spray-air mixing process (Payri et al., 2013; Som and Aggarwal, 2010).

The Forstall and Shapiro (1950) proposed relationship according to Eq. (3-29), which can be presented for the particular case of a non-evaporating non-isothermal jet breakup as

$$L\left(\frac{dL}{dt}\right) = L_{bu}u_{bu} \tag{4-28}$$

where $\frac{dL}{dt} \approx \bar{u}_p[m/s]$ is the tip penetration velocity, $u_{bu}[m/s]$ is the continuous liquid column tip velocity and $L_{bu}[m]$ is the breakup length. It should be noted that Eq.(4-28) holds for $L > L_{bu}$.

Taking L_{bu}~Λ; noting that $L_{bu}u_{bu} \equiv L_{bu}^2/t_{bu}$ in Eq.(4-28); and by separating variables give

$$\int_0^{L_p} L\,dL \sim \int_0^t 4\pi^2 \frac{\omega_{max}}{R_0 k_{opt}^3}\,dt \tag{4-29}$$

Solving for $L_p$in Eq.(4-29) gives the penetration length as:

$$L_p = 3.7657\vartheta\left(\frac{\omega_{max}}{R_0 k_{opt}^3}t\right)^{1/2} \tag{4-30}$$

where ϑ is a constant parameter that combines the proportionality constant.

Figure 4-6, according to Eq.(4-30) (shown by lines) and experimental data (shown by markers), from the Sandia National Laboratory (ECN, 2014), for spray A type injector – see Pickett et al. (2010) for the detailed description of the injector – with Dodecane (nC12) fuel (see Table 4-2 for the pertinent input

data), shows a good agreement between simulated results and experimental data.

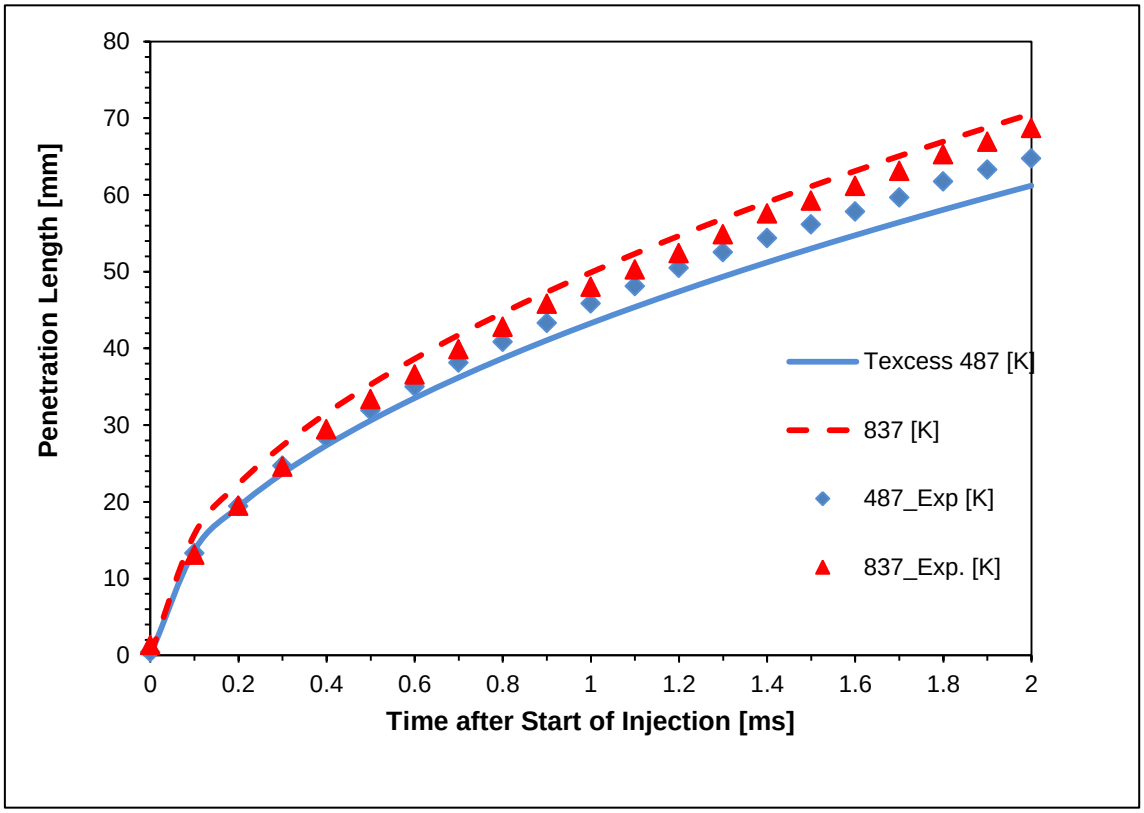

Figure 4-6 Simulated Penetration Length and Experimental Data from the Sandia National Laboratory (ECN, 2014)

The figure suggests that higher ambient temperature contributes to faster liquid penetration for a non-evaporating spray, as a consequence of higher surface tension gradient; this is expected as the non-isothermal condition affects both the primary and the secondary breakup mechanisms. However, it should be expected that the penetration length be decreased for evaporating spray compared to the length of the non-evaporating spray, as noted in the finding of Hiroyasu and Arai (1990).

Table 4-2 Pertinent Input Data (ECN, 2014)

S/No	*Quantity*	*Units*	*Value*
1	Nominal ambient density	kg/m^3	22.80
2	Nominal fuel density	kg/m^3	752
3	Nominal fuel temperature	K	363
4	Discharge coefficient	-	0.89
5	Injector nozzle diameter	mm	0.09

In comparison of Eq.(4-30) with spray penetration correlation for evaporating spray proposed by Dent (1971), Eq.(4-30) is modified for evaporating spray as:

$$L_p = 3.7657\left(\frac{T_i}{T_\infty}\right)^{1/4}\left(\frac{\omega_{max}}{R_0 k_{opt}^3}t\right)^{1/2} \tag{4-31}$$

where $\vartheta \cong \left(\frac{T_i}{T_\infty}\right)^{1/4}$.

Figure 4-7, according to Eq.(4-31), exemplifies the Hiroyasu and Arai (1990) experimental observation and Payri et al. (2013) CFD simulation for an evaporating spray.

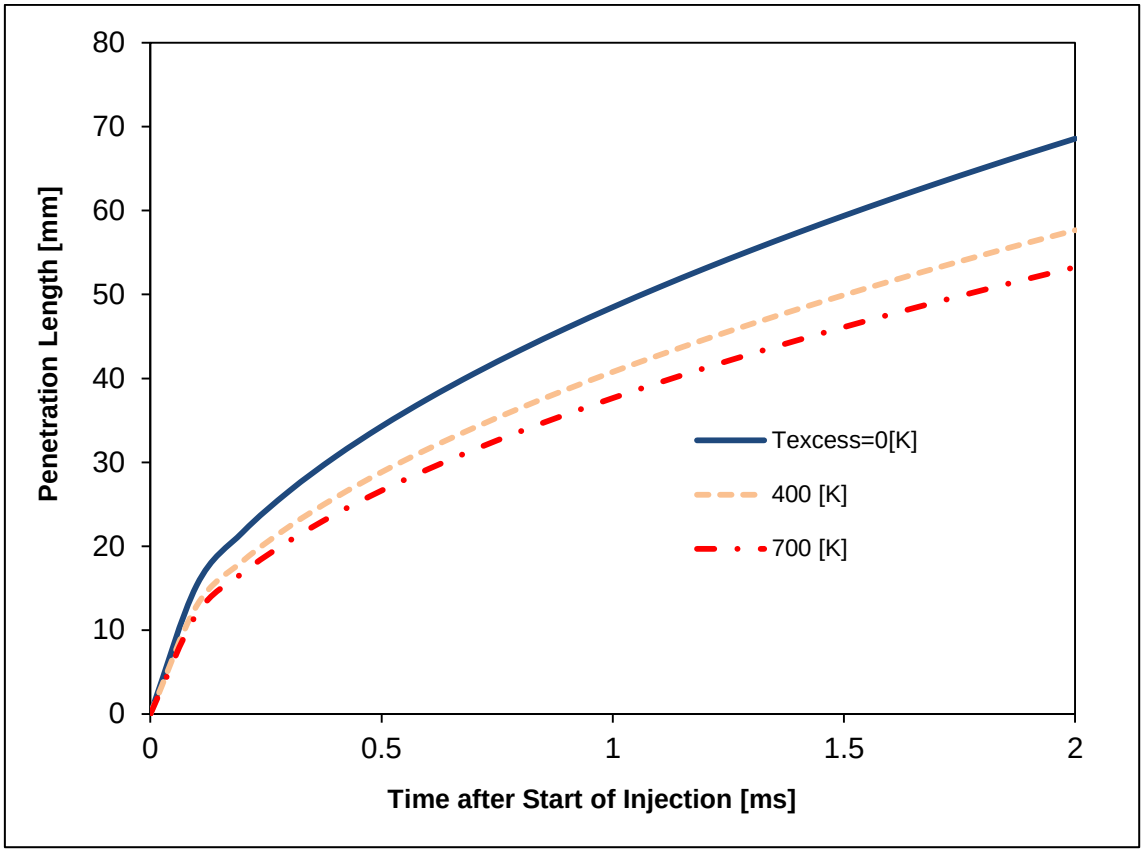

Figure 4-7 Penetration Length for an Evaporating Spray

The relation for the half spray angle, $\theta/2$, in Trinh and Chen (2006) as proposed by Reitz and Bracco (1982) sufficed; therefore, Eq.(3-27) is applied in the following analysis.

The spray angle can be related to the maximum penetration length (the liquid length) by considering the mechanistic model formulation in Siebers (1999), simplified in Payri et al. (2013), to obtain

$$L_{pmax} = 2\frac{b}{a}K_p C_d^{1/2} R_0 \sqrt{\frac{\rho_l}{\rho_g}\frac{1}{\tan\theta/2}} \tag{4-32}$$

where a is a constant taken as 0.66; b is a constant taken to be 0.41(Siebers, 1999); K_p is a constant depending on ambient condition and evaporation; and C_d is the discharge coefficient.

Considering Eq.(3-26) and noting $\bar{u}_z = C_d\left(2\Delta p_{inj}/\rho_l\right)^{1/2}$, thus, Eq.(4-32) becomes

$$L_{pmax} = 0.2833\alpha C_d^{3/2} R_0 \frac{k_{opt}}{\omega_{max}} \left(\frac{\Delta P_{inj}}{\rho_g}\right)^{1/2} \tag{4-33}$$

Where $\alpha \equiv K_p/\Omega$ and ΔP_{inj} is orifice pressure drop.

The present model, Eq.(4-33), is validated against experimental data presented in Siebers (1999) for the breakup of Cetane liquid, see Figure 4-8. The nominal data for the analysis were: orifice pressure drop (136 [MPa]), orifice diameter (246 [μm]), discharge coefficient (0.78 [-]), and fuel injection temperature (400 [K]). Better agreement is observed at higher ambient densities, which may be due to the dominancy of non-isothermal related instabilities at higher ambient density (heat intensification), over other secondary phenomena that exist, which are not stressed in the model (as opposed to velocity related instabilities). However, the model has good predictions of experimental data in the typical region of diesel engine's operations, as seen in Figure 4-8.

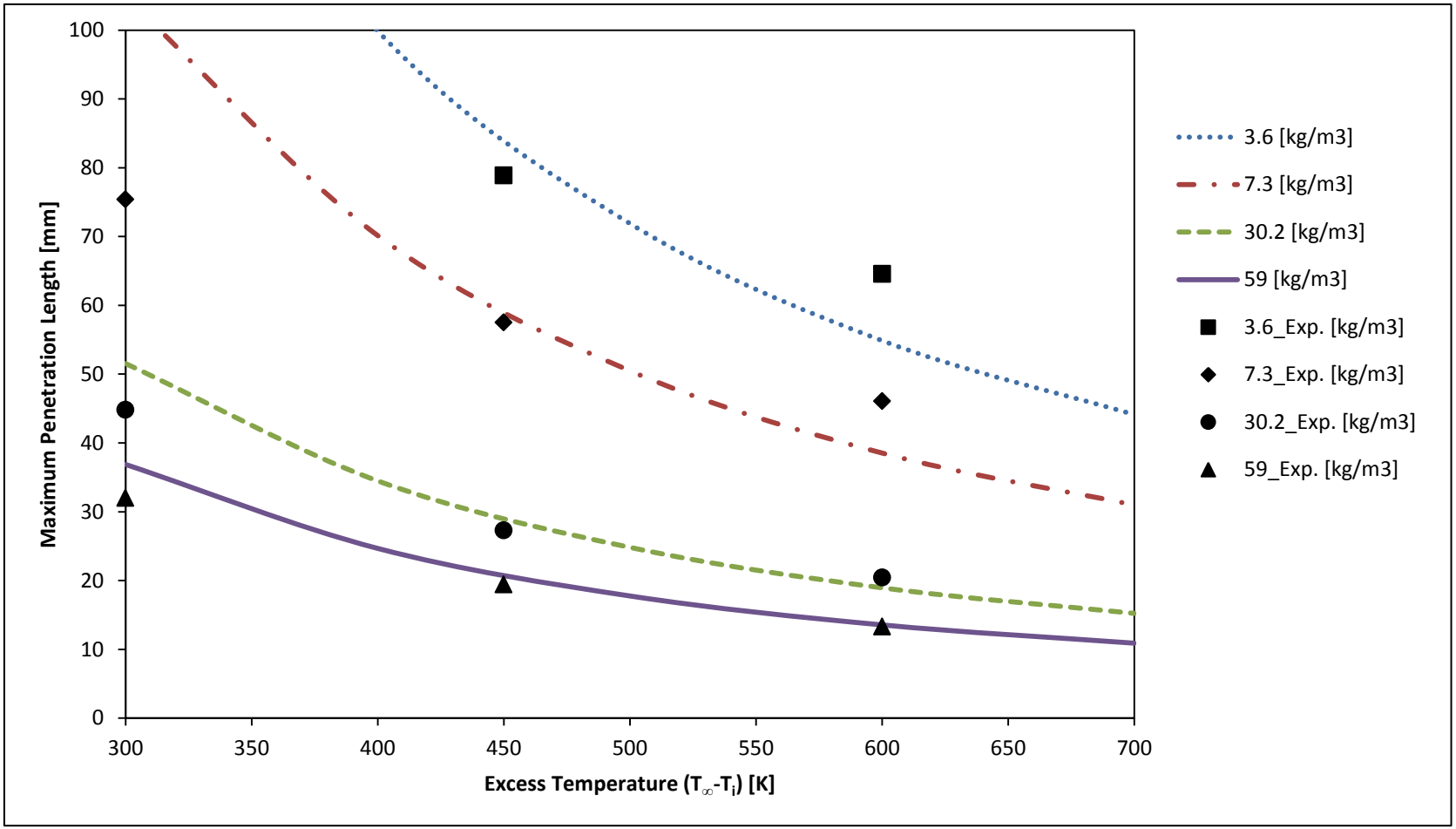

Figure 4-8 Maximum Penetration Length as a Function of Excess Temperature and Ambient Density

4.4.1 Isothermal Approximation

For isothermal case, $\sigma(z) = \sigma = const. \implies \frac{\partial \sigma'(z)}{\partial z} = 0$, therefore, for this case Eq.(4-20) is simplified to:

$$\omega = \frac{-ik\rho_l \bar{u}_z}{(\rho_l + \rho_g)} \pm \left\{ \frac{\rho_l \rho_g k \bar{u}_z^2 - (\rho_l + \rho_g) k\sigma \left(k^2 - \frac{1}{R_o^2}\right)}{(\rho_l + \rho_g)^2} \right\}^{1/2} \tag{4-34}$$

The breakup controlling wave is expected to be the one with maximum growthrate, to occur at: $\frac{\partial Re(\omega)}{\partial k} = 0$. Hence, solving Eq.(4-34) for the breakup controlling wavenumber gives the case presented in Eq.(3-33).

Similarly, the shortwave and dripping flow assumptions result in Eqs (3-34) and (3-35), respectively, which are well established equations in the literature (Tjahjadi, Stone and Ottino, 1992; Eggers and Villermaux, 2008).

4.5 Conclusion of Chapter Four

The theory of liquid fuel jet instabilities has been developed under several assumptions, which include the assumption that the jets breakup processes are isothermal. However, liquid fuels are normally injected into an elevated combustion-chamber temperature to maintain a desirable homogeneous combustible mixture – liquid vapour and air. Therefore, a new linear theory model for the instability and breakup of non-isothermal liquid jets, with consideration of a spatially variation of surface tension along the liquid-gas interface, is presented. The spatial variation of surface tension is obtained through temperature-dependent surface tension and transient heat-transfer from the combusting gases to the liquid jet. The classical interface hydrodynamic breakup theory and solution of heat-transfer through semi-infinite medium are coupled through the surface tension gradient. The model is shown to maintain plausibility of investigating liquid fuel breakup mechanisms under the combustion-chamber operating conditions, as validated results agreed with experimental data.

5 INSTABILITY AND BREAKUP MODEL FOR TRANSIENT NON-ISOTHERMAL JET

5.1 Background

Investigation of the behaviour of liquid fuel jet breakup during the transient operations and in combustor environment, in which the liquid fuel is injected, is crucial to the understanding of the overall aspects of jet breakup and droplet size distribution. The degree of the fuel/air mixing in the Diesel engine combustor requires adequate knowledge of the jet breakup processes, specifically the primary breakup (breakup of jet). The liquid jet experiences a high degree of acceleration during start-up and short-down operations. It is expected that the transient operation being dominant in pulsed injection techniques (which are being deployed in most contemporary combustor systems), since there are more than one start-up and short-down operations per cycle. The effects of the transient operations and the non-isothermal conditions on the overall liquid breakup process should be emphasised.

Furthermore, in automotive applications, the liquid fuel is injected into elevated temperature environment (order of 10^3K over a length scale of 10^{-3}m), which can cause significant thermal fluctuations. The surface tension, which dictates interfacial breakup mechanism, is a function of the local temperature; hence elevated temperature environment, combustor temperature, associated thermal fluctuations result in local variation of the surface tension (as seen in Chapter 4), thereby potentially impacting the liquid breakup processes: primary and secondary. The variation of the surface tension, as a result of the local temperature, modifies the flow field gas-liquid interface, which in turn alters the interfacial temperature distribution through the modified interfacial flow (Herrmann and Lopez, 2009). In what follows, the interfacial temperature distribution is carried downstream by the jet velocity, which gives rise to a transient spatially variation of surface tension (i.e. surface tension gradient) along the liquid-gas interface.

The impact of the two important phenomena on liquid jet instability and breakup – jet acceleration and non-isothermal conditions – has not been fully investigated. Naturally, these effects are difficult to address by both experimental and CFD investigations. The transient effects and non-isothermal conditions on jet breakup have been separately considered in Chapter 3 and Chapter 4, respectively. This chapter presents a new model that simultaneously captures both the transient effects and non-isothermal conditions. The model combined both hydrodynamic model and heat transfer equations, coupled through the surface-tension gradient, and is a novel address of this conjugated problem. Continued modelling in that area may benefit the development of the next generation of liquid fuel injectors and combustors, as simplified models have a qualitative agreement with experimental results.

5.2 Model Formulation

Though chapters 3 and 4 have considered some of the aspects of this chapter, however, one wishes to reemphasis some of the governing equations in the previous chapters in this chapter.

A free cylindrical liquid jet, of axial time-dependent velocity, moving in a hot quiescent ambient gas is considered in the analysis. The coordinate system moves with the jet, with the reference being set at the nozzle exit and whose coordinate z coincides with the jet centre line, as shown in

Figure 5-1. Fundamental conservation equations (continuity and momentum) are applied to both the liquid-phase and the surrounding gas-phase. As usual, the axi-symmetric quality, varicose deformation, is assumed for the unbounded flow; and the dominant disturbances parameters, which has been emphasised in Chapter 3, is considered. Therefore, the conservation equations, Eqs (2-1) through (2-4), become

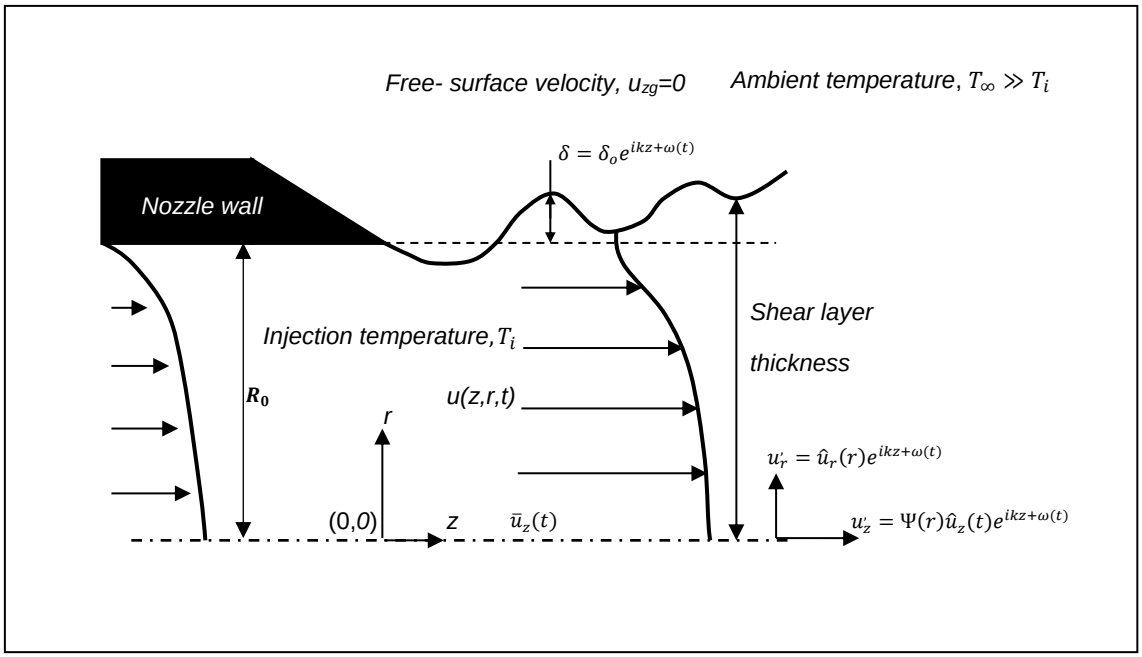

Figure 5-1 Free-surface Liquid Jet in Hot Ambient

The continuity equation

$$\frac{u_r}{r} + \frac{\partial u_r}{\partial r} + \frac{\partial u_z}{\partial z} = 0 \qquad (5\text{-}1)$$

The momentum equation

r-direction momentum

$$\frac{\partial u_r}{\partial t} + u_r\left(\frac{\partial u_r}{\partial r}\right) + u_z\left(\frac{\partial u_r}{\partial z}\right) = -\frac{1}{\rho}\left(\frac{\partial p}{\partial r}\right) \qquad (5\text{-}2)$$

z-direction momentum

$$\frac{\partial u_z}{\partial t} + u_r\left(\frac{\partial u_z}{\partial r}\right) + u_z\left(\frac{\partial u_z}{\partial z}\right) = -\frac{1}{\rho}\left(\frac{\partial p}{\partial z}\right) \qquad (5\text{-}3)$$

Notice that Eqs (5-1) through (5-3) are similar informs to Eq.(3-1)through (3-3), but, the analysis takes a different form.

The Boundary conditions

The governing equations are subject to the following three basic boundary conditions:

(i) To satisfy the kinematic boundary condition, thus,

$$u_{r=R_0} = \frac{\partial \delta}{\partial t} + u_z \frac{\partial \delta}{\partial z} \tag{5-4a}$$

(ii) To satisfy dynamic boundary condition at the liquid-gas interface for spatial variation of surface tension (i.e. surface tension gradient) along the liquid-gas interface due to temperature gradient, thus, the following holds

$$p_l - p_g = \sigma(z)K; \text{ at } \quad r = R_0 + \delta \tag{5-4b}$$

with $K = div\,(\nabla G/|\nabla G|)$ where $G(r,z) = 0$ denotes the surface for which K has to be determined, it follows thus:

$$K = \frac{1}{R_0} - \frac{\delta}{R_0^2} - \frac{\partial^2 \delta}{\partial z^2} \equiv \frac{1 - \delta/R_0}{R_0} - \frac{\partial^2 \delta}{\partial z^2} \tag{5-4c}$$

where R_0 and δ denotes the unperturbed jet radius and surface perturbation, respectively.

(iii) To satisfy axi-symmetric assumption, thus,

$$\left.\frac{\partial u_r}{\partial r}\right|_{r=0} = 0 \tag{5-4d}$$

5.2.1 Formulation Assumptions

Perturbed parameters are represented as a sum of base and perturbation values, according to the theory of small perturbation decomposition (Reitz and Bracco, 1982), thus, the linearization process follows by decomposing velocity, u, and pressure, p, respectively, as follow

$$u_r = \bar{u}_r + u_r' \tag{5-5a}$$

$$u_z = \bar{u}_z(t) + u_z' \tag{5-5b}$$

and

$$p = \bar{p}(t) + p' \tag{5-5c}$$

with the jet surface being prescribed by

$$r = R_o + \delta \tag{5-5d}$$

where bar and prime parameters represent base and perturbed parameters, respectively, whereas R_o and δ represent unperturbed jet surface and surface perturbation, respectively.

With Eqs (5-5) being sufficient, thus, the perturbed parameters are assumed to be possibly presented as follow

$$p' = \Psi(r)\hat{p}(t)e^{ikz+\omega(t)} \tag{5-6a}$$

$$u_z' = \Psi(r)\hat{u}_z(t)e^{ikz+\omega(t)} \tag{5-6b}$$

and

$$\delta = \delta_o e^{ikz+\omega(t)} \tag{5-6c}$$

The combination of Eqs (5-4b) and (5-6) make the difference in the previous two chapters (Chapter 3 and Chapter 4). These forms are less restrictive than the ones postulated by the classical hydrodynamic stability theory. These forms enable time and temperature dependency of perturbation to be non-linear and assume a different form for each parameter.

It is assumed that the jet's bulk velocity (base velocity) is simplified to be of a uniform axial velocity (no radial variation), thus, $\frac{\partial \bar{u}_z}{\partial r} = 0$. As high speed jets with relatively moderate bulk velocity changes in time are considered, bulk radial velocity is assumed to be negligible: $\bar{u}_r \approx 0$.

5.3 Analysis

The analysis follows by considering the hydrodynamic and heat transfer governing equations and, thereafter, coupling the hydrodynamic analysis and

the heat transfer analysis through the surface tension gradient. However, the heat transfer analysis of §4.2.3 sufficed in this present analysis; henceforth heat transfer analysis refers to §4.2.3.

5.3.1 Hydrodynamic Formulation

The hydrodynamic formulation proceeds by substituting the linearized parameters, Eqs (5-5), into Eqs (5-1) through (5-3), since the conservation equations hold for both the unperturbed and perturbed flow, and considering all the hydrodynamic assumptions in the resulting equations. Thereafter, noting that $u_i' \frac{\partial u_i'}{\partial i} = u_i' \frac{\partial u_j'}{\partial i} = 0$, where $i, j \in [r, z]$, results in the following equations for the perturbed continuity equation, r-direction momentum equation and z-direction momentum equation, respectively.

$$\frac{u_r'}{r} + \frac{\partial u_r'}{\partial r} + \frac{\partial u_z'}{\partial z} = 0 \tag{5-7}$$

$$\frac{\partial u_r'}{\partial t} = -\frac{1}{\rho}\frac{\partial p'}{\partial r}, \tag{5-8}$$

and

$$\frac{\partial u_z'}{\partial t} + \bar{u}_z \frac{\partial u_z'}{\partial z} = -\frac{1}{\rho}\frac{\partial p'}{\partial z} \tag{5-9}$$

With the complete description of the perturbed flow, by Eqs (5-7) through (5-9), $\frac{1}{r}\frac{\partial}{\partial r}[r(\,)]$ and $\frac{\partial(\,)}{\partial z}$are operated, respectively, on Eq.(5-8) and Eq.(5-9) to obtain

$$\frac{1}{r}\frac{\partial u_r'}{\partial t} + \frac{\partial^2 u_r'}{\partial r \partial t} + \frac{\partial^2 u_z'}{\partial z \partial t} + \bar{u}_z \frac{\partial^2 u_z'}{\partial z^2} = -\frac{1}{\rho r}\frac{\partial p'}{\partial r} - \frac{1}{\rho}\frac{\partial^2 p'}{\partial r^2} - \frac{1}{\rho}\frac{\partial^2 p'}{\partial z^2} \tag{5-10}$$

Differentiating Eq.(5-7) with respect to time (t) results in

$$\frac{1}{r}\frac{\partial u_r'}{\partial t} + \frac{\partial^2 u_r'}{\partial r \partial t} + \frac{\partial^2 u_z'}{\partial z \partial t} = 0 \tag{5-11}$$

Substituting Eq.(5-11) into Eq.(5-10)and, finally, using Eq.(5-6b) in the resulting equation to obtain

$$r^2\frac{\partial^2\Psi}{\partial r^2}+r\frac{\partial\Psi}{\partial r}-k^2r^2\left(1+\frac{\rho\bar{u}_z\hat{u}_z}{\hat{p}}\right)\Psi=0 \tag{5-12}$$

It has been noted in §3.3 and §4.3.1, for high injection pressure systems, that $\hat{p}\gg\rho\bar{u}_z\hat{u}_z$; it implies that Eq.(5-12) becomes:

$$r^2\frac{\partial^2\Psi}{\partial r^2}+r\frac{\partial\Psi}{\partial r}-k^2r^2\Psi=0 \tag{5-13}$$

The two independent solutions to Eq.(5-13), second-order linear differential equation, are $I_0(kr)$and $K_0(kr)$, where I_0 and K_0 are the modified zero-order Bessel function of the first and second kinds, respectively. However, boundary conditions dictate that, for the liquid phase side, $r\to 0, I_0(kr)$ is bounded; whereas $K_0(kr)$ is unbounded, hence, Ψ for the liquid phase is

$$\Psi_l=\mathrm{A}I_0(kr) \tag{5-14a}$$

and for the gas phase, $r\to\infty, K_0(kr)$ is bounded; whereas $I_0(kr)$ is unbounded, thus, Ψ for the gas phase is

$$\Psi_g=BK_0(kr) \tag{5-14b}$$

Eq.(5-7) is equivalent to $\frac{1}{r}\frac{\partial}{\partial r}(ru_r')=-\frac{\partial u_z'}{\partial z}$, which can be integrated to obtain

$$u_r'=-\frac{1}{r}\int r\frac{\partial u_z'}{\partial z}dr \tag{5-15}$$

By using Eqs(5-14) in Eq.(5-6a) and eliminating integration constants with the axi-symmetric condition, hence, Eq.(5-15) gives, for the liquid phase and the gas phase, respectively, the following:

$$u_{rl}'=-iAI_1(kr)\hat{u}_{zl}(t)e^{ikz+\omega(t)} \tag{5-16a}$$

and

$$u_{rg}'=iBK_1(kr)\hat{u}_{zg}(t)e^{ikz+\omega(t)} \tag{5-16b}$$

By imposing the kinematic boundary condition, Eq.(5-4a), on Eq.(5-6c) gives

$$u'_{r=R_0} = \delta_o \left(\frac{d\omega(t)}{dt} + ik\bar{u}_z \right) e^{ikz+\omega t} \tag{5-17}$$

Equating Eq.(5-17) to Eqs (5-16) gives, respectively, for the liquid and gas region

$$\hat{u}_{zl} = -\frac{\delta_o}{iAI_1(kr)} \left(\frac{d\omega(t)}{dt} + ik\bar{u}_z \right) \tag{5-18a}$$

and

$$\hat{u}_{zg} = \frac{\delta_o}{iAI_1(kr)} \left(\frac{d\omega(t)}{dt} + ik\bar{u}_z \right) \tag{5-18b}$$

Substitute Eqs (5-14) and (5-18) into Eq.(5-6a) to give

$$u'_{zl} = \delta_0 \frac{I_0(kr)}{I_1(kR_o)} \left(i\frac{d\omega(t)}{dt} - k\bar{u}_z \right) e^{ikz+\omega(t)} \tag{5-19a}$$

and

$$u'_{zg} = -\delta_0 \frac{K_0(kr)}{K_1(kR_o)} \left(i\frac{d\omega(t)}{dt} - k\bar{u}_z \right) e^{ikz+\omega(t)} \tag{5-19b}$$

Using Eqs (5-19) in the perturbed z-momentum equation, Eq.(5-9), gives for the liquid and gas, respectively, the following

$$\frac{\partial p'_l}{\partial z} = \rho_l \delta_0 \frac{I_0(kr)}{I_1(kr)} \left\{ -i\frac{d^2\omega(t)}{dt^2} + k\frac{d\bar{u}_{zl}}{dt} - i\left(\frac{d\omega(t)}{dt} \right)^2 + 2k\bar{u}_{zl}\frac{d\omega(t)}{dt} + ik^2\bar{u}_{zl}^2 \right\} e^{ikz+\omega(t)} \tag{5-20a}$$

and

$$\frac{\partial p'_g}{\partial z} = \rho_g \delta_0 \frac{K_0(kr)}{K_1(kr)} \left\{ i\frac{d^2\omega(t)}{dt^2} - k\frac{d\bar{u}_{zg}}{dt} + i\left(\frac{d\omega(t)}{dt} \right)^2 - 2k\bar{u}_{zg}\frac{d\omega(t)}{dt} - ik^2\bar{u}_{zg}^2 \right\} e^{ikz+\omega(t)} \tag{5-20b}$$

Subtract the gas phase equation, Eq.(5-20b), from the liquid phase equation, Eq.(5-20a), to obtain:

$$\frac{\partial(p_l' - p_g')}{\partial z} = \begin{pmatrix} \rho_l \frac{I_0(kr)}{I_1(kr)}\left\{-i\frac{d^2\omega(t)}{dt^2} + k\frac{d\bar{u}_{zl}}{dt} - i\left(\frac{d\omega(t)}{dt}\right)^2 + 2k\bar{u}_{zl}\frac{d\omega(t)}{dt} + ik^2\bar{u}_{zl}^2\right\} \\ -\rho_g \frac{K_0(kr)}{K_1(kr)}\left\{i\frac{d^2\omega(t)}{dt^2} - k\frac{d\bar{u}_{zg}}{dt} + i\left(\frac{d\omega(t)}{dt}\right)^2 - 2k\bar{u}_{zg}\frac{d\omega(t)}{dt} - ik^2\bar{u}_{zg}^2\right\} \end{pmatrix} \delta_0 e^{ikz+\omega} \tag{5-21}$$

On the dynamic boundary condition, Eq.(5-4b), noting Eq.(5-6c) and that $(\bar{p}_l - \bar{p}_g)\big|_{r=R_0} = \frac{\sigma(z)}{R_0}$ for unperturbed state, gives

$$\frac{\partial(p_l' - p_g')}{\partial z} = \left(\frac{\partial\sigma(z)}{\partial z} + ik\sigma(z)\right)\left(k^2 - \frac{1}{R_0^2}\right)\delta_0 e^{ikz+\omega(t)} \tag{5-22}$$

Combining Eqs (5-21) and (5-22); prescribing all parameters at the jet's surface, for an interfacial breakup mechanism and, thereafter, taking $\bar{u}_{zg} = 0$, which is the case for a quiescent ambient condition here considered (henceforth $\bar{u}_{zl}$ becomes $\bar{u}_z$) give the dispersion equation as:

$$\begin{aligned} -i\left(\frac{I_0(kR_o)}{I_1(kR_o)}\rho_l + \frac{K_0(kR_o)}{K_1(kR_o)}\rho_g\right)\left[\frac{d^2\omega(t)}{dt^2} + \left(\frac{d\omega(t)}{dt}\right)^2\right] \\ + \frac{I_0(kR_o)}{I_1(kR_o)}\rho_l\left[k\frac{d\bar{u}_z}{dt} + 2k\bar{u}_z\frac{d\omega(t)}{dt} + ik^2\bar{u}_z^2\right] \\ -\left(\frac{\partial\sigma(z)}{\partial z} + ik\sigma(z)\right)\left(k^2 - \frac{1}{R_0^2}\right) = 0 \end{aligned} \tag{5-23}$$

As in spraying systems' operating conditions short waves (in comparison to jet radius) are expected, $kR_o \to \infty$, hence Eq.(5-23) is approximated to become

$$-i(\rho_l+\rho_g)\left[\frac{d^2\omega(t)}{dt^2}+\left(\frac{d\omega(t)}{dt}\right)^2\right]+\rho_l\left[k\frac{d\bar{u}_z}{dt}+2k\bar{u}_z\frac{d\omega(t)}{dt}+ik^2\bar{u}_z^2\right] - \left(\frac{\partial\sigma(z)}{\partial z}+ik\sigma(z)\right)\left(k^2-\frac{1}{R_0^2}\right)=0 \quad (5\text{-}24)$$

For the accelerating non-isothermal jets of practical interest, it is taken that typical breakup time (of a jet element at nozzle tip) is small, so that jet's bulk velocity (and acceleration) variation in that period can be neglected.

Typical wave growth velocity:

$$v\approx\frac{1}{k}max\left\{Re\left(\frac{d\omega(t)}{dt}\right)\right\} \quad (5\text{-}25)$$

Typical breakup time is taken as:

$$\Delta t\approx\frac{R_o}{v} \quad (5\text{-}26)$$

The assumption above is state in the view of:

$$\frac{d\bar{u}_z}{dt}.\Delta t\ll\bar{u}_z, \text{ and } \frac{d^2\bar{u}_z}{dt^2}.\Delta t\ll\frac{d\bar{u}_z}{dt} \quad (5\text{-}27)$$

Therefore, for the accelerating non-isothermal jets of interest, relevant instability and breakup can be analysed for instantaneous constant jet velocity and jet acceleration:

$$\bar{u}_z\approx const.,\frac{d\bar{u}_z}{dt}\approx const.=a \quad (5\text{-}28)$$

Then, the solution for the dispersion equation, Eq.(5-24), should occur at $\frac{d\omega(t)}{dt}\rightarrow const.$, (with $\frac{d^2\omega(t)}{dt^2}=0$), therefore,

$$\frac{d\omega(t)}{dt} = -i\frac{\rho_l k\bar{u}_z}{(\rho_l+\rho_g)} \pm \left\{ \frac{\rho_l\rho_g k^2\bar{u}_z^2 - (\rho_l+\rho_g)k\sigma\left(k^2-\frac{1}{R_0^2}\right)}{(\rho_l+\rho_g)^2} - \frac{i(\rho_l+\rho_g)\left[\rho_l ka - \left(k^2-\frac{1}{R_0^2}\right)\frac{d\sigma(z)}{dz}\right]}{(\rho_l+\rho_g)^2} \right\}^{1/2} \quad (5\text{-}29)$$

Eq.(5-29) represents complex growth rate, $\omega' = \omega_r' + i\omega_i'$, where its real part ω_r' represents the growth or decay rates of the disturbance. On the frame of temporal analysis of the present work, one seeks complex solutions of ω' to the dispersion relation for any given real wavenumber, k. Therefore, the real part of $\omega' = \omega_r' + i\omega_i'$ represents the growth rate of the disturbance, which indicates the degree of instability of the liquid jet. In view of the foregoing, Eq.(5-30) is obtained, after a considerable algebraic exercise and rearrangement, as:

$$Re(\omega') = \frac{2^{-1/2}}{(\rho_l+\rho_g)}\left(\left(\left[\rho_l\rho_g k^2\bar{u}_z^2 - (\rho_l+\rho_g)k\sigma\left(k^2-\frac{1}{R_0^2}\right)\right]^2 + \left[(\rho_l+\rho_g)\left(\rho_l ka - \left(k^2-\frac{1}{R_0^2}\right)\frac{d\sigma(z)}{dz}\right)\right]^2\right)^{1/2} + \rho_l\rho_g k^2\bar{u}_z^2 - (\rho_l+\rho_g)k\sigma\left(k^2-\frac{1}{R_0^2}\right)\right)^{1/2} \quad (5\text{-}30)$$

Eq.(5-30) features two important parameters of practical interest (jet acceleration and surface tension gradient), which have not been simultaneously considered in the majority of the literature.

The coupling of the hydrodynamic analysis and the heat transfer is achieved through the surface tension gradient, $d\sigma/dz$, see details in §4.2.3.

In most liquid breakup applications, the drop size, the jet breakup length and the breakup frequency spectrum are most pertinent. This information could be gotten from the instability analysis, which is the practice, on the assumption that

the most unstable wave with initial disturbance amplitude, δ_o, grows exponentially to a magnitude equal to radius, R_o, in time, t^*, with the typical breakup length, L_{bu}, being estimated as:

$$L_{bu} = \frac{\bar{u}_z}{\omega'_{max}} \ln\left(\frac{R_0}{\delta_0}\right) \tag{5-31}$$

Eq.(5-31) is satisfactory in the current analysis, as the perturbations earlier postulated enable time dependency of perturbation.

Figure 5-2 shows cylindrical liquid jet instability and breakup under accelerated and non-isothermal conditions at injection velocity of 300[m/s]. Pertinent parameters used for Figure 5-3 and Figure 5-2 are: injector radius ($R_0 = 0.003$[m]), liquid density ($\rho_l = 1000$[kg/m3]), gas density ($\rho_g = 40$[kg/m3]), surface tension ($\sigma = 0.24$[N/m]) and surface tension gradient (200[Pa]), which is carefully computed based on typical average operating conditions in internal combustion engine, see Chapter 4 for details.

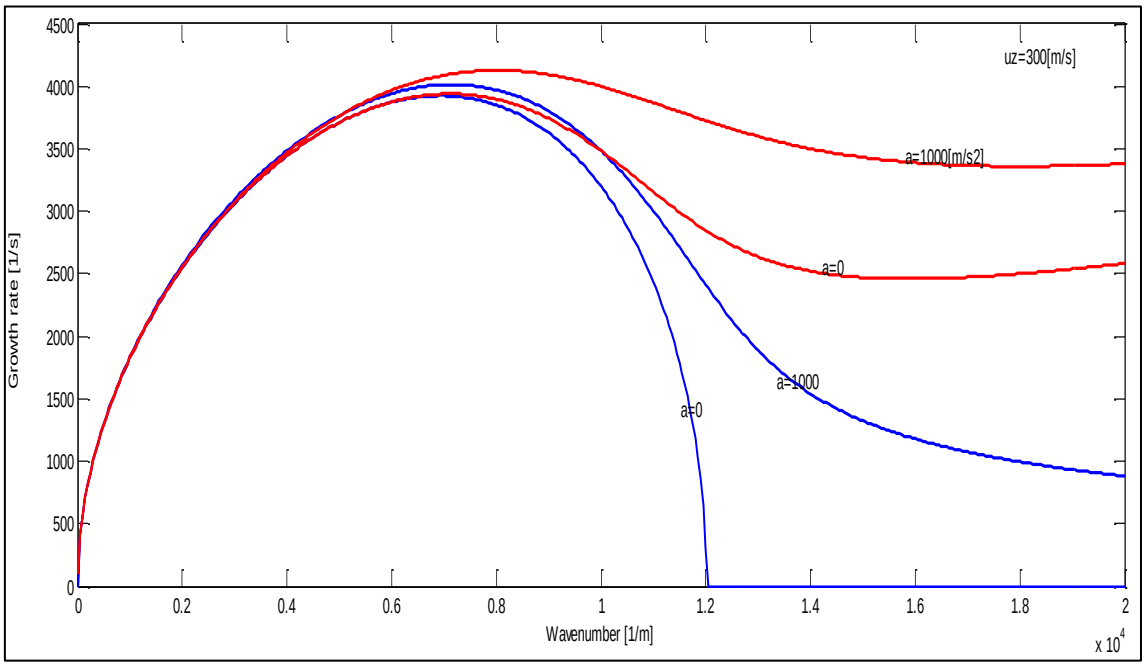

Figure 5-2 Effects of Acceleration (a = 0, 1000[m/s^2]) and Surface Tension Gradient (200[Pa]) on Liquid Jet Instability and Breakup at Injection Velocity of 300[m/s]

The blue lines, in Figure 5-2 and Figure 5-3, indicate a wholly accelerated jet breakup case, whereas the red lines indicate simultaneous consideration of non-isothermal condition (surface tension gradient) and accelerated condition. It is observed from the figures (Figure 5-2 and Figure 5-3) that increasing the acceleration shifts the wavenumber spectrum, which indicates droplet distribution, to the right with higher breakup rate (since growth rate is a measure of instability).

The trend is maintained with the consideration of the surface tension gradient; however, corresponding parameters are higher. Most significantly is the broader wavenumber spectrum which may be attributed to combine jet thinning, caused by jet acceleration, and modified intermolecular forces, caused by surface tension modification by heat transfer at liquid jet interface. Thus, inconsistencies between experimental and simulations results, as observed in Dumouchel, (2008), may be attributed to the failure of existing models to simultaneously consider acceleration and surface tension gradient.

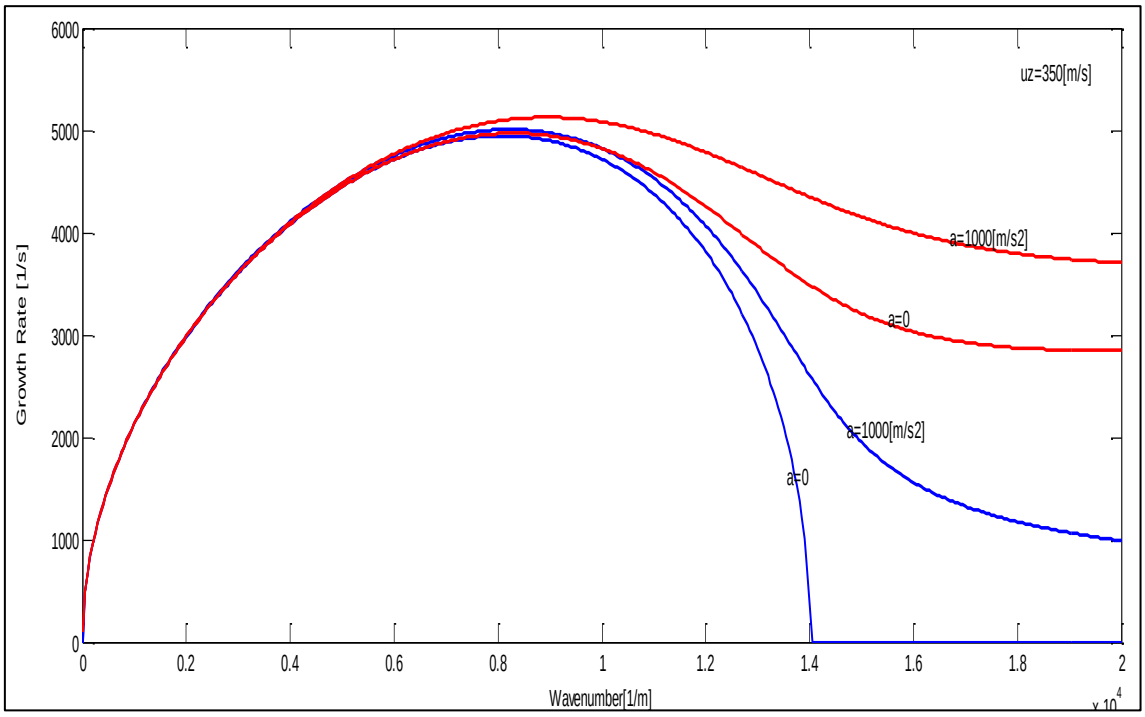

Figure 5-3 Effects of Acceleration (a = 0, 1000[m/s^2]) and Surface Tension Gradient (200[Pa]) on Liquid Jet Instability and Breakup at Injection Velocity of 350[m/s]

Figure 5-3 is similar to Figure 5-2, but with higher injection velocity (350[m/s]). The maximum growth rate and the corresponding wavenumber show higher values, compared to Figure 5-2. This observation indicates that increasing the injection velocity increases the disturbance growth rate as a result of increased relative velocity, which exemplify the classical theory (Lefebvre, 1989)

Figure 5-4 shows the effects of acceleration and non-isothermal condition (measured by surface tension gradient) on liquid jet breakup length. The figure shows a decreased breakup length with increasing jet acceleration. However, the breakup length shows little variation as acceleration approaches higher values, which may be attributed to the thinning effect of accelerated jet (Domann and Hardalupas, 2004) and, ultimately, to the too large interfacial breakup response timescale compare to velocity change timescale at high acceleration. This observation is in qualitative agreement with numerical observations under the isothermal condition of Domann and Hardalupas (2004). The figure indicates that the accelerated non-isothermal jet shows lower breakup length, over the accelerated isothermal jet, at relatively low jet accelerations; whereas higher breakup length is observed at relatively high jet accelerations. In general, it is observed, on the average, that the accelerated non-isothermal jet has a higher breakup length over the accelerated isothermal jet, which may be attributed to the modification of the surface tension that controls the interfacial liquid jet breakup, as interfacial forces may resist the jet thinning caused by the jet acceleration.

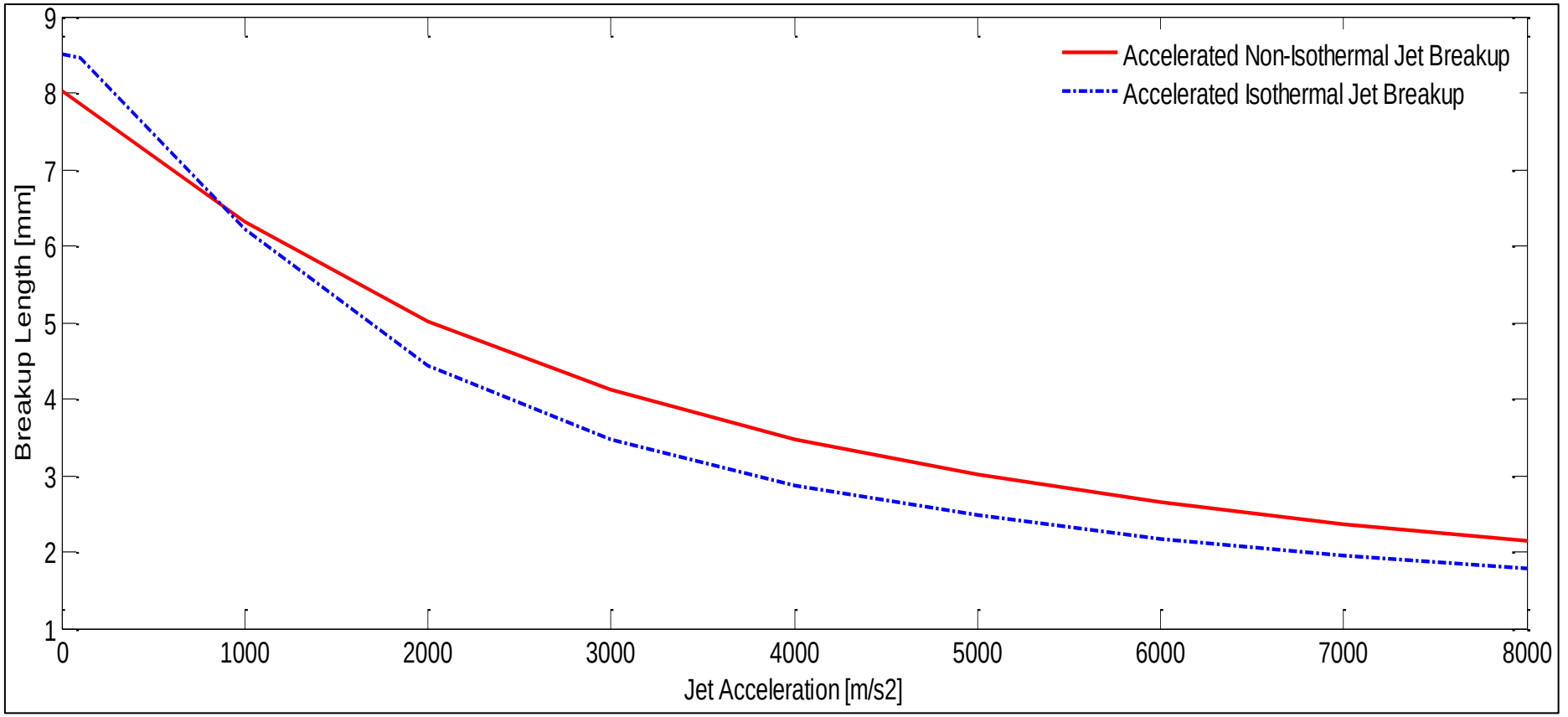

Figure 5-4 Effects of Acceleration and Non-Isothermal Condition on Liquid Breakup Length at Average Injection Parameters: σ=0.024[N/m], dσ/dz=200[Pa], ρ_l=900 [kg/m^3], ρ_g=900 [kg/m^3], R_0=0.003[m]

The findings imply that transient effects and non-isothermal condition have impact on liquid jet breakup. This may be attributed to some of the discrepancies between experimental results and CFD simulations for liquid jet breakup (Dumouchel, 2008), since it is presently difficult to consider both transient effect and non-isothermal condition in a single simulation.

5.4 Accelerated Isothermal Jet Approximation

For the accelerated isothermal case, $\sigma(z) = \sigma = const. \implies \frac{\partial \sigma'(z)}{\partial z} = 0$, therefore, for this case Eq.(5-30) is simplified to:

$$Re(\omega') = \frac{2^{-1/2}}{(\rho_l + \rho_g)} \left(\left(\left[\rho_l \rho_g k^2 \bar{u}_z^2 - (\rho_l + \rho_g) k\sigma \left(k^2 - \frac{1}{R_0^2} \right) \right]^2 + \left[(\rho_l + \rho_g) \rho_l k a \right]^2 \right)^{1/2} + \rho_l \rho_g k^2 \bar{u}_z^2 - (\rho_l + \rho_g) k\sigma \left(k^2 - \frac{1}{R_0^2} \right) \right)^{1/2} \quad (5\text{-}32)$$

Eq.(5-32) is similar to Eq.(3-23), which presents instability and breakup model for transient jets already treated in Chapter 3.

5.5 Steady Non-isothermal Jet Approximation

For the steady non-isothermal case, $\bar{u}_z = const. \implies a \equiv \frac{d\bar{u}_z}{dt} = 0$, therefore, for this case Eq.(5-30) is simplified to:

$$Re(\omega') = \frac{2^{-1/2}}{\left(\rho_l + \rho_g\right)}\left(\left(\left[\rho_l\rho_g k^2\overline{u}_z^2 - \left(\rho_l + \rho_g\right)k\sigma\left(k^2 - \frac{1}{R_0^2}\right)\right]^2 + \left[\left(\rho_l + \rho_g\right)\left(k^2 - \frac{1}{R_0^2}\right)\frac{d\sigma(z)}{dz}\right]^2\right)^{1/2} + \rho_l\rho_g k^2\overline{u}_z^2 - \left(\rho_l + \rho_g\right)k\sigma\left(k^2 - \frac{1}{R_0^2}\right)\right)^{1/2} \quad (5\text{-}33)$$

Eq.(5-33) is similar to Eq.(4-20), which presents instability and breakup model for steady non-isothermal jets already treated in Chapter 4.

5.6 Conclusion of Chapter Five

The theory of liquid jet instabilities has been developed under several assumptions, which include the assumption that the jets breakup processes are quasi-steady and isothermal. Accelerated liquid fuels are normally injected into an elevated combustion-chamber temperature to maintain a desirable homogeneous combustible mixture – liquid vapour and air. The accelerated jet breakup may be induced by cavitation, turbulent, hydrodynamic and aerodynamic forces interaction and variation in fluid properties. The absolute majority of studies have been devoted to the extensive study on some of the effects that cause jet instability and breakup, while others are still at their infant study. In particular, relatively few researchers have studied the combined effects of jet acceleration and non-isothermal condition on jet instability and breakup, despite its practical relevance in liquid fuel spray and combustion. Specifically, liquid fuel jets are highly transient under pulsed injection technique, which has been demonstrated to maintain better fuel economy and emissions reduction. Liquid jet acceleration and non-isothermal conditions have a significant role in the breaking of interfacial surfaces.

A new analytical hydrodynamic instability and breakup model, which captured both jet acceleration and non-isothermal condition, for liquid jet is presented. The analytical model investigates the impact of two important phenomena on liquid jet instability and breakup; jet acceleration and non-isothermal conditions.

These effects are naturally difficult to address by both experimental and CFD investigations. The new model analysis combined both hydrodynamic model and heat transfer equations, coupled through the surface tension gradient, and is a novel address of this conjugated problem. Continued modelling in that area may benefit the development of the next generation of liquid fuel injectors and combustors, as simplified models have a qualitative agreement with experimental results.

6 A MECHANISTIC MODEL FOR THE BREAKUP LENGTH IN JET BREAKUP

6.1 Background

The breakup of bulk liquid, which may be a jet, sheet or film, is a result of several complex physical interactions: aerodynamic, surface tension, viscous and inertial. These determine the breakup characteristics, namely, breakup time and length, droplet size, spray angle and velocity distribution. An understanding of the interaction is crucial to the characterisation of the breakup mechanism. Much experimental work on primary breakup of liquid streams of Newtonian fluids free of external forcing has been reviewed in Dumouchel (2008). Amongst the properties of breaking jets of most interest are the breakup length and the drop size. The graphical representation of the breakup length, which defines the primary breakup and secondary breakup regions, and the injection velocity, mostly referred to as the stability curve, is illustrated in Figure 2-3. The figure indicates the Rayleigh, first-wind induced or wind assisted, second-wind induced and atomisation regime of primary breakup.

There are divided opinions regarding the predominant breakup mechanisms for the atomisation regime, which include: aerodynamics interaction (Turner et al. 2012), turbulence (Trinh and Chen, 2006) and cavitaion (Andriotis, Gavaises and Arcoumanis, 2008). Given the uncertain detailed mechanisms of the atomisation regime, some workers in this field assert that the jet breakup length increases with increasing velocity (Shibata, Koshizuka and Oka, 2004), while others (Gulder, Smallwood and Snelling 1992; Lasheras and Hopfinger, 2000) have suggest that the breakup is right at the nozzle exit, therefore, breakup length is negligible. However, there is a strong experimental evidence, which suggests that the atomisation regime breakup length at low velocity is comparable to the jet diameter (Yule and Salters, 1995; Dumouchel, 2001). Hiroyasu and Arai (1990) investigated the structures of fuel sprays in diesel engine in the near-injector region of the flow and suggest liquid core length, which is the breakup length, exists. Experimental measurements have contributed significantly to the understanding and development of empirical and

semi-empirical models for the breakup length (Sallam et al., 1999, 2002; Siebers, 1999).

Based on extensive experimental data, liquid breakup length correlations for turbulent jets are mainly grouped into three categories (Lee et al., 2007), as follows: (a) the onset of turbulent primary breakup along the liquid surface (b) the end of turbulent primary breakup along the liquid surface and (c) breakup of the entire liquid column as a result of the turbulent primary breakup mechanism, the atomisation regime. The widely accepted and used empirical correlation for breakup length in breakup of the entire liquid column due to the turbulent primary breakup mechanism is the one introduced by Wu and Faeth (1995), which was also verified in Sallam et al. (2002):

$$L_{bu}^{*} = \frac{L_{bu}}{d_j} = 9.37 We_0^{0.34} \qquad (6\text{-}1)$$

where L_{bu}^{*} is the dimensionless breakup length, L_{bu} is the breakup length, d_j is the nozzle exit diameter and $We_0 \equiv \rho_j r_j U_0^2/\sigma$ is the Weber number of the jet; also, ρ_j is the density of the liquid jet, U_0 is the jet velocity at the nozzle exit andσ is the surface tension of the liquid jet.

The Wu and Faeth (1995) empirical breakup length correlation offers good predictive performance despite the fact it doesn't account for aerodynamic interactions of the jet with the surrounding gas, nor for any viscous effects.

The following suggested model offers a mechanistic model based theoretical breakup length, that accounts for the jet's aerodynamic drag (by surrounding gas), complementing the classical viscous hydrodynamic instability breakup model. This is necessary because CFD investigations are complemented by semi-empirical relations (Kalaaji et al., 2003), which in most cases limit parametric investigations.

6.2 Modelling of Breakup Length of the Atomisation Regime

The considered problem is illustrated in Figure 6-1a. The control volume is defined to include the intact segment of the jet, just down to the breaking tip. The momentum balance on that control volume is illustrated in Figure 6-1b.

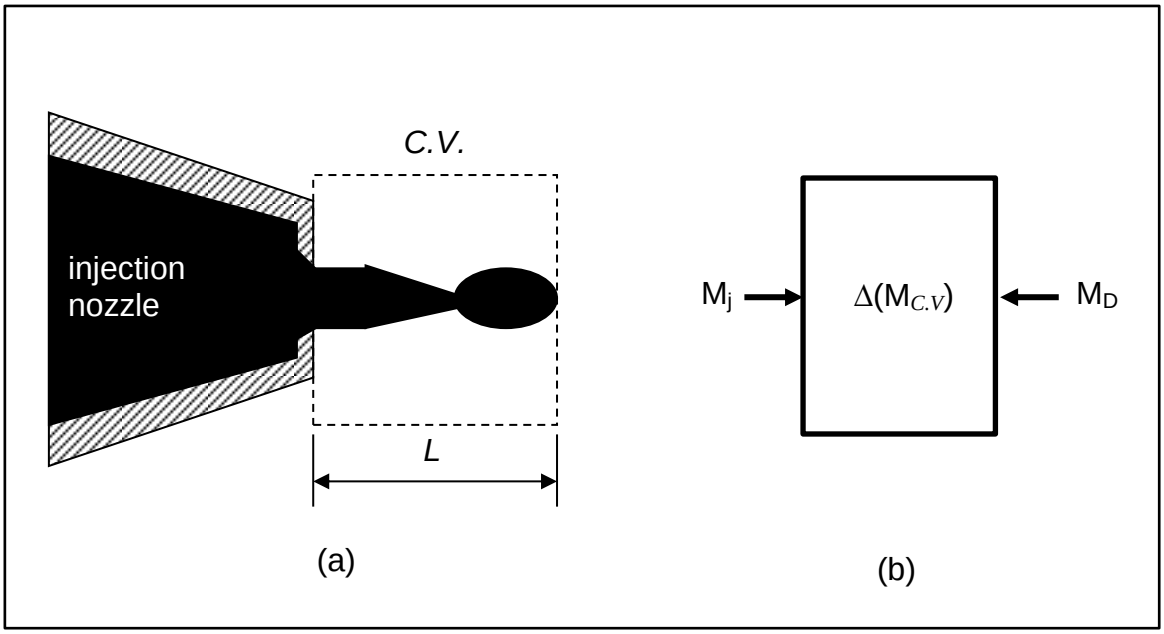

Figure 6-1 The Atomisation Processes of a Cylindrical Jet (a) C.V on the Jet (b) Momentum Balance on the C.V.

The horizontal momentum balance on the C.V of a cylindrical liquid column jet gives:

$$\Delta(M_{C.V}) = M_j - M_D \qquad (6\text{-}2)$$

where M_j is the jet momentum rate entering the control volume, $\Delta(M_{C.V})$ is the rate change of C.V momentum and M_D is the drag rate of momentum on the dynamic C.V. It is assumed that no liquid is detaching from the jet core, other than at the breakup tip.

Explicitly expressing the terms in Eq.(6-2), one arrives at Eq.(6-3)

$$\frac{d(mU)_{c.v}}{dt} = \pi\rho_j r_j^2 U_0^2 - \frac{1}{2}\rho_g C_D A_f U^2 \qquad (6\text{-}3)$$

where m is mass of the jet, U_0 is injection velocity, ρ_g is density of the gas, A_f is the frontal area, C_D is the drag coefficient, t is time and U is the axial velocity of jet.

Expanding Eq.(6-3) and assuming the frontal area of the moving jet is hemispherical:

$$U\frac{dm}{dt} + m\frac{dU}{dt} = \pi\rho_j r_j^2 U_0^2 - \rho_g C_D \pi r_j^2 U^2 \tag{6-4}$$

The mass in the control volume at a given time is $m = \rho_j \pi r_j^2 L(t)$, where ρ_j is the density of liquid, r_j is the radius of jet and $L(t)$ is the distance travelled by the jet from the nozzle exit, which is a function of time. Substituting for mass in Eq.(6-4) and simplifying the resulting equation, one obtains Eq.(6-5):

$$\frac{1}{L}dL + \frac{1}{U}dU = \frac{U_0^2}{UL}dt - \frac{\rho_g}{\rho_j}C_D\frac{U}{L}dt \tag{6-5}$$

Letting $U \equiv \frac{dL}{dt}$ in Eq.(6-5)and simplifying the resulting equation, one obtains:

$$\frac{U}{U_o^2 - U^2\left(\frac{\rho_g}{\rho_j}C_D + 1\right)}dU = \frac{1}{L}dL \tag{6-6}$$

Integrating Eq.(6-6), gives:

$$\frac{1}{-2\left(\frac{\rho_g}{\rho_j}C_D + 1\right)}\ln\left[\frac{U_o^2 - U^2\left(\frac{\rho_g}{\rho_j}C_D + 1\right)}{-\frac{\rho_g}{\rho_j}C_D U_o^2}\right] = \ln\frac{L}{\varphi} \tag{6-7}$$

where φ is an integration constant, which may be taken to account for nozzle discharge characteristics, e.g discharge coefficient.

In the case of liquid injection into gas ambient, $\rho_j \gg \rho_g$ can be assumed. That gives $\frac{\rho_g}{\rho_j}C_D \ll 1$, and therefore, Eq.(6-7) could be simplified to yield:

$$U_{bu}^2 - \frac{\rho_g}{\rho_j}C_D U_o^2 \varphi^2 L_{bu}^{-2} = U_o^2 \tag{6-8}$$

where the indices bu and *0* stand for parameters at breakup and parameters at nozzle exit, respectively.

Also, making the estimation of: $U_{bu} \approx L_{bu}/t_{bu}$, Eq.(6-8) becomes:

$$L_{bu}^4 - U_o^2 t_{bu}^2 L_{bu}^2 - \frac{\rho_g}{\rho_j} C_D U_o^2 \varphi^2 t_{bu}^2 = 0 \tag{6-9}$$

Solving Eq.(6-9) for L_{bu} one gets:

$$L_{bu} = \frac{U_o t_{bu}}{\sqrt{2}} \left(1 + \varphi \frac{\left(\left(\frac{U_o t_{bu}}{\varphi} \right)^2 + 4 \frac{\rho_g}{\rho_j} C_D \right)^{1/2}}{U_o t_{bu}} \right)^{1/2} \tag{6-10}$$

The breakup time, t_{bu}, was estimated for turbulent round liquid jets (Lee et al., 2007):

$$t_{bu} \sim 2^{3/2} \left(\frac{\rho_j r_j^3}{\sigma} \right)^{1/2} + Oh 6 r_j^{3/2} \sqrt{\frac{\rho_j}{\sigma}} \tag{6-11}$$

where $Oh = \mu_j / \sqrt{\rho_j r_j \sigma}$ is the Ohnesorge number.

The breakup time is on the consideration given to convection of ligament along surface of a turbulent liquid jet, and the effect of liquid viscosity to increase breakup, for the hydrodynamic instability breakup to form a ligament that is ready to produce a drop.

Substituting Eq.(6-11) into Eq.(6-10), the dimensionless breakup length, L_{bu}^* is obtained:

$$L_{bu}^* = \frac{We_0^{1/2} \left(6Oh + 2^{3/2} \right)}{2^{3/2}} \left(1 + \frac{\left(We_0 \left(6Oh + 2^{3/2} \right)^2 + 4 \frac{\rho_g}{\rho_j} C_D \varepsilon^2 \right)^{0.5}}{We_0^{1/2} (6Oh + 2^{3/2})} \right)^{0.5} \tag{6-12}$$

Where $We_0 \equiv \frac{U_0^2 \rho_j r_j}{\sigma}$ is the Weber number at the nozzle exit and $\varepsilon \equiv \frac{\varphi}{r_j}$ is the non-dimensionalised integration constant.

A simplification could be made for an inviscid case. By letting $Oh \to 0$, Eq.(6-12) is simplified:

$$L_{bu}^{*} = We_0^{0.25}\left(We_0^{0.5} + 0.71\left(2We_0 + \frac{\rho_g}{\rho_j} C_D \varepsilon^2\right)^{0.5}\right)^{0.5} \quad (6\text{-}13)$$

6.3 Results and discussion

The developed model was validated with the experimental data on the breakup of cylindrical liquid jets presented in Dumouchel (2001). Dumouchel (2001) investigated water, CSL2 and mixture of Methanol/glycerol liquid jets breakup length with the liquid jets properties, shown in Table 6-1., and nozzle diameter of 4.0×10^{-4} [m]. It is noted that CSL2 is a non-flammable liquid with properties similar to gasoline.

Figure 6-2, Figure 6-3 and Figure 6-4 show the model results for breakup length as function of the Weber number, compared to experimental data, and to Wu and Faeth's (1995) correlation, for water, CSL2 and Methanol/glycerol, respectively. C_D was taken as 0.5 and phi as 2.51. It is noted that the proposed model is in good agreement with the Water and CSL2 experimental data (Figure 6-2 and Figure 6-3), and with Wu and Faeth's empirical correlation for the atomisation regime (of the stability curve, see Figure 2-3). Typically, the liquid jet atomisation region has a limit of $1.0 \times 10^2 \leq We_0 \leq 1.1 \times 10^6$, according to the experimental investigation of Wu and Faeth (1995). However, both the proposed model and Wu and Faeth's empirical correlation show a poor agreement with the methanol/glycerol experimental data (see Figure 6-4); this may be attributed to significant deviation in nozzle internal flow characteristic, for example discharge coefficient (C_d), as shown in Table 6-1. Ultimately, as expected, the deviation may also be attributed to surface tension behaviour of

binary liquids, which is fundamentally different to that of pure liquids in a dynamic system (a phenomenon referred to as dynamic surface tension, see Fang and Joos (1992)).

The discharge coefficient is a characteristic that is used to measure the issuing jet velocity as function of the injection pressure. The discharge coefficient is obtained, according to Dumouchel (2001), by weighing the mass of liquid collected during a controlled time interval. The discharge coefficient is thus defined by:

$$C_d \equiv \frac{\dot{Q}}{\pi r_j^2}\left(\frac{\rho_j}{2\Delta p_i}\right)^{0.5} \tag{6-14}$$

where $\dot{Q}$ and Δp_i are the liquid volume flow rate and injection pressure, respectively.

The discharge coefficient gives an indication of the loss of energy concentrated in the injector, and is usually independent of the injection pressure. The coefficient allows the estimation of the issuing mean velocity or the volume flow rate for a given injection pressure to be possible.

However, increasing the value of phi to 50 sees the model having agreement with the experimental data (see Figure 6-5). This observation shows that the breakup length may be dependent on the internal nozzle flow, as it was herein postulated that phi may account for internal nozzle flow. In fact, the postulation is plausible as the model predicted experimental data with close discharge coefficient at phi of 2.51, whereas phi of 50 for a relative deviation in discharge coefficient (see Table 6-1). It, therefore, offers a theoretical modelling framework for the prediction of the breakup length for both pure liquid and liquid mixture.

Table 6-1 Liquid Input Data Dumouchel (2001)

S/No	Liquid	Property				
		Discharge Coefficient [-]	ρ_L [kg/m^3]	μ [kg/ms]	σ [N/m]	Oh [-]
1	Water	0.84	995	1.0×10^{-3}	7.3×10^{-2}	0.0059
2	CSL2	0.83	760	9.5×10^{-4}	2.4×10^{-2}	0.0111
3	Methanol/glycerol	0.62	990	1.1×10^{-2}	3.44×10^{-2}	0.0942

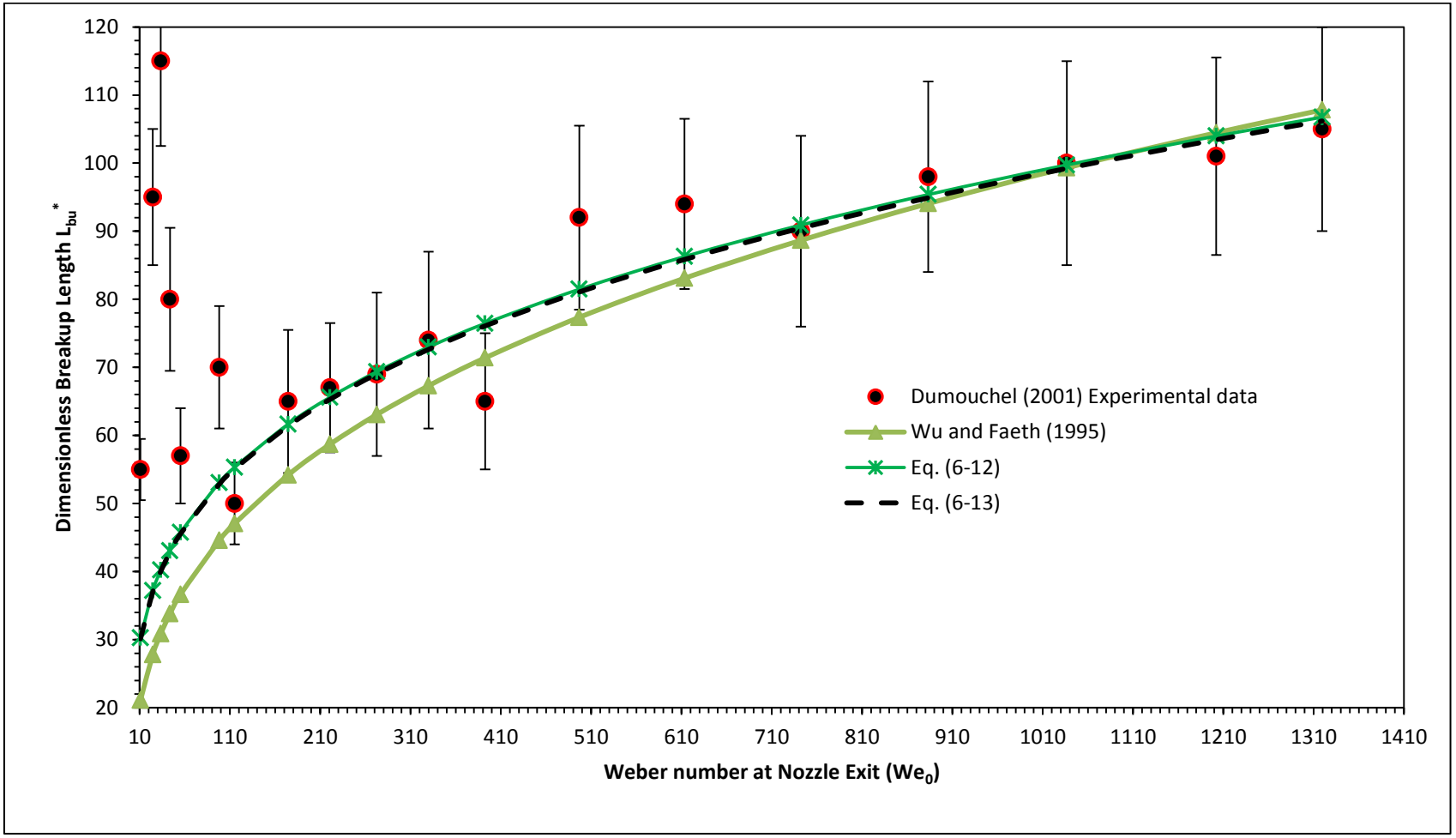

Figure 6-2 Stability Curve for Water: Experimantal Data, Empirical Correlation (Eq (6-1)), and Present Model Predictions (Eqs(6-12) and (6-13))

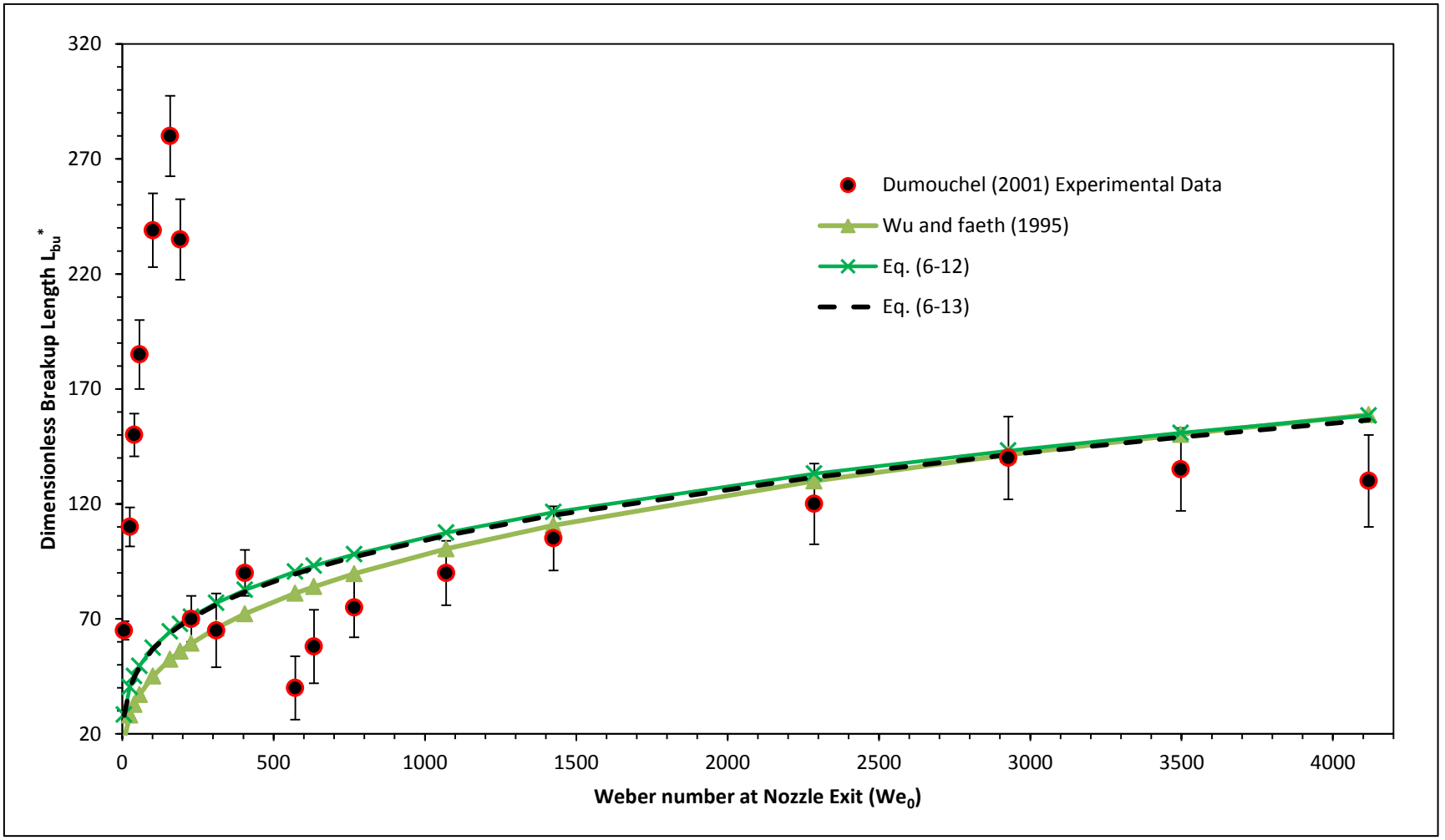

Figure 6-3 Stability Curve for CSL2: Experimantal Data, Empirical Correlation (Eq (6-1)), and Present Model Predictions (Eqs(6-12) and (6-13))

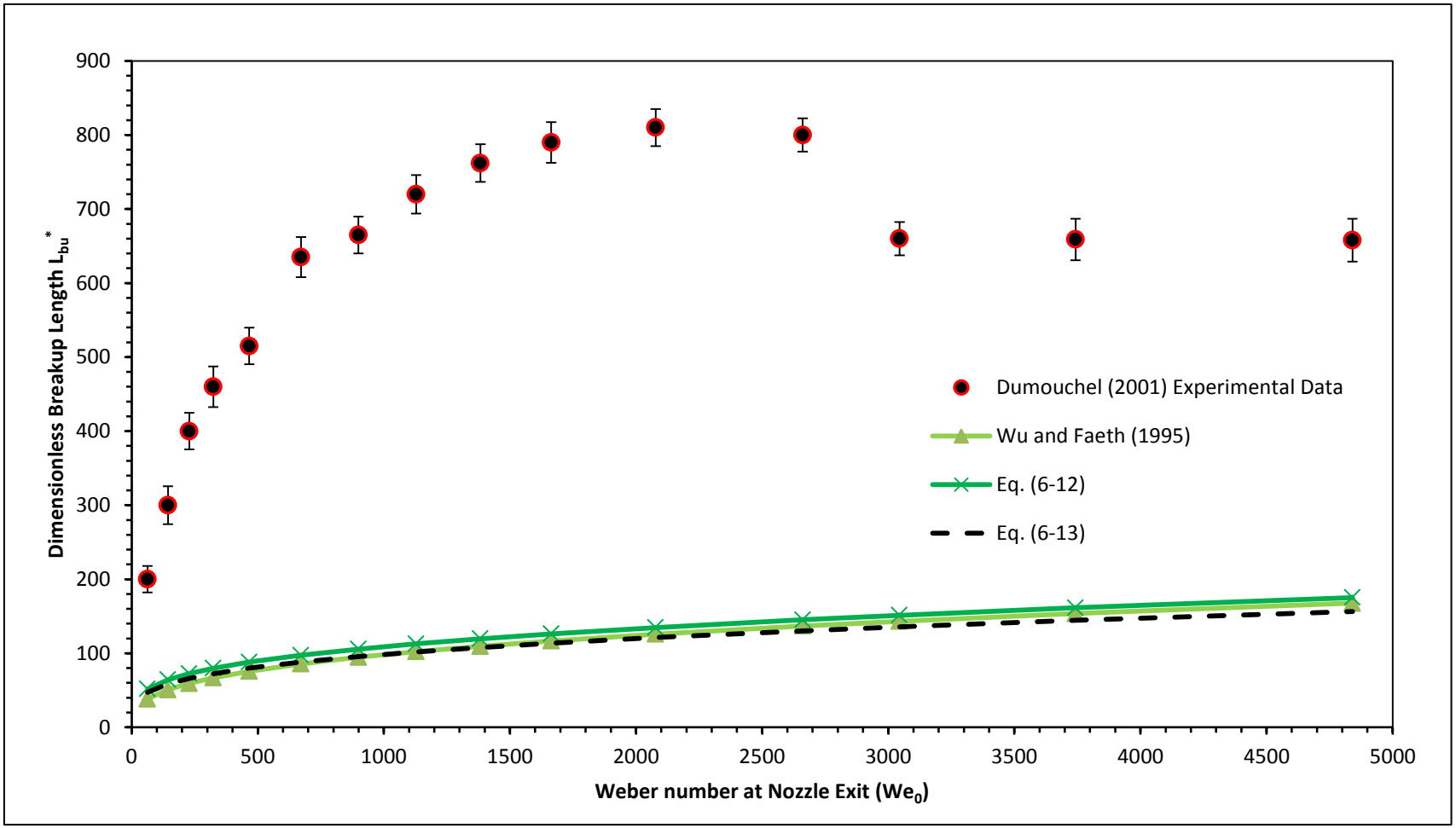

Figure 6-4 Stability Curve for Methanol/Glycerol: Experimantal Data, Empirical Correlation (Eq (6-1)), and Present Model Predictions (Eqs(6-12) and (6-13)): with phi 2.51

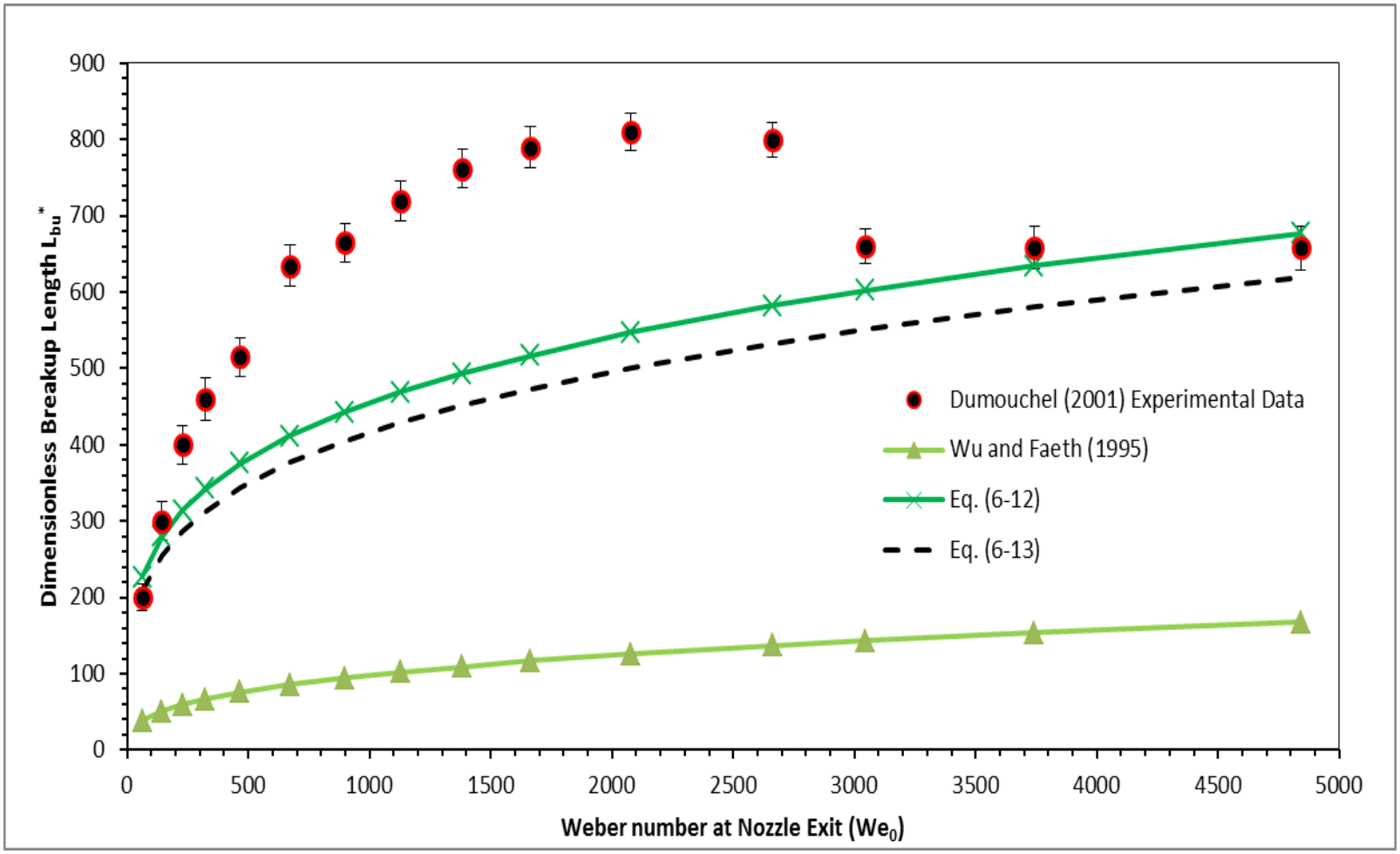

Figure 6-5 Stability Curve for Methanol/Glycerol: Experimantal Data, Empirical Correlation (Eq (6-1)), and Present Model Predictions (Eqs(6-12) and (6-13)): with phi 50

Results shown in Figure 6-2 and Figure 6-3 indicate that the inviscid simplification may be plausible for pure liquid fuel injections in high rate injection applications.

6.4 Conclusion of Chapter Six

The suggested model offers a basic mechanistic approach to the breakup length prediction, based on a simple momentum balance between the injected jet and the aerodynamic drag force due to the surrounding gas, which complements the classic hydrodynamic instability breakup mechanism. Hydrodynamic instability theory is often complemented by semi-empirical relations for it to predict the breakup length (Kalaaji et al., 2003). This model offers a simple complementing mechanistic model for that purpose, and it is shown that obtained results compare well with published experiments, and with the established empirical correlation of Wu and Faeth (1995). A simplified version of the model, taking into account an inviscid hydrodynamic model is shown to maintain plausibility of breakup length predictions in fuel-injection relevant conditions. Therefore, the model offers a theoretical modelling framework for the prediction of the breakup length. However, there is a significant coupling between the model constant parameter and the internal nozzle flow.

7 DROPLET BREAKUP IN SIMULTANEOUS LAMINAR DRAG AND TURBULENCE VORTEX

7.1 Background

The outcome of primary liquid breakup is relatively large parent droplets, which are subjected to further breakup by secondary breakup mechanisms caused by aerodynamic drag force and turbulence. The droplet breakup occurs first by deformation. However, breakup occurs if the droplet deformation goes beyond a certain limit. Droplet breakup is characterised, in the context of laminar flow, by five distinct breakup mechanisms: vibration, bag, transition, stripping and catastrophic; but a fundamentally different mechanism occurred for a turbulence flow field.

Droplet breakup mechanisms limits are mostly characterized in Weber number (We)-Ohnesorge number (Oh) representation (Reitz and Diwakar, 1986). According to the We-Oh representation, the critical Weber number found for low-viscosity liquids ranges from 7.2 to 16.8 (Reitz and Diwakar, 1986). Absolute majority of classical models for We-Oh droplet breakup criterion are empirically developed, which may be handicap for predictive purposes. However, analytical criterion for We-Oh droplet breakup presentation has been proposed by Sher and Sher (2012). The proposed analytical criterion has a good estimation of the droplet breakup limit despite its failure to capture turbulent effects, but it seems it is stressed for low We-Oh applications. It is expected that turbulence eddies may be introduced into the flow field, with the application of high-injection-pressure (HIP) fuel system in modern engines. Therefore, the total dependence on the classical We-Oh droplet breakup presentation might be constrained for non-entirely inertially-driven flow field, for example, the effects of turbulence flow field.

One of the significant developments in diesel direct injection (DDI) engines is the utilization of electronically controlled HIP fuel system, which is aimed at achieving high-power-density low-emission DDI engine (Jansons, Campbell and Rhee, 1998). In the HIP fuel system liquid fuel is injected at a very high

pressure, as high as near 200MPa and is expected to increase progressively (see Figure 2-7). The high pressure is later converted to a corresponding high velocity, at near sonic speed, by the injector nozzle, which gives rise to a turbulent flow field around droplets. Experimental work has shown the importance of flow field characteristics on droplet breakup (Wierzba, 1990). Further experimental results, for low Oh values, have shown that turbulence flow has a remarkable influence on the droplet breakup process in gaseous flow field (Previsch, 1998). It seems that existing We-Oh droplet breakup criterion models are inherently handicap for turbulence induced droplet breakup, which is expected in the modern DDI engines.

The prevalence of turbulent flow on droplet breakup has long been noted by Clift, Grace and Weber (1978), but recognised the inherent experimental difficulty to establish the relationship between droplet breakup and turbulent flow fields. The authors, however, noted two basic established conditions used in investigating droplet breakup in turbulence flow field: 1. breakup occurs when local shear stress imposed by the continuous-phase exceeds the surface tension and the disperse-phase dissipative viscous force; 2. breakup occurs only when the energy carried by eddies is smaller than droplet diameter. The turbulent eddies must exert sufficient stress to deform the fluid particle and also transfer sufficient energy to stretch the interfacial area (Andersson and Andersson, 2006). It is expected that for a droplet fragmentation to occur the turbulence lengthscale should be of the order of the droplet size. However, an order of magnitude analysis conducted to determine effects of different time and length scales on the breakup of droplet in turbulent flow fields shows that eddies in an order of magnitude larger than the droplet diameter are most significant and influential in droplet breakup (Previsch, 1998).

The breaking of a droplet is generally assumed to occur if Weber (We) > 12 – 13 (Stiesch, 2010; Faeth, 2002). The general criterion for droplet breakup holds only for the laminar flow around the droplet; hence, the breakup criterion may be changed considerably when a droplet is shot into a turbulent flow field, as the case for droplet instability and breakup in diesel sprays (Vuorinen et al.,

2010). This expectation is attributed to a wide range of dynamic forces due to the growing eddies (Vuorinen et al., 2010). Han, Luo and Liu (2011) have theoretically shown the prevalence of turbulent flow field on droplet breakup. Nevertheless, minimum breakup criterion for droplets in gaseous flow field has not been fully investigated. Moreover, there has been no consensus in droplet breakup criterion from CFD simulations of spray flows, especially in turbulent flow fields, see Liao and Lucas (2009), Vuorinen et al. (2010) and Han et al. (2011) for a complete review.

There is inherent difficulty to experimentally and analytically capture all the phenomena of droplet breakup in turbulence flow field. This difficulty and some other inherent advantages have necessitated many researchers in the field to resort to CFD applications Han et al. (2011). It is important to note that some important specific details of the atomisation process can be achievable through the use of simplified basic mathematical models. Therefore, in this chapter, a simplified mathematical model for the critical Weber number, which accounts for the turbulent effects, is developed. The proposed model differs from previous analytical models in its physics – consideration of energy criterion and dual-timescale for turbulent energy transfer in droplet dispersion.

7.2 Mathematical modelling

The fate of a droplet that travels through ambient depends on the droplet velocity, on the droplet thermo-physical properties and on the ambient properties, which are related, in part, by the Weber number. The Weber number is the ratio between disruptive forces and cohesive forces. When a drop travels in ambient, deformation occurs, which may lead to droplet breakup. The droplet breakup will occur only if the Weber number locally exceeds a certain critical value. Forces inducing droplet deformation are categorized, to a large extent, into two distinct mechanisms: turbulent and lamina drag forces, as shown in Figure 7-1. Therefore, previous study, which focused on laminar drag induced droplet breakup (Sher and Sher, 2012), is considered by incorporating turbulent effects into the breakup mechanism, through the time scales of the droplet's trajectory and droplet breakup (a balance of deformed surface energy and

breakup dissipation). The principle of isotropic turbulence is considered valid, as the breakup was to be considered local.

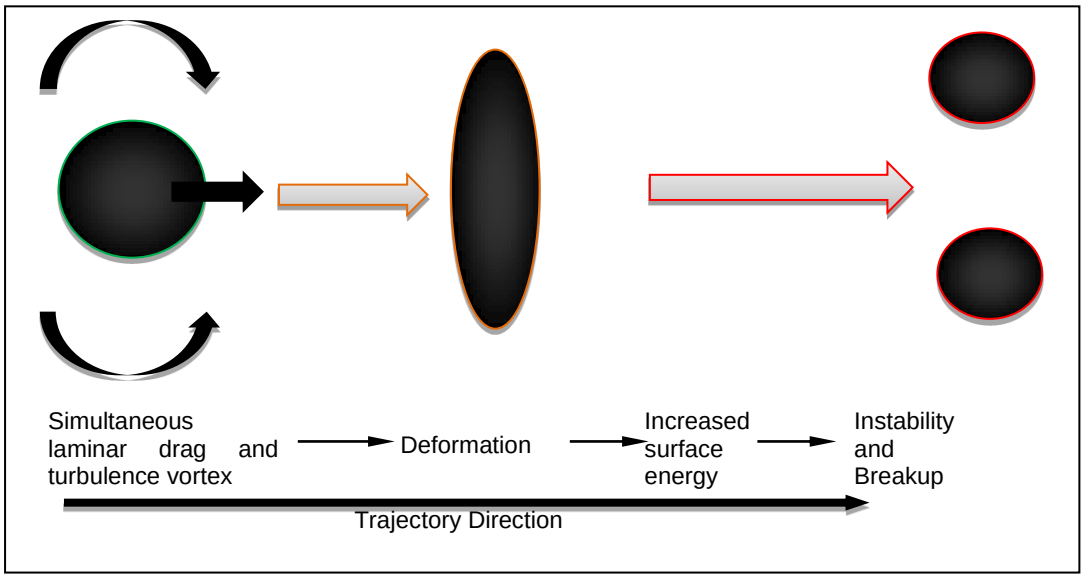

Figure 7-1 Droplet Breakup Processes

The energy criterion, according to (Sher and Sher, 2012), for a disturbed parent droplet to disintegrate can be written, for a symmetrical breakup process, as

$$E_s = ne_s + E_{diss} \tag{7-1}$$

where $E_s[Nm]$ is the deformed droplet extended surface energy; $n[-]$ is the number of daughter droplets; $e_s[Nm]$ is the surface energy of a drop and $E_{diss}[Nm]$ is the dissipative energy, which accounts for viscous effect.

The disturbed droplet surface energy, drop surface energy and the dissipative energy can be obtained according to Sher and Sher (2012) as follow:

Deformed droplet extended surface energy is estimated as

$$E_s = \sigma . 2\pi \int_0^{\pi} R^2(\theta) \sin(\theta)\, d\theta = \sigma \pi r_e^2 \left(\frac{3^2}{2^6 . 5} We^2 + 4 \right) \tag{7-2}$$

where $\sigma[N/m]$ is the surface tension, $We = \frac{\rho_g U^2 r_e}{\sigma}[-]$ is the continuous phase, the ambient, Weber number and U[m/s] is the droplet instantaneous trajectory velocity, $r_e[m]$is the radius of a spherical droplet of the same volume (V) as the deformed droplet; $r_e \equiv (3V/4\pi)^{1/3}$ this implied that the radius of daughter droplet is $r_d \equiv n^{-1/3} r_e$.

Daughter droplet surface energy is determine as

$$e_s = 4n^{-2/3}\sigma\pi r_e^2 \tag{7-3}$$

Dissipative energy is estimated by

$$E_{diss} = \mu_l \left(\frac{du}{dx}\right)^2 Vt = \mu_l \left(\frac{r_e/t}{r_e}\right)^2 \frac{4}{3}\pi r_e^3 t = \frac{4}{3}\pi r_e^3 \mu_l \frac{1}{t} \tag{7-4}$$

where $\mu_l[kg/ms]$ is the dynamic viscosity of the dispersed phase.

Substitute the deformed droplet extended surface energy, product droplet surface energy and the dissipative energy into Eq.(7-1) to obtain

$$\sigma\pi r_e^2 \left(\frac{3^2}{2^6.5} We^2 + 4\right) = 4n^{1/3}\sigma\pi r_e^2 + \frac{4}{3}\pi r_e^3 \mu_l \frac{1}{t} \tag{7-5}$$

It is argued, in the present work, that the droplet breakup is due to the simultaneous mechanisms of drag induced deformation (laminar drag breakup) and turbulence vortex induced breakup, the faster breakup mechanism being the relatively dominant. The breakup time is proposed, in a similar way to the dual-timescale for turbulent energy transfer in droplet dispersion (Pai and Subramaniam, 2007), as follows:

$$\frac{1}{t} \sim \frac{1}{t'} + \frac{1}{t_{bu}} \tag{7-6}$$

The laminar drag breakup timescale, t_{bu}, and the turbulence breakup timescale, t', are coupled to the dissipation timescale in the breaking droplet, which is the timescale in the energy balance for droplet breakup.

The turbulence time scale, $t'[s]$, is generally given as (Stiesch, 2010)

$$t' = \frac{l}{u'} \equiv \frac{l}{I_{rt}U} \tag{7-7}$$

where $l[m]$ is the turbulence lengthscale, $u'[m/s]$ is the fluctuating velocity and $I_{rt} = u'/U[\%]$ is the relative turbulence intensity.

It is expected that for a droplet fragmentation to occur the turbulence lengthscale should be of the order of the droplet size, which supports some researchers' submissions that eddy close to droplet size or order of magnitude larger than the droplet diameter has the most contributing factor in its disintegration process (Andersson and Andersson, 2006). It implies that $l \sim \varphi r_e$, hence, $t' \sim \varphi r_e / I_{rt}U$, where the parameter φ is an experimental fit.

$$\frac{1}{t'} \sim \frac{I_{rt}\sqrt{We}}{\varphi r_e}\sqrt{\frac{\sigma}{\rho_l r_e}} \tag{7-8}$$

The trajectory of the droplet in the continuous phase of the two-phase flow field is readily described by the particle's equation of motion, which relates acceleration and drag force on the bases of momentum balance, given as

$$\rho_l V_p \frac{dU}{dt} = -\frac{1}{2}\rho_g C_D A_f U^2 \tag{7-9}$$

where $V_p[m^3]$ is the droplet volume, $C_D[-]$ is the drag coefficient, $A_f[m^2]$ is the frontal area of the particle, which is given as $A_f = \pi r_e^2$ for spherical droplet, and $U[m/s]$ is the mean flow velocity.

Eq.(7-9) can be written as

$$\frac{dU}{dt} = -\frac{3}{2^3} C_D \frac{\rho_g}{\rho_l r_e} U^2 \tag{7-10}$$

Integration of Eq.(7-10), between U_o at zero time – initial droplet velocity, and an arbitrary point in time, t, where the velocity is U, gives

$$\frac{1}{t_{bu}} = \frac{3}{2^3} C_D \frac{\rho_g}{\rho_l r_e} \frac{U_o U}{U_o - U} \tag{7-11}$$

Since $We = \frac{\rho_l U^2 r_e}{\sigma}$, hence $U = \sqrt{We}\sqrt{\frac{\sigma}{\rho_l r_e}}$. Therefore, Eq.(7-11) becomes

$$\frac{1}{t_{bu}} = \frac{3}{2^3} C_D \frac{\sqrt{\rho_g r_e \sigma}}{\rho_l r_e^2} \frac{\sqrt{We_0}\sqrt{We}}{\sqrt{We_0} - \sqrt{We}} \tag{7-12}$$

where $We_0[-]$ is the initial Weber number and $We[-]$ is the local Weber number.

Substituting Eqs (7-12) and (7-8) into (7-6) gives

$$\begin{aligned} \sigma\pi r_e^2 \left(\frac{3^2}{2^6.5} We_{bu}^2 + 4 \right) &= 4n^{1/3} \sigma\pi r_e^2 \\ &+ \frac{4}{3}\pi r_e^3 \mu_l \left(\frac{3}{2^3} C_D \frac{\sqrt{\rho_g r_e \sigma}}{\rho_l r_e^2} \frac{\sqrt{We_0}\sqrt{We_{bu}}}{\sqrt{We_0} - \sqrt{We_{bu}}} \right. \\ &\left. + \frac{I_{rt}\sqrt{We_{bu}}}{2^3 \varphi r_e} \sqrt{\frac{\sigma}{\rho_l r_e}} \right) \end{aligned} \tag{7-13}$$

Taking $\mu_l = Oh\sqrt{\rho_l r_e \sigma}$ in Eq.(7-13), expanding and simplifying result in

$$\sigma\frac{3^2}{2^8.5}We_{bu}^2 = \left(n^{1/3}-1\right)+\frac{1}{2^3}C_D Oh\sqrt{\frac{\rho_g}{\rho_l}}\frac{\sqrt{We_0}\sqrt{We_{bu}}}{\sqrt{We_0}-\sqrt{We_{bu}}} + \frac{1}{3\varphi}OhI_{rt}\sqrt{We_{bu}} \quad (7\text{-}14)$$

where $Oh[-]$ is the Ohnesorge number.

It is assumed that the parent droplet is approximately broken into two new daughter droplets, which supports (Stiesch, 2010), hence *n=2* is adopted. It is evident from Figure 7-2 that Eq.(7-14) has two extrema (minimum and maximum). It should be noted that for a decelerating droplet, which is the case under investigation, the physical region is where the minimum occurred in the figure, because it is expected that $We_0 > We_{bu}$. The figure equally supports the theory that turbulence effects enhance droplet breakup (Trinh and Chen, 2006), since the critical initial Weber number decreases with increasing relative turbulence intensity.

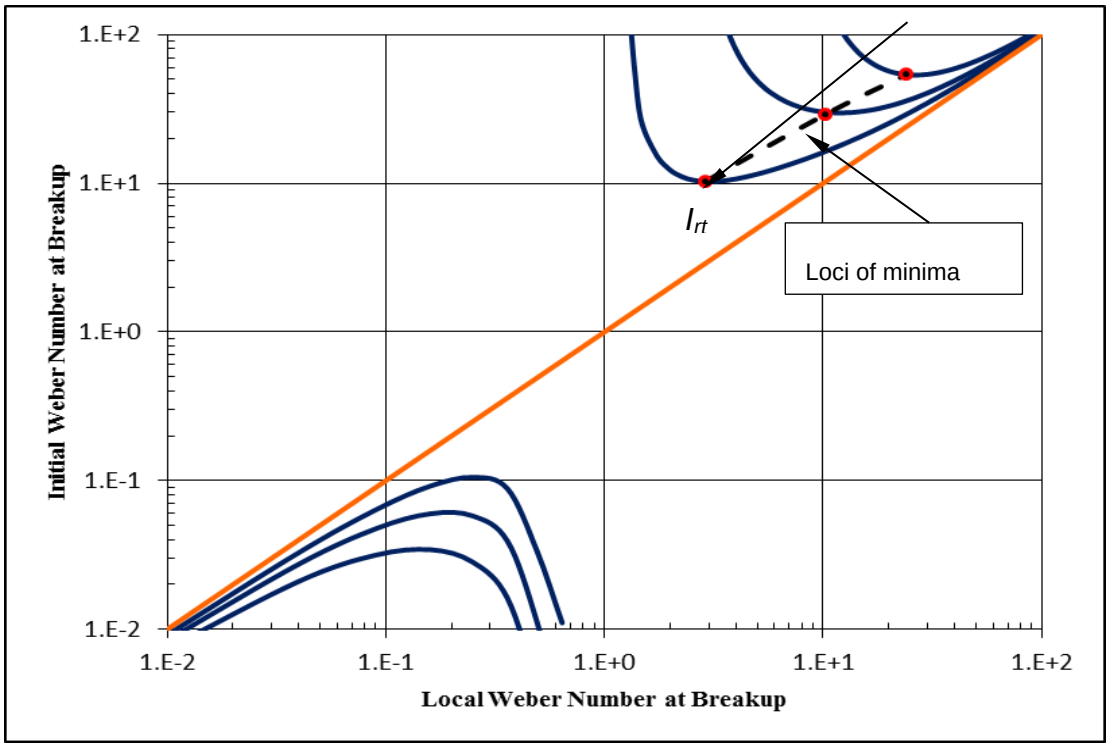

Figure 7-2 Initial Weber Number, We_0 vs. Local Weber Number at Breakup, We_{bu} at varying I_{rt}

The critical breakup conditions correspond to the minimum values, which can be obtained at $\left.\frac{d\sqrt{We_0}}{d\sqrt{We_{bu}}}\right| = 0$ from Eq.(7-14). However, Eq.(7-14) is not straight forward to analytical solution and is, therefore, transformed to the following form.

$$\frac{3^2}{2^8.5}\left(\sqrt{We_{bu}}\right)^4 = \left(n^{1/3}-1\right) + \frac{1}{2^3}C_D Oh\sqrt{\frac{\rho_g}{\rho_l}}\frac{\sqrt{We_0}\sqrt{We_{bu}}}{\sqrt{We_0}-\sqrt{We_{bu}}} + \frac{1}{3\varphi}OhI_{rt}\sqrt{We_{bu}} \quad (7\text{-}15)$$

Two asymptotic solutions, for the critical condition $\left.\frac{d\sqrt{We_0}}{d\sqrt{We_{bu}}}\right|_{cr} = 0$, is obtained for Eq.(7-15) as follow:

Surface energy is much larger than breakup products' surface energy

This case is where critical surface energy is much larger than that of the expected breakup products, in that $\left(n^{1/3}-1\right) \ll \frac{3^2}{2^8.5}\left(\sqrt{We_{bu}}\right)^4$, this means that at critical breakup conditions, the initial surface energy is predominantly viscously dissipated. This condition dictates that Eq.(7-15) being

$$\frac{3^2}{2^8.5}\left(\sqrt{We_{bu}}\right)^3 = \frac{1}{2^3}C_D Oh\sqrt{\frac{\rho_g}{\rho_l}}\frac{\sqrt{We_0}}{\sqrt{We_0}-\sqrt{We_{bu}}} + \frac{1}{3\varphi}OhI_{rt} \quad (7\text{-}16)$$

Differentiating Eq.(7-16) with respect to $\sqrt{We_{bu}}$ to obtain

$$\frac{3^3}{2^8.5}\left(\sqrt{We_{bu}}\right)^2 = \frac{1}{2^3}C_D Oh\sqrt{\frac{\rho_g}{\rho_l}}\left[\frac{\left(\frac{d\sqrt{We_0}}{d\sqrt{We_{bu}}}\right)\left(\sqrt{We_0}-\sqrt{We_{bu}}\right)-\left(\frac{d\sqrt{We_0}}{d\sqrt{We_{bu}}}-1\right)\sqrt{We_0}}{\left(\sqrt{We_0}-\sqrt{We_{bu}}\right)^2}\right] \quad (7\text{-}17)$$

Noting $\left.\frac{d\sqrt{We_0}}{d\sqrt{We_{bu}}}\right|_{cr} = 0$ at the critical condition, hence, Eq.(7-17) becomes

$$\frac{3^3}{2^8.5}\left(\sqrt{We_{bu}}\right)^2 = \frac{1}{2^3}C_D Oh\sqrt{\frac{\rho_g}{\rho_l}}\left[\frac{\sqrt{We_0}}{\left(\sqrt{We_0}-\sqrt{We_{bu}}\right)^2}\right] \quad (7\text{-}18)$$

Rearranging Eq.(7-16); diving the resulting equation by Eq.(7-18) and solving for $\sqrt{We_0}$ give

$$\sqrt{We_0} = \frac{2^2}{3}\sqrt{We_{bu}} - \frac{2^8.5}{3^4}\left(\frac{1}{\varphi}\right)\frac{OhI_{rt}}{\left(\sqrt{We_{bu}}\right)^2} \quad (7\text{-}19)$$

Combine Eq.(7-16) and Eq. (7-19) to obtain

$$\frac{2^2}{3}\sqrt{We_{bu}} - \frac{2^8.5}{3^4}\left(\frac{1}{\varphi}\right)\frac{OhI_{rt}}{\left(\sqrt{We_{bu}}\right)^2} = \frac{\left(\frac{3^2}{2^8.5}\left(\sqrt{We_{bu}}\right)^3 - \frac{1}{3\varphi}OhI_{rt}\right)\sqrt{We_{bu}}}{\frac{3^2}{2^8.5}\left(\sqrt{We_{bu}}\right)^3 - \frac{1}{3\varphi}OhI_{rt} - \frac{1}{2^3}C_D Oh\sqrt{\frac{\rho_g}{\rho_l}}} \quad (7\text{-}20)$$

In order to simplify the solution method for Eq(7-20), it is here noted, for the class of system under consideration, that $\frac{3^2}{2^8.5}\left(\sqrt{We_{bu}}\right)^3 \gg \frac{1}{3\varphi}OhI_{rt}$ thus

$$\sqrt{We_{bu}} \cong \left(\frac{2^7.5}{3^2} C_D Oh \sqrt{\frac{\rho_g}{\rho_l}}\right)^{1/3} \tag{7-21}$$

Substitute Eq.(7-21) into Eq.(7-19) to obtain

$$\sqrt{We_{0,cr}} = \frac{2^2}{3}\left(\frac{2^7.5}{3^2} C_D Oh \sqrt{\frac{\rho_g}{\rho_l}}\right)^{1/3} - \frac{2^8.5}{3^4}\left(\frac{1}{\varphi}\right) Oh \left(\frac{2^7.5}{3^2} C_D Oh \sqrt{\frac{\rho_g}{\rho_l}}\right)^{-2/3} I_{rt} \tag{7-22}$$

Viscous dissipation is negligible

The second asymptotic case is where the viscous dissipation is negligible, in that $Oh \to 0$. This means that at critical breakup conditions the initial surface energy is almost completely converted to products surface energy. This second case yields

$$\sqrt{We_{0,cr}} \sim \sqrt{We_{bu}} = \left(\frac{2^8.5}{3^2}\right)^{1/4} \left(n^{1/3} - 1\right)^{1/4} \tag{7-23}$$

The critical Weber number is, therefore, obtained by linearly combining Eqs (7-22) and (7-23), and simplifying for $We_{0,cr}$ to obtain

$$We_{0,cr} = \left(3.45\left(n^{\frac{1}{3}} - 1\right)^{\frac{1}{4}} + 5.52\left(C_D Oh \sqrt{\frac{\rho_g}{\rho_l}}\right)^{\frac{1}{3}} - 0.92\left(\frac{1}{\varphi}\right) Oh^{\frac{1}{3}}\left(C_D \sqrt{\frac{\rho_g}{\rho_l}}\right)^{-\frac{2}{3}} I_{rt}\right)^{1/2} \tag{7-24}$$

7.3 Model Validation

Though drop drag coefficients vary with droplet deformation and turbulence intensity of the flow field (Snyder et al., 2006), but use of constant average coefficients have been effective for earlier considerations of drop motion (Sher and Sher, 2012). There are two classical average values for a deforming droplet drag coefficients: 1. $C_D = 0.44$ for droplet in turbulent flow field (Stiesch, 2010) and 2. $C_D \in \{1.5,2.5\}$ for droplet in laminar flow field (Previsch, 1998). However, Hsiang and Faeth (1995) noted that C_D varies from values 0.44-0.5 at the start of breakup to 4.8-5.4 when the maximum deformation condition is reached. The two base cases for the drag coefficient are used for the model, Eq.(7-24), validation (as shown in Figure 7-3 and Figure 7-4) for n-heptane and methanol fuel droplets in turbulent flow field with the table of input parameters shown in Table 7-1.

Table 7-1Input Parameters (Previsch, 1998)

Fuel	$\boldsymbol{\rho_l[kg/m^2]}$	$\frac{\boldsymbol{\rho_g}}{\boldsymbol{\rho_l}}[-]$	$\boldsymbol{\sigma[N/m]}$	$\boldsymbol{Oh}[-]$
n-Heptane	684	0.0087	0.0201	0.0064
Methanol	791	0.0076	0.0226	0.0082

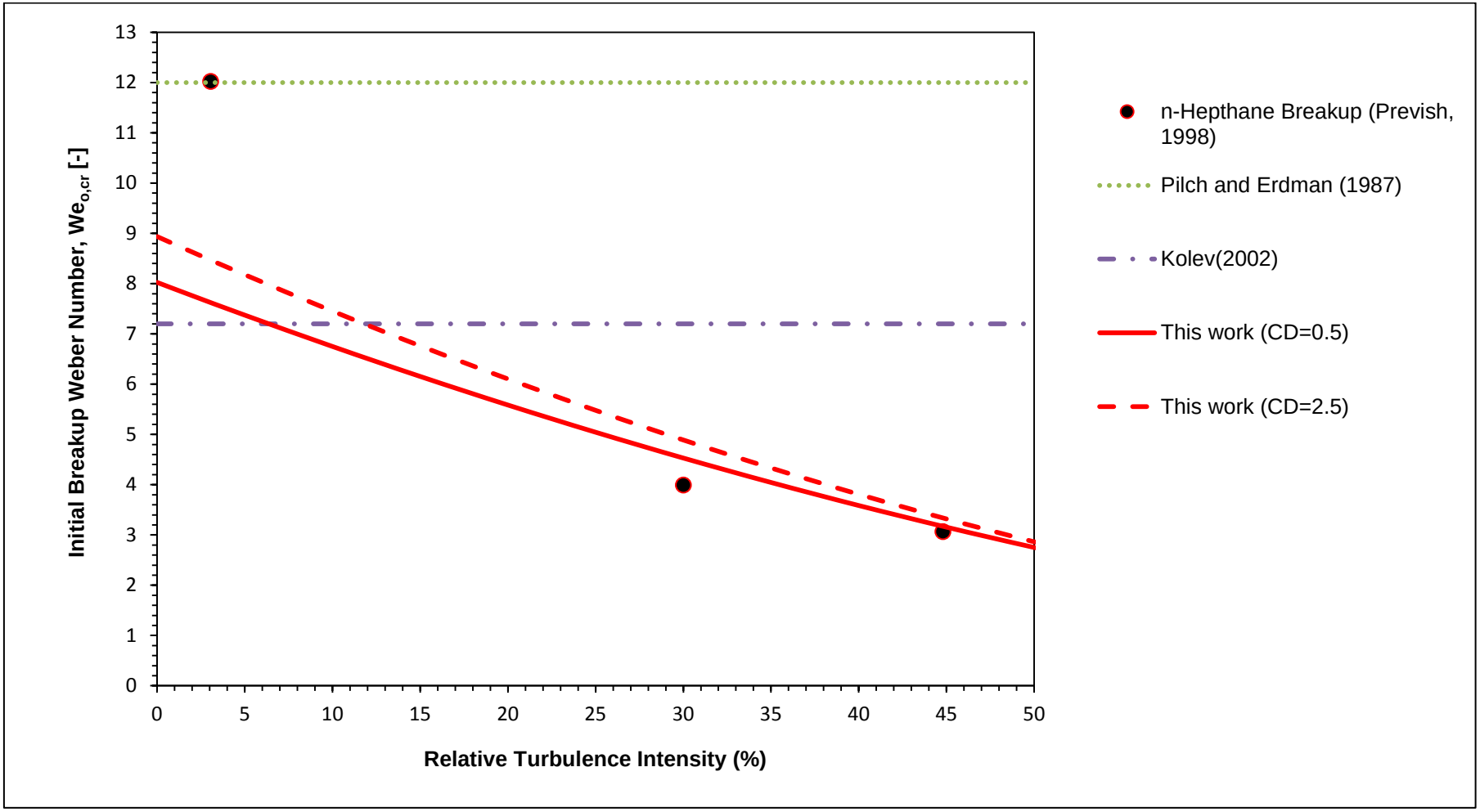

Figure 7-3 Theoretical Prediction vs Experimental Data for n-Heptane Critical Weber Number

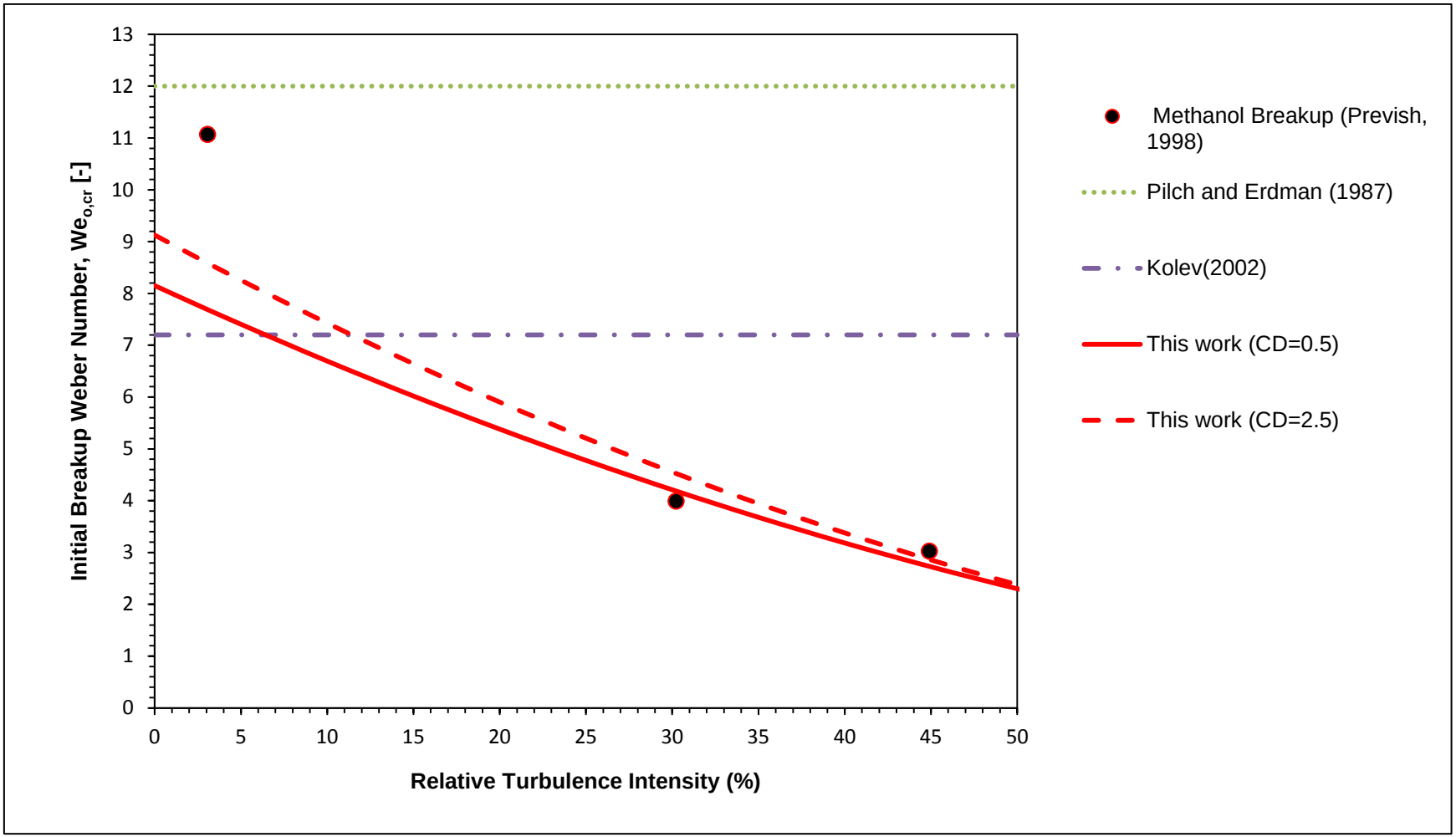

Figure 7-4Theoretical Prediction vs Experimental Data for Methanol Critical Weber Number

The critical Weber number in Previsch's experimental work (Previsch, 1998), circle markers in Figure 7-3 and Figure 7-4, was established at the flow rate where about 5[%] of droplets experienced breakup. For the two fuel types, the critical Weber number of droplet breakup decreases with increasing turbulence intensity whereas two popular empirical criteria, by Pilch and Erdman (1987) and Kolev (2002), for droplet breakup predict constant values for the critical Weber number for the droplet breakup, figures Figure 7-3 and Figure 7-4. Kolev (2002) empirical criterion under-predicts the critical Weber number at low turbulence intensities and over-predicts same at high turbulence intensities; whereas Pilch and Erdman (1987) criterion over-predicts the critical Weber number of droplet breakup in turbulent flow field. The ambiguity in the empirical models predictions may be attributed to the non-consideration of turbulence effects. It is obvious from Figure 7-3 and Figure 7-4 that the analytical model, Eq.(7-24), gives a fair prediction of the experimental data. The analytical model has poor prediction at moderate low turbulence intensities. However, Snyder et al. (2006) have shown from their extensive literature survey that particle trajectory in transition from laminar to turbulent flow field is accompanied with rapid C_D rise well above the standard value, which is often referred to as the "drag crisis". Thus, the deviation of the model predictions from the experimental data, at moderate low turbulence intensities, may be attributed to the "drag crisis", since constant C_D is used in the model, which is collaborated by the model prediction at higher C_D value, as shown in the figures (Figure 7-3 and Figure 7-4).

7.3.1 Model Simulation: Effects of Elevated Ambient Density

The properties of the ambient in which the fuel is injected have a role to play in the breakup of liquid droplets. For instance, in a diesel engine the liquid fuel is injected into the combustion chamber near the end of the compression stroke with an elevated density of the combustion chamber (the ambient)of about 52 [kg/m^3]. Figure 7-5 is the simulated critical Weber number with the variation of gas-liquid density ration and turbulence intensity based on Eq.(7-24).

The figure shows that increasing the density ratio (gas density/liquid density) increases the critical Weber number. This is expected as larger aerodynamic force is needed to break a droplet moving in a quiescent denser ambient as a result of dynamic deceleration. It is also observed from the figure that turbulence effects are predominant for low density ratio, whereas the turbulence effects are less for high density ratio. This observation is hypothesised to be attributed to the damping of turbulent vortex by the high dense environment, which necessitates agitation of high ambient density, for example liquid-liquid interaction, to enhance breakup (Andersson and Andersson, 2006). However, turbulence effects are still prevalent in droplet breakup even in an elevated ambient density for the gas-liquid interaction, without necessarily agitating the continuous phase (the ambient).

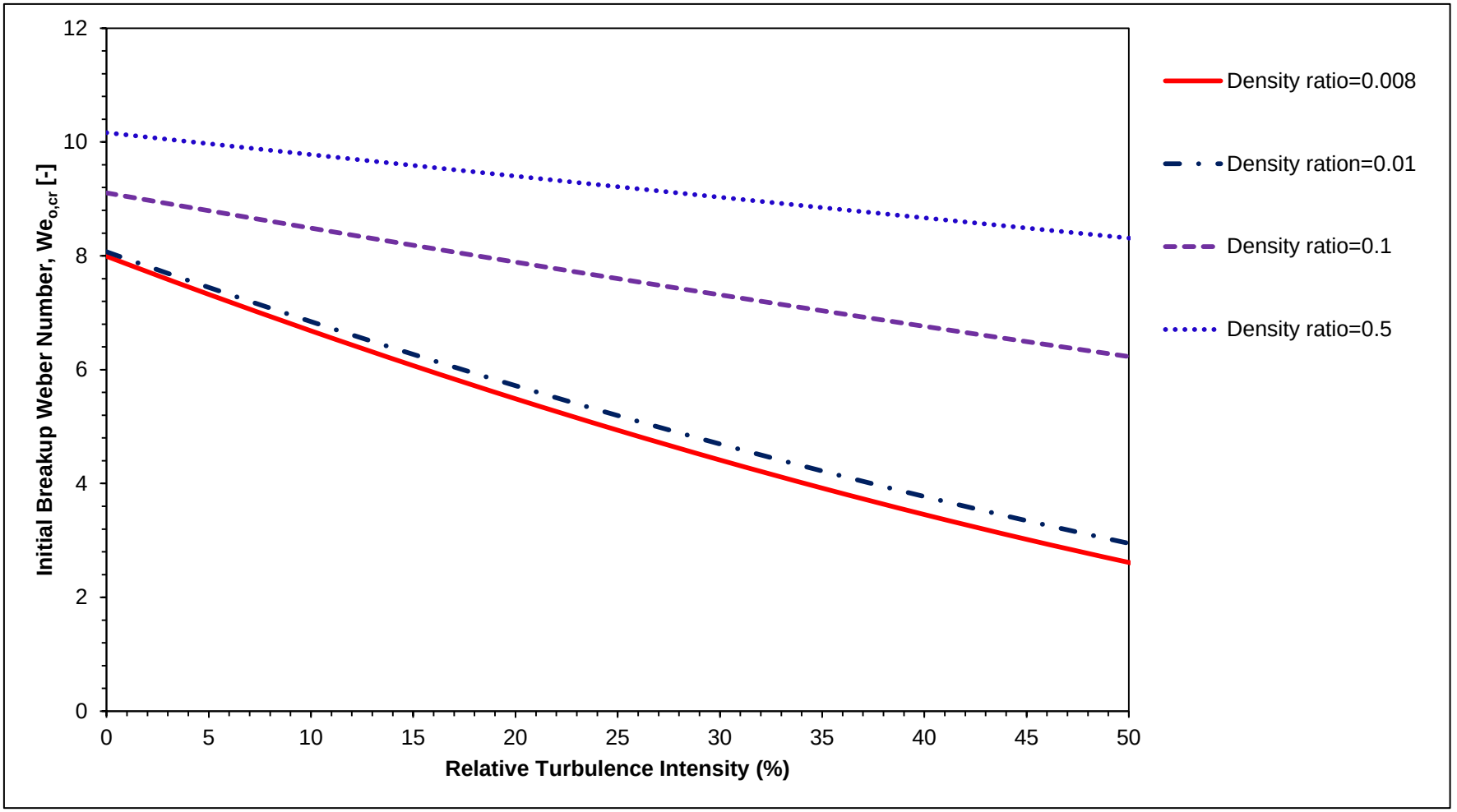

Figure 7-5 Effects of Elevated Ambient Density on Critical Weber Number

7.4 Another Look at the We-Oh Presentation

Absolute majority of classical models for We-Oh droplet breakup criterion are empirically developed (Pilch and Erdman, 1987; Kolev, 2002), which may be handicap for predictive purposes. However, a good analytical criterion on We-Oh for droplet breakup was proposed in Sher and Sher (2012). It is expected that with the application of HIP fuel system in modern engines may introduce turbulence eddies, which should be accounted for in the We-Oh criterion for droplet breakup. The effective shear stress, τ_e, which is the shear stress due to the laminar shear stress and the turbulence shear stress, is given as

$$\tau_e = \tau_l + \tau' \tag{7-25}$$

where τ_l is the laminar shear stress and τ' is the turbulence shear stress.

Eq.(7-25) can be presented as (Muralidhar and Biswas, 1999)

$$\tau_e = \mu \frac{dU}{dy} - \rho\overline{u'v'} \tag{7-26}$$

Taking $v' \sim \alpha u'$ and dividing Eq.(7-26) by ρU^2 gives

$$C_D = \alpha I_{rt}^2 + \frac{3\pi}{Re} \tag{7-27}$$

where $C_D \equiv \frac{\tau_e}{\rho U^2}$ is the effective drag coefficient; $\mu \frac{dU}{dy} / \rho U^2 \equiv \frac{3\pi}{Re}$ is laminar drag coefficient for a spherical body and $Re \equiv \frac{\rho U r_e}{\mu}$ is the Reynolds' number.

With $Re = \frac{\sqrt{We}}{Oh}$ in Eq.(7-27) and solving for I_{rt} to obtain

$$I_{rt} = \left(\frac{C_D}{\alpha} - \frac{3\pi}{\alpha} \frac{Oh}{\sqrt{We}} \right)^{1/2} \tag{7-28}$$

Taylor's series expansion of Eq.(7-28) is

$$\left(\frac{C_D}{\alpha}-\frac{3\pi}{\alpha}\frac{Oh}{\sqrt{We}}\right)^{\frac{1}{2}}=\sum_{n}^{\infty}\left(\frac{3\pi}{\alpha}\frac{Oh}{\sqrt{We}}\right)^{n}(-1)^{n}\left[\left(\frac{C_D}{\alpha}\right)^{\frac{1}{2}-n}\binom{\frac{1}{2}}{n}\right] \quad \text{for } \left|\frac{C_D}{\alpha}\right|>\left|\frac{3\pi}{\alpha}\frac{Oh}{\sqrt{We}}\right| \tag{7-29}$$

Neglecting $\left(\frac{3\pi}{\alpha}\frac{Oh}{\sqrt{We}}\right)^{n}; n=2,\dots,\infty$ gives

$$I_{rt}\approx\left(\frac{C_D}{\alpha}\right)^{1/2}-\frac{1.5\pi}{\sqrt{\alpha C_d}}\frac{Oh}{\sqrt{We}} \tag{7-30}$$

Substituting Eq.(7-30), for breakup condition, in Eq.(7-12) results in

$$\frac{3^2}{2^8.5}We_{bu}^2=\left(n^{1/2}-1\right)+\frac{1}{2^3}C_D Oh\sqrt{\frac{\rho_g}{\rho_l}}\frac{\sqrt{We_0}\sqrt{We_{bu}}}{\sqrt{We_0}-\sqrt{We_{bu}}}+\frac{1}{3\varphi}Oh\sqrt{\frac{C_D}{\alpha}}\sqrt{We_{bu}}-\frac{\pi}{2\varphi\sqrt{\alpha C_D}}Oh^2 \tag{7-31}$$

It is evident that Eq.(7-31), from Figure 7-6, has a minimum value, which corresponds to the critical Weber number.

The critical Weber number is obtained from the summation of two limiting values of the Ohnesorge number,

1: $Oh \ll 1$, the case where viscous effect is negligible, which gives

$$We_{0,cr}=\frac{2^4.5^{1/2}}{3}\left(n^{1/3}-1\right)^{1/2} \tag{7-32}$$

2: $Oh \gg 1$, the case where surface tension has a negligible influence on droplet deformation and breakup(Faeth, 2002), gives (see Appendix B for the detailed analysis):

$$We_{0,cr} = \left(\frac{1}{3}\frac{\pi}{2\varphi\alpha}\right)^2 \left(\frac{1}{2}C_D\sqrt{\frac{\rho_g}{\rho_l}} + \frac{1}{3\varphi}\left(\frac{C_D}{\alpha}\right)^{1/2}\right)^{-4} Oh^2 \quad (7\text{-}33)$$

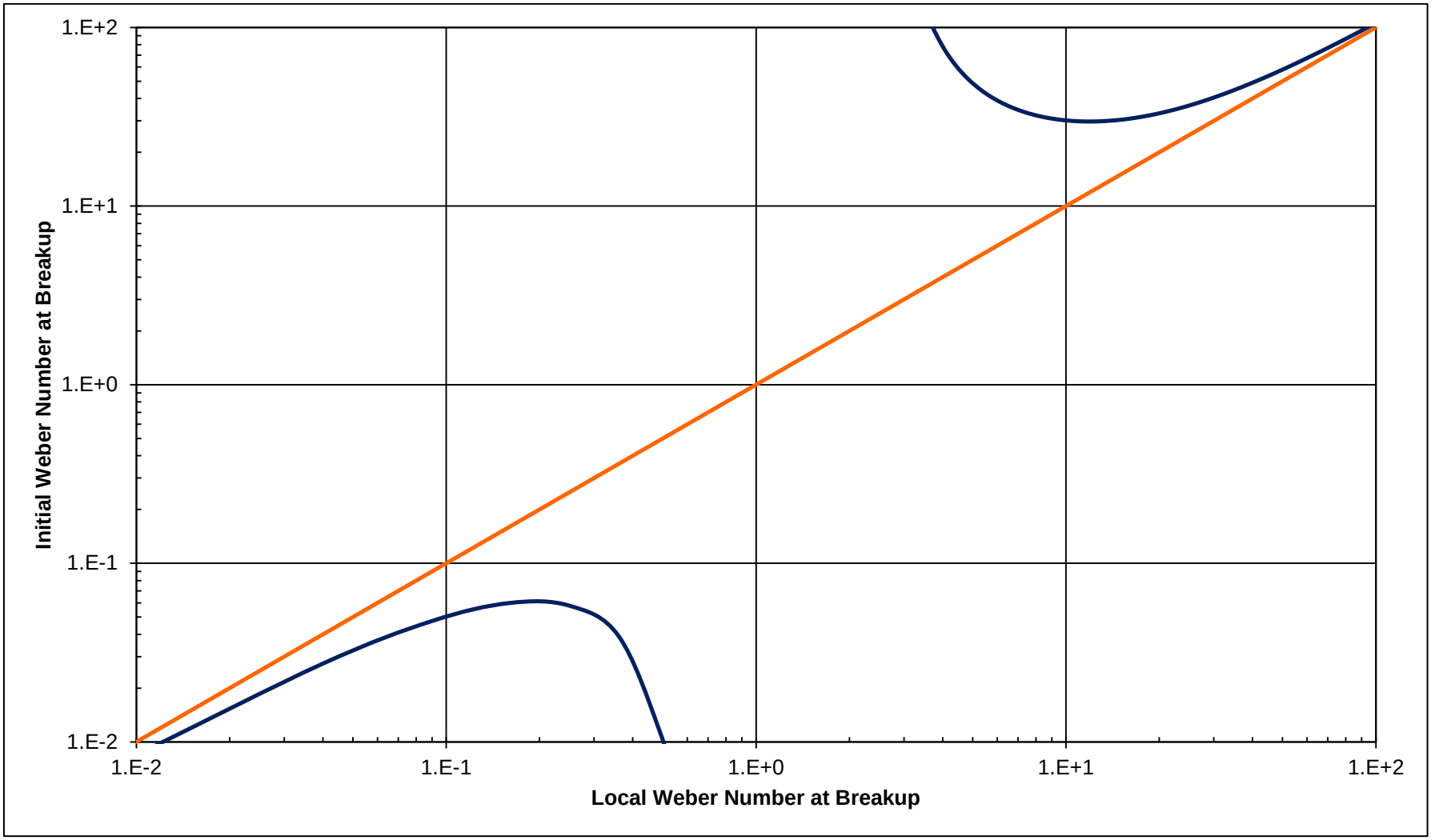

Figure 7-6 Initial Weber number, We_0 vs. local Weber number at breakup, We_{bu}

It should be noted that Eqs (7-32) and (7-33) are in agreement with the Faeth's(2002) submission, for breakup transition, in that $We_{0,cr} = const.;\ Oh \ll 1$ and $We_{0,cr} \sim Oh^2;\ Oh \gg 1$, respectively.

The critical initial Weber number of droplet breakup is, therefore, obtained from the summation of the two cases as follows

$$We_{0,cr} = 11.93\left(n^{1/3} - 1\right)^{1/2} + 0.27\left(\frac{1}{\varphi\alpha}\right)^2\left(0.5C_D\sqrt{\frac{\rho_g}{\rho_l}} + \frac{0.33}{\varphi}\left(\frac{C_D}{\alpha}\right)^{1/2}\right)^{-4} Oh^2 \quad (7\text{-}34)$$

Eq.(7-34) gives the analytical criterion, on the We-Oh presentation, for droplet breakup, as a function of the fluid densities ratio and the Ohnesorge number. Eq.(7-34) is plotted in Figure 7-7, and is compared with empirical models and available experimental data (Hsiang and Faeth, 1995; Hinze, 1955; Loparev 1975; Hanson, Domich, and Adams, 1963; Lane, 1951). Figure 7-7 shows the droplet deformation and droplet breakup regime on the We-Oh presentation. The green data marks represent droplet deformation without breakup and the red data marks represent droplet breakup. Although Pilch and Erdman (1987) and Kolev (2002) empirical models perfectly established the breakup criterion, however, it should be noted that the two models are not predictive and most importantly do not account for the ambient properties. The two analytical breakup criteria, Eq.(7-34) and Sher and Sher (2012), both also established the breakup criterion, even though the Sher and Sher (2012) analytical criterion is stressed for a moderate We-Oh region.

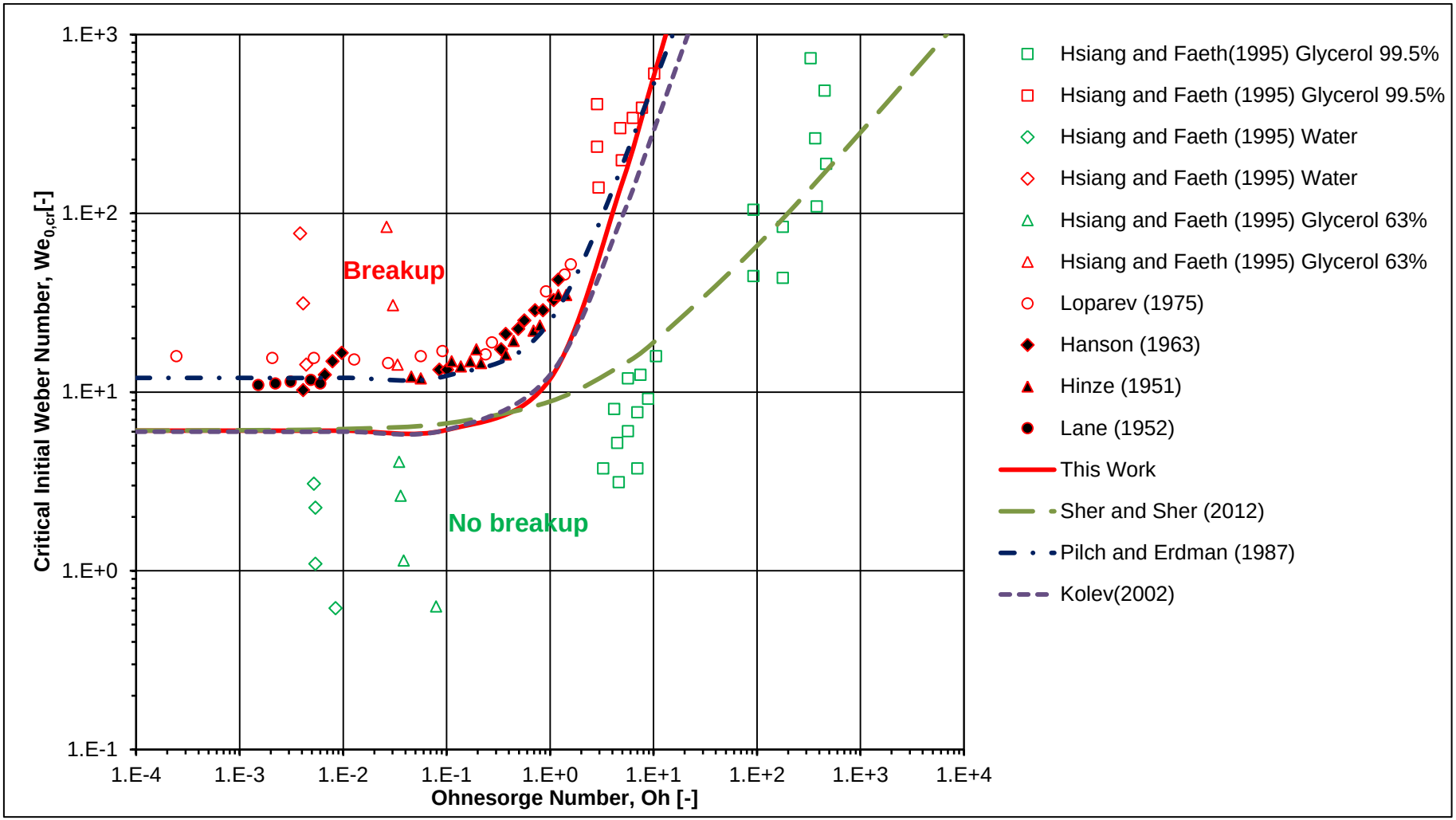

Figure 7-7 We-Oh Droplet Breakup Regime; n=2, C_D=0.5 and ρ_g/ρ_l=0.003

7.5 Conclusion of Chapter Seven

The utilisation of high-injection-pressure (HIP) fuel system in direct diesel injection (DDI) requires liquid fuel being injected at a very high pressure, which is later converted to a corresponding high velocity by the injector nozzle, which gives rise to a turbulent flow fields around droplets. Experimental work has shown the importance of flow field characteristics on droplet breakup. Further experimental results, for low Oh values, have shown that turbulence flow has a remarkable influence on the droplet breakup process in gaseous flow field. Hence, droplet breakup criterion, for the classical droplet breakup assumptions, may be changed considerably when a droplet is shot into a turbulent flow fields as the case for droplet instability and breakup in diesel sprays. This expectation is attributed to a wide range of dynamic forces due to the growing eddies. There is inherent difficulty to experimentally and analytically capture all the phenomena of droplet breakup in a turbulent flow field. In this work, simplified mathematical models for the droplet breakup criteria, on the We-I_{rt} and We-Oh, which account for the turbulent effects, are suggested. The We-I_{rt} and We-Oh analytical breakup criteria are in good agreement with published experimental data. The present We-Oh analytical criterion stressed the importance of turbulence effects on We-Oh breakup criterion at high We-Oh applications. It is envisaged that the analytical models be incorporated into larger CFD codes to complement CFD droplet breakup simulations.

8 CONCLUSION AND FUTURE WORK

8.1 Conclusion

An analytical investigation into the liquid fuel breakup mechanisms – jet and droplet breakups – was carried out. The investigation covers transient effects on jet breakup, non-isothermal conditions on jet breakup, liquid jet breakup length and turbulence induced droplet breakup, as they are applied to internal combustion engines. The models showed good predictions of available experimental data within the operational conditions of ICEs, specifically diesel engines. Continued research in these areas could benefit the development of the next generation of liquid fuel injectors and combustors – by accounting for these effects in their design. The following subsections expand the conclusions, according to the set objectives of the research work.

8.1.1 Transient Primary Breakup Model

The quasi-steady assumption may be attributed to some of the deviations observed in the literature between theoretical predictions and experimental data. There are three basic methods of investigating liquid breakup mechanisms: experimental, numerical and analytical. The experimental and numerical methods of liquid breakup investigation could be too difficult and expensive to resolve all the different length and time scales. However, some important specific details of the breakup mechanisms could be addressed by the analytical method of investigation. Therefore, a new instability and breakup model of transient liquid jet, with the consideration of the jet instantaneous velocity and acceleration, is developed. The model was developed from the conservation equations for two-phase flow, on the classical interfacial breakup theory, by the modification of the linear perturbation process that considers time-dependent base flow and perturbed parameters. The analytical model accounts for the transient effects on liquid jet breakup.

Results obtained compared fairly well with experimental data obtained for penetration length, breakup length and spray angle. Furthermore, the model could be reduced to its steady jet approximation equivalent. The model is

shown to maintain the plausibility of investigating liquid jet breakup mechanisms of accelerating liquid jets, which are dominant in the modern practical fuel injection techniques, like the pulse injection strategy.

8.1.2 Non-Isothermal Primary Breakup Model

The classical theory of liquid fuel jet instabilities has been developed under several assumptions, which include the assumption that the jet breakup processes are isothermal and steady. However, liquid fuel injection is normally transient in operation, in an elevated combustion-chamber. This non-isothermal injection introduces a variation of the surface-tension with temperature along the liquid-gas interface. Therefore, a new linear theory model is developed for the instability and breakup of non-isothermal liquid jets, with consideration of a spatially variation of surface tension along the liquid-gas interface. The spatial variation of surface tension is obtained through the temperature-dependent surface tension and transient heat-transfer from the combusting gases to the liquid jet. The classical interfacial hydrodynamic breakup theory and solution of heat-transfer through semi-infinite medium are coupled through the surface tension gradient. The analytical model accounts for the non-isothermal effects on jet breakup.

The model shows that liquid fuel breakup under non-isothermal environments may differ significantly from the isothermal case. More so, the model could be reduced to its isothermal jet approximation equivalent. The model showed good predictions of available experimental data regarding maximum penetration length at different ambient temperatures, within the operational conditions of contemporary ICEs, specifically diesel engines.

8.1.3 Transient Non-Isothermal Primary Breakup Model

The theory of liquid jet instabilities has been developed under several assumptions, which include the assumption that the jets breakup processes are quasi-steady and isothermal. Accelerated liquid fuels are normally injected into an elevated combustion-chamber temperature to maintain a desirable homogeneous combustible mixture – liquid vapour and air. The accelerated jet

breakup may be induced by cavitation, turbulent, hydrodynamic and aerodynamic forces interaction and variation in fluid properties. The absolute majority of studies have been devoted to the extensive study on some of the effects that cause jet instability and breakup, while others are still at their infant study. In particular, relatively few researchers have studied the combined effects of jet acceleration and non-isothermal condition on jet instability and breakup, despite its practical relevance in liquid fuel spray and combustion. Specifically, liquid fuel jets are highly transient under pulsed injection technique, which has been demonstrated to maintain better fuel economy and emissions reduction. Liquid jet acceleration and non-isothermal conditions have a significant role in the breaking of interfacial surfaces, since the surface tension, which is temperature dependent, predominantly controls interfacial breakup.

Therefore, a new analytical hydrodynamic instability and breakup model, which captured both jet acceleration and non-isothermal conditions, for liquid jet, is presented. The analytical model investigates the impact of two important phenomena on liquid jet instability and breakup; jet acceleration and non-isothermal conditions. These effects are naturally difficult to address by both experimental and CFD investigations. The new model analysis combined both hydrodynamic model and heat transfer equations, coupled through the surface-tension gradient, and is a novel address of this conjugated problem.

Simulated results suggest liquid jets instability to be enhanced by increase in excess-temperature up to a high injection velocity, where the non-isothermal effects become minimal, beyond which the breakup mechanism coincides with the isothermal condition. Furthermore, liquid jet acceleration is shown to have appreciable effects on the macro structure of the spray. The non-isothermal condition is shown to be significant in transient liquid fuel injection. The model showed good predictions of experimental data regarding temporal penetration length and maximum penetration length at different injection pressures, and different ambient temperatures, within the operational conditions of contemporary ICEs, specifically diesel engines. Continued research in this regard, of transient and non-isothermal effects on jet breakup, could benefit the

development of the next generation of liquid fuel injectors and combustors – by accounting for these effects in their design.

8.1.4 Breakup Length

In jet atomisation, breakup length is the length of the continuous jet segment, before its breakup to discontinuous droplets. A basic mechanistic approach to the breakup length prediction, based on a simple momentum balance between the injected jet and the aerodynamic drag force due to the surrounding gas, which complements the classic hydrodynamic instability breakup mechanism, is suggested. It is shown that obtained results compare well with published experiments, and with the established empirical correlation of Wu and Faeth (1995). A simplified version of the model, taking into account an inviscid hydrodynamic model is shown to maintain plausibility of breakup length predictions in fuel-injection relevant conditions.

8.1.5 Droplet Breakup in Turbulent Flow Field

The utilisation of high-injection-pressure (HIP) fuel systems in direct diesel injection (DDI) requires liquid fuel being injected at a very high pressure, which is later converted to a corresponding high velocity by the injector nozzle, which gives rise to a turbulent flow fields around droplets. Experimental work has shown the importance of flow field characteristics on droplet breakup. Further experimental results, for low Oh values, have shown that turbulence flow has a remarkable influence on the droplet breakup process in gaseous flow field. Hence, droplet breakup criterion, for the classical droplet breakup assumptions, may be changed considerably when a droplet is shot into a turbulent flow field as the case for droplet breakup in diesel sprays. This expectation is attributed to a wide range of dynamic forces due to the growing eddies. There is inherent difficulty to experimentally and analytically capture all the phenomena of droplet breakup in a turbulent flow field.

New droplet breakup criteria models, which combine an energy criterion and a dual-timescale for turbulent shear in droplet dispersion, are suggested for droplet breakup. The suggested analytical breakup criteria, on We-I_{rt} and We-

Oh representations, are proposed on the basis of the critical Weber number. The We-I_{rt} and We-Oh analytical breakup criteria are in good agreement with published experimental data and successfully predict the breakup regime – for the very low and very high We-Oh conditions. The suggested model stressed the importance of turbulence effects on We-Oh breakup criterion at high We-Oh applications.

The analytical models could enhance CFD simulation capability for droplet breakup, as it is envisaged to be incorporated into larger CFD codes. Continued research in this area could favour the development of the next generation of liquid fuel injectors.

8.2 Future Work

In the present work, perturbed parameters are postulated to take forms that are less restrictive than the ones postulated by the classical hydrodynamic instability and breakup theory. These forms enable time dependency of perturbation to be non-linear, with the principle of separable variable still being maintained, and assume a different form for each parameter. However, in the investigation the liquid jet breakup is modelled on the assumption that the cylindrical jet maintains a constant diameter along the jet axis prior to breakup. This approach does not allow the investigation of the fact that there are likely to be changes in the growth rate along the liquid jet prior to breakup due to the thinning of the liquid jet diameter of an accelerating jet. Therefore, the suggested transient temporal instability and breakup model should be coupled with spatial interface tracking. One possible step to incorporate the spatial interface tracking is by the adoption of the proposed interface tracking method by Domann and Hardalupas (2004), which is based on the tracking of the total surface disturbance at any fixed time as a superposition of all unstable wavenumbers, characterised by the breakup controlling wave length.

The ever growing energy demands, interests for friendlier environment and steady supply of energy, are strongly influencing internal combustion engine researchers to consider renewable bio-fuels as an alternative to conventional fuels. Therefore, extending the capability of instability and breakup models to

include biodiesel breakup investigation is of interest. However, it has been observed that the constant parameters in the classical instability and breakup model are tuned separately for biodiesel and conventional diesel (Pogorevc, Kegl, and Skerget, 2008). Furthermore, it is observed for biodiesel that the primary breakup constant parameters have significant effects on the change in spray structure, as the tuning parameters are mostly expressed in terms of liquid thermo-physical properties, namely, viscosity and density. Furthermore, the literature has shown a significant difference between biodiesel spray and diesel spray droplets sizes, for biodiesel droplet size being higher by 40%, which is attributed to the high viscosity of bio-diesel (Boggavarapu and Ravikrishna, 2013). Specifically, the non-isothermal condition on jet breakup would be very significant, since the viscosity of biodiesel is non-linear with temperature. Therefore, the accelerating and non-isothermal jet instability and breakup model should be reconstructed to apply for a biodiesel liquid fuel. The basic approach is to drop the inviscid assumption made in the current analysis. However, the analysis may not yield analytical solution, as desired, but careful simplification, on the basis of order of magnitude, may potentially yield an approximate analytical solution.

Investigation of sprays by analytical models, in general, provides information on pertinent spray parameters, which are limited to an extent by the simplifications deployed in the modelling of extremely complicated breakup processes. However, a large number of CFD studies are reported in the literature for the investigation of liquid breakup structure up to some levels of complexities. These CFD codes in most cases are computationally expensive. Thus, it is envisaged that the analytical model developed could be integrated into larger CFD software to complement CFD spray investigations, which could see the computational cost of CFD reduced significantly; with an improved predictive capability (Mancaruso et al., 2014). One basic approach is to write a User Defined Function (UDF) for CFD modelling, on the basis of the developed models. Writing a UDF is challenging, nevertheless it is a matter of interest in this regard. ANSYS FLUENT is a popular spray modelling platform, as it supports several approaches for modelling atomisation and sprays. In ANSYS

FLUENT, UDF is basically a C program or a C function that can be dynamically loaded with ANSYS FLUENT to enhance its features. A C program is a high-level general-purpose programming language, which has the capabilities for structured programming and allows lexical variable scope and recursion. Whereas a C function is a combination of statements within a C program environment that together perform a task. The C function can easily be called dynamically to perform a specific task.

REFERENCES

Andersson, R. and B. Andersson. 2006. “Modelling the Breakup of Fluid Particles in Turbulent Flows.” *AIChE J.* 52 (11): 2031–2038.

Andriotis, A., M. Gavaises and C. Arcoumanis. 2008. “Vortex Flow and Cavitation in Diesel Injector Nozzles.” *Journal of Fluid Mechanics* 610: 195–215. doi:10.1017/S0022112008002668.

Awasthi, I., G. Gogos and T. Sundararajan. 2013. “Effects of Size on Combustion of Isolated Methanol Droplets.” *Combustion and Flame* 160 (9): 1789–1802. doi:10.1016/j.combustflame.2013.03.023.

Bae, C. and J. Kang. 2006. “The Structure of a Break-up Zone in the Transient Diesel Spray of a Valve-Covered Orifice Nozzle.” *International Journal of Engine Research* 7 (4): 319–334.

Beale, J.C. and R.D. Reitz. 1999. “Modelling Spray Atomization with the Kelvin-Helmholtz/Rayleigh-Taylor Hybrid Model.” *Atomization and Sprays* 9: 623–650.

Beaumgarten, C. 2006. *Mixture Formation in Internal Combustion Engines*. Heidelberg: Springer-Verlag.

Bianchi, G. M., F. Minelli, R. Scardovelli and S. Zaleski. 2007. “3D Large Scale Simulation of the High-Speed Liquid Jet Atomization.” *SAE Technical Paper* 2007-01-02.

Boggavarapu, P. and R. V. Ravikrishna. 2013. “A Review on Atomization and Sprays of Biofuels for IC Engine Applications.” *International Journal of Spray and Combustion Dynamics* 5 (2): 85–122. doi:10.1260/1756-8277.5.2.85.

Carslaw, H.S. and J.C. Jaeger. 1959. *Conduction of Heat in Solids*. 2nd ed. Oxford: Clarendon Press.

Chen, P., W. Wang, W. L. Roberts and T. Fang. 2013. “Spray and Atomization of Diesel Fuel and Its Alternatives from a Single-Hole Injector Using a Common Rail Fuel Injection System.” *Fuel* 103: 850–861. doi:10.1016/j.fuel.2012.08.013.

Chhetri, A.B. and K.C. Watts. 2013. “Surface Tensions of Petro-Diesel, Canola, Jatropha and Soapnut Biodiesel Fuels at Elevated Temperatures and Pressures.” *Fuel* 104: 704–710. doi:10.1016/j.fuel.2012.05.006.

Clift, R., J.R. Grace and M.E. Weber. 1978. *Bubbles, Drops and Particles*. New York: Academic Press.

Constantine, R.D. and G.G. Evangelos. 2009. *Diesel Engine Transient Operation: Principles of Operation and Simulation Analysis*. London: Springer-Verlag.

Cossali, G.E., M. Marengo and M. Santini. 2005a. “Single-Drop Emperical Models for Spray Impact on Solid Walls: A Review.” *Atomization and Sprays* 15 (6): 699–736.

Cossali, G.E., M. Marengo and M. Santini. 2005b. “Secondary Atomisation Produced by Single Drop Vertical Impacts onto Heated Surfaces.” *Experimental Thermal and Fluid Science* 29 (8): 937–946. doi:10.1016/j.expthermflusci.2004.12.003.

Dent, J. C. 1971. “A Basis for the Comparison of Various Experimental Methods for Studying Spray Penetration.” *SAE Technical Paper*: 710571.

Desantes, J.M., R. Payri, F.J. Salvador and A. Gil. 2006. “Development and Validation of a Theoretical Model for Diesel Spray Penetration.” *Fuel* 85 (7-8): 910–917. doi:10.1016/j.fuel.2005.10.023.

Domann, R. and Y. Hardalupas. 2004. “Breakup Model for Accelerating Liquid Jets.” In *Proceedings of 42nd AIAA Aerospace Science Meeting and Exhibition, Reno, Nevada*, Paper AIAA–2004–1155.

Dumouchel, C. 2001. “Measurement of Breakup Length of Cylindrical Liquid Jets. Application to Low-Pressure Car Injector.” *Atomization and Sprays* 11: 201–226.

Dumouchel, C. 2008. “On the Experimental Investigation on Primary Atomization of Liquid Streams.” *Journal of Experimental Fluids* 45: 371–422.

ECN. 2014. “Sandia National Laboratory.” www.sandia.gov/ecn/dieselSprayCombustion.php. [cit. 15-04-2004]

Eggers, J. 2006. “A Brief History of Droplet Formation.” In *Nonsmooth Mechanics and Analysis. Advances in Mechanics and Mathematics, Vol. 12.*, edited by P Alart, O Maisonneuve, and R.T Rockafellar, 163–172. New York: Springer.

Eggers, J. and E. Villermaux. 2008. “Physics of Liquid Jets.” *Reports on Progress in Physics* 71 (3): 036601. doi:10.1088/0034-4885/71/3/036601.

Faeth, G.M. 2002. “Dynamics of Secondary Drop Breakup — A Rate Controlling Process in Dense Sprays.” In *ILASS-Europe, 9-11 September, Zaragoza*, 1–11.

Fang, J.P. and P. Joos. 1992. "The Dynamic Surface Tension of SDS—Dodecanol Mixtures: 1. The Submicellarsystems." *Journal Colloids and Surfcaces* 65(2–3): 113–120.

Ferziger, J.H. and M. Peric. 2002. *Computational Methods for Fluid Dynamics*. Berlin: Springer.

Forstall, W. and A.H. Shapiro. 1950. “Momentum and Mass Transfer in Coaxial Gas Jets.” *ASME Journal of Applied Mechanics* 17: 399–408.

Furlani, E.P. 2005. “Temporal Instability of Viscous Liquid Microjets with Spatially Varying Surface Tension.” *Journal of Physics A: Mathematical and General* 38 (1): 263–276. doi:10.1088/0305-4470/38/1/020.

Gorokhovski, M. and M. Herrmann. 2008. “Modelling Primary Atomization.” *Annual Review of Fluid Mechanics* 40: 343–366. doi:10.1146/annurev.fluid.40.111406.102

Gulder, O.L., G.J. Smallwood and D.R. Snelling. 1992. “Diesel Spray Structure Investigation by Laser Diffraction and Sheet Illumination.” *SAE Technical Paper*: 1992057.

Han, L., H. Luo and Y. Liu. 2011. “A Theoretical Model for Droplet Breakup in Turbulent Dispersions.” *Chemical Engineering Science* 66 (4): 766–776. doi:10.1016/j.ces.2010.11.041.

Hansen, K.G., J. Madsen, C.M. Trinh, C.H. Ibsen, T. Solberg and B.H. Hjertager. 2002. “A Computational and Experimental Study of the Internal Flow in a Scaled Pressure-Swirl Atomizer.” In *ILASS-Europe, 9-11September,*. Zaragoza.

Hanson, A.R., E.G. Domich and H.S. Adams. 1963. “Shock-Tube Investigation of the Breakup of Drops by Air Blasts.” *Physics of Fluids* 6: 1070–1080.

Hardalupas, Y. and N. Chigier. 1994. “Characteristics of Sprays Produced by Coaxial Airblast Atomizers.” *Journal of Propulsion and Power* 10: 453–460.

Hayashi, J., J. Fukui and F. Akamatsu. 2013. “Effects of Fuel Droplet Size Distribution on Soot Formation in Spray Flames Formed in a Laminar Counterflow.” *Proceedings of the Combustion Institute* 34 (1): 1561–1568. doi:10.1016/j.proci.2012.06.019.

Herrmann, M. and J. M. Lopez. 2009. “A Numerical Method for Detailed Simulations of Atomization in Non-Isothermal Environments.” In *ICLASS 2009, 11th Triennial International Annual Conference on Liquid Atomization and Spray Systems, July 2009, Vail, Colorado USA*.

Hinze, J.O. 1955. “Fundamentals of Hydrodynamic Mechanism of Splitting in Dispersion Processes.” *AIChE J.* 1: 289–295.

Hiroyasu, H. and M. Arai. 1990. “Structures of Fuel Sprays in Diesel Engines.” *SAE Technical Paper*: 19900475.

Hossainpour, S. and A.R. Binesh. 2009. “Investigation of Fuel Spray Atomization in a DI Heavy-Duty Diesel Engine and Comparison of Various Spray Breakup Models.” *Fuel* 88 (5) (May): 799–805. doi:10.1016/j.fuel.2008.10.036.

Hsiang, L.P. and G.M. Faeth. 1995. “Drop Properties after Secondary Breakup.” *International Journal of Multiphase Flow* 19 (5): 721–735.

Ibrahim, A.A., M.A. Jog and S.M. Jeng. 2005. “Computational Simulation of Two-Phase Flow in Simplex Atomizers.” In *Proceedings of ILASS-AMERICAS*. Irvine, California.

Jansons, M., S. Campbell.and K.T. Rhee. 1998. “Diesel Engine Response to High Fuel-Injection Pressures.” SAE Technical Paper: 982683. doi:10.4271/982683.

Jarrahbashi, D. and W.A. Sirignano. 2013. “Three-Dimensional Segment Analysis of Transient Liquid Jet Instability.” In *25th Annual Conference on Liquid Atomization and Spray Systems, May 2013, Pittsburgh, PA*.

Jiang, X., G.A. Siamas, K. Jagus and T.G. Karayiannis. 2010. “Physical Modelling and Advanced Simulations of Gas–liquid Two-Phase Jet Flows in Atomization and Sprays.” *Progress in Energy and Combustion Science* 36 (2) (April): 131–167. doi:10.1016/j.pecs.2009.09.002.

Kalaaji, A., B. Lopez, P. Attané and A. Soucemarianadin. 2003. “Breakup Length of Forced Liquid Jets.” *Physics of Fluids* 15 (9): 2469–2479. doi:10.1063/1.1593023.

Karimi, K. 2007. “Characterisation of Multiple-Injection Diesel Sprays at Elevated Pressures and Temperatures.” University of Brighton.

Karimi, K., E.M. Sazhina, W.A. Abdelghaffar, C. Crua, T. Cowell, M.R. Heikal and M.R. Gold. 2006. “Developments in Diesel Spray Characterisation and Modelling.” In *THIESEL Conference on Thermo-and Fluid-Dynamic Processes in Diesel Engine*. Valencia, Spain.

Kennaird, D.A, C. Crua, J. Lacoste, M.R. Heikal, M. R. Gold and N.S. Jackson. 2002. “In-Cylinder Penetration and Breakup of Diesel Sprays Using a Common Rail Injection System.” *SAE Technical Paper*: 2002–01–1626.

Kim, D.J. and J.K. Lee. 2008. “Analysis of the Transient Atomization Characteristics of Diesel Spray Using Time-Resolved PDPA Data.” *International Journal of Automotive Engineering* 9 (3): 297–305. doi:10.1007/s12239.

Kolev, N.I. 2002. *Multiphase Flow Dynamics 1. Fundamental*. Berlin: Springer-Verlag.

Kourmatzis, A., P.X. Pham and A.R. Masri. 2013. “Air Assisted Atomization and Spray Density Characterization of Ethanol and a Range of Biodiesels.” *Fuel* 108 (June): 758–770. doi:10.1016/j.fuel.2013.01.069.

Kumar, V., S. Joshi, J. Schuetze, M. Braun, M. Sami. 2013 “Modeling Primary Atomization”. In *ILASS-Americas, 25th Annual Conference on Liquid Atomization and Spray Systems*, May, Pittsburgh, PA.

Lane, W.R. 1951. “Shatter of Drops in Streams of Air.” *Ind. Engng. Chem.* 43: 1312–1317.

Lasheras, J.C., and E.J. Hopfinger. 2000. “Liquid Jet Instability and Atomization in a Coaxial Gas Stream.” *Annual Review of Fluid Mechanics* (1873): 275–308.

Lee, K., C. Aalburg, F.J. Diez, G.M. Faeth and K.A. Sallam. 2007. “Primary Breakup of Turbulent Round Liquid Jets in Uniform Crossflows.” *AIAA Journal* 45 (8) (August): 1907–1916. doi:10.2514/1.19397.

Lefebvre, A.H. 1989. *Atomization and Spray*. New York: Hemisphere Publishing Cooperation.

Liao, Y. and D. Lucas. 2009. “A Literature Review of Theoretical Models for Drop and Bubble Breakup in Turbulent Dispersions.” *Chemical Engineering Science* 64 (15): 3389–3406. doi:10.1016/j.ces.2009.04.026.

Lin, S.P. 2006. “Three Types of Linear Theories for Atomizing Liquids.” *Atomization and Sprays* 16: 147–158.

Lin, S.P. and R.D. Reitz. 1998. “Drop and Spray Formation from a Liquid Jet.” *Annual Review of Fluid Mechanics* 30: 85–105.

Liu, A.B., D. Mather and R.D. Reitz. 1993. “Modelling the Effects of Drop Drag and Breakup on Fuel Sprays.” *SAE Technical Paper*: 930072.

Loparev, V.P. 1975. “Experimental Investigation of the Atomization of Drops of Liquid Under Conditions of a Gradual Rise of the External Forces.” *Izvestya Akad. Nauk SSSR, Mekh. Zhidkosti* Gaza 3: 174–178.

Madsen, J. 2006. *Computational and Experimental Study of Sprays from the Breakup of Water Sheets*. *PhD Thesis,* Aalborg Universitet, http://vbn.aau.dk/fbspretrieve/13581720/PhD_Thesis_Madsen.pdf.

Mahr, B. 2002. “Future and Potential of Diesel Injection System.” In *THIESEL Conference on Thermo-and Fluid-Dynamic Processes in Diesel Engine*. Valencia: THIESEL.

Mancaruso, E., R. Marialto, L. Sequino and B.M. Vaglieco. 2014. “Comparison of Spray Characteristics Measured in an Optical Single Cylinder Diesel Engine with 1D Model.” *SAE Technical Paper* 2014-04-01.

Marek, M. 2013. “The Double-Mass Model of Drop Deformation and Secondary Breakup.” *Applied Mathematical Modelling* 37 (16-17): 7919–7939. doi:10.1016/j.apm.2013.03.025.

Mashayek, F. and N. Ashgriz. 2006. “Nonlinear Instability of Liquid Jets with Thermocapillarity.” *Journal of Fluid Mechanics* 283 (April): 97–123. doi:10.1017/S0022112095002242.

Ming, H., L. Shenlun, L. Haifeng and F.L. Chia-fon. 2012. “Investigation on Spray Characteristics of Water Emulsified Diesel with Different Injection Pressure and Ambient Temperature.” In *ICLASS, 2-6 September,*. Heidelberg.

Mohan, B., W. Yang and S.K. Chou. 2014. “Development of an Accurate Cavitation Coupled Spray Model for Diesel Engine Simulation.” *Energy Conversion and Management* 77: 269–277. doi:10.1016/j.enconman.2013.09.035.

Moreira, A.L., A.S. Moita, E. Cossali and M. Marengo. 2006. “Secondary Atomization of Drop Impactions onto Heated Surfaces.” In *13th Int. Symp. on Applications of Laser Techniques to Fluid Mechanics*, 26-29 June, Lisbon, Portugal.

Muralidhar, K. and G. Biswas. 1999. *Advanced Engineering Fhuid Mechanics*. Revised Ed. Narosa Publishing House.

Naber, D. and D.L. Siebers. 1996. “Effects of Gas Density and Vaporization on Penetration and Dispensation of Diesel Spray.” *SAE Technical Paper*: 960034.

Naterer, G.F. 2003. *Heat Transfer in Single Amd Multiphase Systems*. New York: CRC Press.

Oko, C.O.C. 2011. *Introduction to Heat Transfer: An Algorithmic Approach*. 2nd ed. Port Harcourt: University of Port Harcourt Press.

Pai, M.G. and S. Subramaniam. 2007. “Modeling Droplet Dispersion and Interphase Turbulent Kinetic Energy Transfer Using a New Dual-Timescale Langevin Model.” *International Journal of Multiphase Flow* 33 (3): 252–281. doi:10.1016/j.ijmultiphaseflow.2006.08.007.

Park, S.H., H.J. Kim, H.K. Suh and C.S. Lee. 2009. “A Study on the Fuel Injection and Atomization Characteristics of Soybean Oil Methyl Ester (SME).” *International Journal of Heat and Fluid Flow* 30 (1): 108–116. doi:10.1016/j.ijheatfluidflow.2008.11.002.

Payri, F., R. Payri, F.J. Salvador and M. Bardi. 2012. “Effect of Gas Properties on Diesel Spray Penetration and Spreading Angle for the ECN Injectors.” In *ICLASS, 2-6 September,*. Heidelberg.

Payri, R., J. Gimeno, M. Bardi and A.H. Plazas. 2013. “Study Liquid Length Penetration Results Obtained with a Direct Acting Piezo Electric Injector.” *Applied Energy* 106: 152–162. doi:10.1016/j.apenergy.2013.01.027.

Pickett, L.M, C.L. Genzale, G. Bruneaux, L.M. Malbec, L. Hermant, C. Christiansen and J. Schramm. 2010. “Comparison of Diesel Spray Combustion in Different High-Temperature, High-Pressure Facilities.” *SAE Int. Journal of Engines* 3 (2): 156–181. doi:10.4271/2010-01-2106.

Pilch, M. and C.A. Erdman. 1987. “Use of Breakup Time Data and Velocity History Data to Predict the Maximum Size of Stable Fragments for Acceleration-Induced Breakup of Liquid Droplet.” *International Journal of Multiphase Flow* 13: 741–757.

Pogorevc, P., B. Kegl and L. Skerget. 2008. “Diesel and Biodiesel Fuel Spray Simulations.” *Energy & Fuels* 22 (2): 1266–1274. doi:10.1021/ef700544r.

Postrioti, L., S. Malaguti, M. Bosi, G. Buitoni, S. Piccinini and G. Bagli. 2014. “Experimental and Numerical Characterization of a Direct Solenoid Actuation Injector for Diesel Engine Applications.” *Fuel* 118: 316–328. doi:10.1016/j.fuel.2013.11.001.

Prevish, T.D. 1998. “Secondary Droplet Breakup in Highly Turbulent Flowfield”. PhD Thesis, Pennsylvania State University.

Qian, L., J. Lin and H. Xiong. 2009. “A Fitting Formula for Predicting Droplet Mean Diameter for Various Liquid in Effervescent Atomization Spray.” *Journal of Thermal Spray Technology* 19 (3): 586–601. doi:10.1007/s11666-009-9457-4.

Qian, L., J. Lin, H. Xiong and T.L. Chan. 2011. “Theoretical Investigation of the Influence of Liquid Physical Properties on Effervescent Atomization Performance.” *Journal of Fluids Engineering* 133 (10): 101205. doi:10.1115/1.4004256.

Radev, St., F., R.A. Onofri, A. Lenoble and L. Tadrist. 2013. “Review on the Instability and Optics of Capillary Jets and Glass Fibres.” *Journal of Theoretical and Applied Mechanics* 43 (2): 5–30. doi:10.2478/jtam-2013-0011.

Rangel, R.H. and W.A. Sirignano. 1991. “The Linear and Nonlinear Shear Instability of a Fluid Sheet.” *Physics of Fluids* A3: 2392–2400.

Reitz, R.D. 1987. “Modeling Atomization Processes in High-Pressure Vaporizing Sprays.” *Atomization and Spray Technology* 3: 309–337.

Reitz, R.D. and F.V. Bracco. 1982. “Mechanism of Atomization of Liquid Jet.” *Physics of Fluids* 25 (10): 1730–1742.

Reitz, R.D. and R. Diwakar. 1986. “Effect of Drop Breakup on Fuel Sprays.” *SAE Technical Paper*: 860469.

Sallam, K.A., Z. Dai and G.M. Faeth. 1999. “Drop Formation at the Surface of Plane Turbulent Liquid Jets in Still Gasses.” *International Journal of Multiphase Flow* 25: 116–1180.

Sallam, K.A., Z. Dai and G.M. Faeth. 1999. 2002. “Liquid Breakup at the Surface of Turbulent Round Liquid Jets in Still Gases.” *International Journal of Multiphase Flow* 28 (3): 427–449. doi: 10.1016/S0301-9322(01)00067-2.

Satkoski, C.A., N.S. Ruikar, S.D. Biggs and G.M. Shaver. 2011. “Cycle-to-Cycle Estimation and Control of Multiple Pulse Profiles for a Piezoelectric Fuel Injector.” In *American Control , 29 June- 01 July*. San Francisco.

Sazhin, S.S., S.B. Martynov, T. Kristyadi, C. Crua and M.R. Heikal. 2008. “Diesel Fuel Spray Penetration , Heating , Evaporation and Ignition : Modelling vs . Experimentation” *International Journal of Engineering Systems Modelling and Simulation,* 1(1): 1-19. doi: 10.1504/IJESMS.2008.018845.

Sazhin, S.S., M.R. Turner, J.J. Healey and S.B. Martynov. 2011. “Transient Diesel Fuel Jets and Spray: Mathematical Analysis and Application.” In *ILASS-Europe, 24th European Conference on Liquid Atomization and Spray Systems, Estoril, Sept. 2011*. Estoril.

Sazhin, S.S., S.A. Boronin, S. Begg, C. Crua, J. Healey, N.A. Lebedeva, A.N. Osiptsov, F. Kaplanski and M.R. Heikal. 2013. “Jet and Vortex Ring-Like Structures in Internal Combustion Engines: Stability Analysis and Analytical Solutions.” *Procedia IUTAM* 8: 196–204. doi:10.1016/j.piutam.2013.04.025.

Sazhin, S.S. 2006. “Advanced Models of Fuel Droplet Heating and Evaporation.” *Progress in Energy and Combustion Science* 32 (2) (January): 162–214. doi:10.1016/j.pecs.2005.11.001.

Shepard Jr., W.S. and V. Palan. 2006. “Enhanced Water Removal in a Fuel Cell Stack by Droplet Atomization Using Structural and Acoustic Excitation.” *Journal of Power Sources* 159: 1061–1070.

Sher, I. 2010. “Stability and Breakup of Transient Jets.” In *ILASS-Europe, 6-8 September*. Brno, Czech Republic.

Sher, I. and E. Sher. 2012. “Analytical Criterion for Droplet Breakup.” *Atomization and Sprays* 21 (12): 1059–1063.

Shibata, K., S. Koshizuka and Y. Oka. 2004. “Numerical Analysis of Jet Breakup Behavior Using Particle Method.” *Journal of Nuclear Science and Technology* 41 (7): 715–722.

Shinjo, J. and A. Umemura. 2011a. “Detailed Simulation of Primary Atomization Mechanisms in Diesel Jet Sprays (isolated Identification of Liquid Jet Tip Effects).” *Proceedings of the Combustion Institute* 33 (2): 2089–2097. doi:10.1016/j.proci.2010.07.006.

Shinjo, J. and A. Umemura. 2011b. “Surface Instability and Primary Atomization Characteristics of Straight Liquid Jet Sprays.” *International Journal of Multiphase Flow* 37 (10): 1294–1304. doi:10.1016/j.ijmultiphaseflow.2011.08.002.

Siebers, D.L. 1999. “Scaling Liquid-Phase Fuel Penetration in Diesel Sprays Based on Mixing-Limited Vaporization.” *SAE Technical Paper*: 1999–01–0528.

Sirignano, W.A. and C. Mehring. 2001. “Review of Theory of Distortion Disintegration of Liquid Streams.” *Progress in Energy and Combustion Science* 26: 609–655.

Snyder, M.R, O.M. Knio, J. Katz and O.L. Maitre. 2006. “Numerical Study on the Motion of Microscopic Oil Droplets in High Intensity Isotropic Turbulence.” *Physics of Fluids* 20: 073301.

Soid, S.N. and Z.A. Zainal. 2011. “Spray and Combustion Characterization for Internal Combustion Engines Using Optical Measuring Techniques: A Review” *Journal of Energy* 36: 724–741. doi:10.1016/j.energy.2010.11.022.

Som, S. and K. Aggarwal. 2009. “Assessment of Atomization Models for Diesel Engine Simulations.” *Atomization and Sprays* 19 (9): 885–903.

Som, S. and S.K. Aggarwal. 2010. “Effects of Primary Breakup Modeling on Spray and Combustion Characteristics of Compression Ignition Engines.” *Combustion and Flame* 157 (6): 1179–1193. doi:10.1016/j.combustflame.2010.02.018.

Stiesch, G. 2010. *Modeling Engine Spray and Combustion Processes (Heat and Mass Transfer)*. Berlin: Springer Verlag.

Tanner, F.X. 1997. “Liquid Jet Atomization and Droplet Breakup Modelling of Non-Evaporating Diesel Fuel Sprays.” *SAE Technical Paper:* 1997-0050.

Tjahjadi, M., H.A. Stone and J.M. Ottino. 1992. “Satellite and Subsatellite Formation in Capillary Breakup.” *Journal of Fluid Mechanics* 243: 297–317. doi:10.1017/S0022112092002738.

Trinh, H.P. and C.P. Chen. 2006. “Modelling of Turbulence Effects on Liquid Jet Atomization and Breakup.” *Atomization and Sprays* 16: 907–932.

Turner, M.R., J.J. Healey, S.S. Sazhin and R. Piazzesi. 2012. “Wave Packet Analysis and Breakup Length Calculations for an Accelerating Plannar Liquid Jet.” *Fluid Dynamics Research* 44 (1): 015503.

Vladimir, R., G. Igor and K. Oleg. 2009. *Hydrodynamic Instability Analysis: Perturbation Methods*. Berlin: VDM Verlag Dr. Muller.

Vuorinen, V.A., H. Hillamo, O. Kaario, M. Nuutinen, M. Larmi and L. Fuchs. 2010. “Effect of Droplet Size and Atomization on Spray Formation: A Priori Study Using Large-Eddy Simulation.” *Flow, Turbulence and Combustion* 86 (3-4): 533–561. doi:10.1007/s10494-010-9266-3.

Wang, Y. 2010. “Numerical Methods For Two-Phase Jet Flow”. PhD Thesis, The Florida State University.

Wierzba, A. 1990. “Deformation and Breakup of Liquid Drops in a Gas Stream at Nearly Critical Weber Numbers.” *Experiments Fluids* 9: 59–64.

Wigley, G.M., G.P. Godwin and D. Blondel. 2004. “Imaging and PDA Analysis of a GDI Spray in the Near-Nozzle Region.” *Experiments in Fluids* 36: 565–574.

Wu, P.K. and G.M. Faeth. 1995. “Onset and End of Drop Formation along the Surface of Turbulent Liquid Jets in Still Gases.” *Physics of Fluids* 7 (11): 2915–2917.

Xue, J., M.A. Jog, S.M. Jeng, E. Steinthorsson and M.A. Benjamin. 2002. “Computational Model to Predict Flow in Simplex Fuel Atomizer.” In *38th AIAA/ASME/SAE/ASEE, Joint Propulsion Conference & Exhibit*. Indiana Polis.

Yoon, S.S. and S.D. Heister. 2003. “Categorizing Linear Theories for Atomizing Round Jets.” *Atomization and Sprays* 13: 499–516.

Yule, A.Y., and D.G. Salters. 1995. “On the Distance Required to Atomize Diesel Sprays Injected from Orifice-Type Nozzles.” *Journal of Automobile Engineering* 209: 217–226.

APPENDICES

Appendix A : Analysis of Heat Transfer through Semi-Infinite Medium

In §4.2.3 the physics of the heat transfer from ambient to high speed liquid jet is established. The physics is described as heat transfer from hot ambient to a semi-infinite solid, as describe by Eqs (4-3) and (4-4). The result of the analysis is presented in most literature without the detailed mathematical analysis. Therefore, this appendix presents the detailed analysis of the physics posed in §4.2.3 according to the Carslaw and Jaeger (1959) mathematical analysis approach.

It should be noted in this case that heat is transferred from the surrounding medium into the semi-infinite body.

Is possible to transform Eqs (4-3) and (4-4) into a particular case of heat transfer in which the surface is kept at zero temperature with initial condition being T_i as follows:

From Eq. (4-4c) is possible to state:

$$\eta(r,t) = [T_\infty - T(0,t)] - \frac{\bar{h}}{k_g}\frac{\partial T}{\partial r} \qquad \text{A.1}$$

With Eq.(A.1), Eqs (4-3) and (4-4) are transformed to become

$$\frac{1}{\alpha}\frac{\partial \eta}{\partial r} = \frac{\partial^2 \eta}{\partial r^2} \qquad \text{A.2}$$

$$\eta(r,0) = T_\infty - T_i \qquad \text{A.3a}$$

and

$$\eta(0,t) = 0 \qquad \text{A.3b}$$

The particular solution to the transformed equations, Eqs (A.2) and (A.3), is

$$\eta(r,t) = t^{-1/2} e^{-\left(\frac{r^2}{4\alpha t}\right)} \quad \text{A.4}$$

The integral of Eq.(A.4) will also satisfy Eq.(A.2), thus,

$$\int_0^r t^{-1/2} e^{-\left(\frac{r^2}{4\alpha t}\right)} dr \quad \text{A.5}$$

Eq.(A.5) could be transformed to a popular function by letting $y^2 = r^2/4\alpha t$; to give $dr = 2\sqrt{\alpha t}dy$, hence, Eq.(A.5) becomes:

$$2\alpha^{1/2} \int_0^{r/2\sqrt{\alpha t}} e^{-y^2} dy \quad \text{A.6}$$

Equating Eqs (A.5) and (A.6), and multiplying both sides by $1/\sqrt{\alpha\pi}$ give:

$$\frac{1}{\sqrt{\alpha\pi t}} \int_0^r e^{-\left(\frac{r^2}{4\alpha t}\right)} dr = \frac{2}{\sqrt{\pi}} \int_0^{r/2\sqrt{\alpha t}} e^{-y^2} dy \quad \text{A.7}$$

The right hand side of Eq.(A.7) defines the error function.

If Eq.(A.5) is a particular integral of Eq.(A.2), it is sufficient to say

$$\eta(r,t) = \frac{2\varpi}{\sqrt{\pi}} \int_0^{r/2\sqrt{\alpha t}} e^{-y^2} dy \quad \text{A.8}$$

where ϖ is an integral constant.

The initial condition of the transformed problem dictates $\varpi = T_\infty - T_i$, since $erf(r \to 0) = 1$, hence

$$\eta(r,t) = \frac{2(T_\infty - T_i)}{\sqrt{\pi}} \int_0^{r/2\sqrt{\alpha t}} e^{-y^2}\, dy \qquad \text{A.9}$$

Since $\eta(r,t)$ is known, it is now set to determine $T(r,t)$.

From Eq. (A.1), it appropriate to say

$$\frac{\partial T}{\partial r} - \frac{k_g}{\bar{h}}[T_\infty - T(0,t)] = \frac{k_g}{\bar{h}}\eta(r,t) \qquad \text{A.10}$$

Integrating Eq.(10), and taking $r \sim \xi$ to give

$$T(r,t) - T_i = \kappa e^{\frac{k_g}{\bar{h}}r} - \frac{k_g}{\bar{h}} e^{\frac{k_g}{\bar{h}}r} \int_\infty^r \eta(\xi,t)\, e^{-\frac{k_g}{\bar{h}}r} d\xi \qquad \text{A.11}$$

Eq.(A.11) is transformed accordingly by taking $\xi = r + v$ to give

$$T(r,t) - T_i = \kappa e^{\frac{k_g}{\bar{h}}r} + \frac{k_g}{\bar{h}} \int_0^\infty \eta(r+v,t)\, e^{-\frac{k_g}{\bar{h}}v} dv \qquad \text{A.12}$$

As it is noted before, $\eta(r,t)$ has the limit of $(T_\infty - T_i)$ with $r \to \infty$; hence, κ takes the value of zero, since $T(r,t)$must be finite. Therefore, Eq.(A.12) becomes

$$T(r,t) - T_i = \frac{k_g}{\bar{h}} \int_0^\infty \eta(r+v,t)\, e^{-\frac{k_g}{\bar{h}}v} dv \qquad \text{A.13}$$

Substitute Eq.(A.9) into Eq.(A.13) to obtain

$$T(r,t) - T_i = \frac{2}{\sqrt{\pi}}\left(\frac{k_g}{\bar{h}}\right)(T_\infty - T_i) \int_0^\infty e^{-\frac{k_g}{\bar{h}}v} \int_0^{r/2\sqrt{\alpha t}} e^{-y^2}\, dy dv \qquad \text{A.14}$$

Expanding Eq.(A.14) to get

$$\frac{T(r,t)-T_i}{T_\infty-T_i}=\frac{2}{\sqrt{\pi}}\left[e^{-\frac{k_g}{\bar{h}}v}\int_0^{(r+v)/2\sqrt{\alpha t}}e^{-y^2}\,dy\right]\Bigg|_0^\infty + \frac{2}{\sqrt{\pi}}\int_0^\infty e^{-\frac{k_g}{\bar{h}}v}\frac{d}{dv}\left(\int_0^{(r+v)/2\sqrt{\alpha t}}e^{-y^2}\,dy\right)dv \qquad \text{A.15}$$

Simplify Eq.(15) to obtain

$$\frac{T(r,t)-T_i}{T_\infty-T_i}=\frac{2}{\sqrt{\pi}}\int_0^{r/2\sqrt{\alpha t}}e^{-y^2}\,dy+\frac{1}{\sqrt{\pi\alpha t}}\int_0^\infty e^{-\frac{k_g}{\bar{h}}v-(r+v)/4\alpha t}\,dv \qquad \text{A.16}$$

Further simplification gives

$$\frac{T(r,t)-T_i}{T_\infty-T_i}=\frac{2}{\sqrt{\pi}}\int_0^{r/2\sqrt{\alpha t}}e^{-y^2}\,dy+\frac{e^{\frac{k_g}{\bar{h}}v-\left(\frac{k_g}{\bar{h}}\right)^2\alpha t}}{\sqrt{\pi\alpha t}}\int_0^\infty e^{-\left(r+v+2\frac{k_g}{\bar{h}}\alpha t\right)^2/4\alpha t}\,dv \qquad \text{A.17}$$

The second integral in the right hand side of Eq.(A.17) can be re-organised by taking $y^2=\left(r+v+2\frac{k_g}{\bar{h}}\alpha t\right)^2/4\alpha t$, which implies $dv=2\sqrt{\alpha t}dy$, as follows:

$$\frac{T(r,t)-T_i}{T_\infty-T_i}=\frac{2}{\sqrt{\pi}}\int_0^{r/2\sqrt{\alpha t}}e^{-y^2}\,dy+\frac{2}{\sqrt{\pi}}e^{\frac{k_g}{\bar{h}}r+\left(\frac{k_g}{\bar{h}}\right)^2\alpha t}\int_{\left(r+2\frac{k_g}{\bar{h}}\alpha t\right)/4\alpha t}^\infty e^{-y^2}\,dy \qquad \text{A.18}$$

Eq.(A.18) is expanded to obtain

$$\frac{T(r,t)-T_i}{T_\infty-T_i}=\frac{2}{\sqrt{\pi}}\int_0^{r/2\sqrt{\alpha t}} e^{-y^2}\,dy$$
$$+\frac{2}{\sqrt{\pi}}e^{\frac{k_g}{\bar{h}}r+\left(\frac{k_g}{\bar{h}}\right)^2\alpha t}\left[\int_0^{\infty} e^{-y^2}\,dy-\int_0^{\left(r+2\frac{k_g}{\bar{h}}\alpha t\right)/4\alpha t} e^{-y^2}\,dy\right] \qquad \text{A.19}$$

Simplifying Eq.(A.19), by noting the definition of error function, finally gives the form presented by Eq.(4-21).

Appendix B : Analysis of Droplet Breakup in Turbulent Flow Field

This is the detailed analysis of the problem posed in §7.4 for the case where surface tension has a negligible influence on droplet deformation and breakup.

Rearranging Eq.(30) to obtain

$$\frac{3^2}{2^{8.5}}\left(\sqrt{We_{bu}}\right)^4+\frac{\pi}{2\varphi\sqrt{\alpha C_D}}Oh^2=\left(n^{1/2}-1\right)+\frac{1}{2^3}C_DOh\sqrt{\frac{\rho_g}{\rho_l}}\frac{\sqrt{We_0}\sqrt{We_{bu}}}{\sqrt{We_0}-\sqrt{We_{bu}}}+\frac{1}{3\varphi}Oh\sqrt{\frac{C_D}{\alpha}}\sqrt{We_{bu}} \quad \text{B.1}$$

For $Oh \gg 1$ it implies

$$\frac{\pi}{2\varphi\sqrt{\alpha C_D}}Oh^2=\frac{1}{2^3}C_DOh\sqrt{\frac{\rho_g}{\rho_l}}\frac{\sqrt{We_0}\sqrt{We_{bu}}}{\sqrt{We_0}-\sqrt{We_{bu}}}+\frac{1}{3\varphi}Oh\sqrt{\frac{C_D}{\alpha}}\sqrt{We_{bu}} \quad \text{B.2}$$

Differentiating Eq.(B.2) with respect to $\sqrt{We_{bu}}$ gives

$$0=\frac{1}{2^3}C_DOh\sqrt{\frac{\rho_g}{\rho_l}}\left[\frac{\left(\frac{d\sqrt{We_0}}{d\sqrt{We_{bu}}}\sqrt{We_{bu}}+\sqrt{We_0}\right)\left(\sqrt{We_0}-\sqrt{We_{bu}}\right)-\left(\frac{d\sqrt{We_0}}{d\sqrt{We_{bu}}}-1\right)\sqrt{We_0}\sqrt{We_{bu}}}{\left(\sqrt{We_0}-\sqrt{We_{bu}}\right)^2}\right]+\frac{1}{3\varphi}Oh\sqrt{\frac{C_D}{\alpha}} \quad \text{B.3}$$

Noting $\left.\frac{d\sqrt{We_0}}{d\sqrt{We_{bu}}}\right|_{cr}=0$, therefore, Eq.(B.3) becomes

$$-\frac{1}{3\varphi}Oh\sqrt{\frac{C_D}{\alpha}}=\frac{1}{2^3}C_DOh\sqrt{\frac{\rho_g}{\rho_l}}\left[\frac{\left(\sqrt{We_0}\right)^2}{\left(\sqrt{We_0}-\sqrt{We_{bu}}\right)^2}\right] \quad \text{B.4}$$

Rearranging Eq.(B.2); diving the resulting equation by Eq.(B.4); solving for $\sqrt{We_{bu}}$ and substituting into Eq.(B.2) to obtain

$$\left(\frac{1}{2^3}C_DOh\sqrt{\frac{\rho_g}{\rho_l}}+\frac{1}{3\varphi}Oh\sqrt{\frac{C_D}{\alpha}}\right)\sqrt{We_0}-2\left(\frac{1}{3}\frac{\pi}{2\varphi\alpha}Oh^3\right)^{\frac{1}{2}}\left(\sqrt{We_0}\right)^{\frac{1}{2}}+\frac{\pi}{2\varphi\sqrt{\alpha C_D}}Oh^2=0 \quad \text{B.5}$$

Solving for $\sqrt{We_0}$ and neglecting unphysical solutions, imaginary solution, Eq.(B.6) is obtained.

$$\sqrt{We_0} = \frac{1}{3}\frac{\pi}{2\varphi\alpha}Oh^3\left(\frac{1}{2^3}C_D Oh\sqrt{\frac{\rho_g}{\rho_l}} + \frac{1}{3\varphi}Oh\sqrt{\frac{C_D}{\alpha}}\right)^{-2} \quad \text{B.6}$$